Spiral and Multislice

Computed Tomography of the Body

Mathias Prokop
Michael Galanski

Co-Editors
Aart J. van der Molen
Cornelia M. Schaefer-Prokop

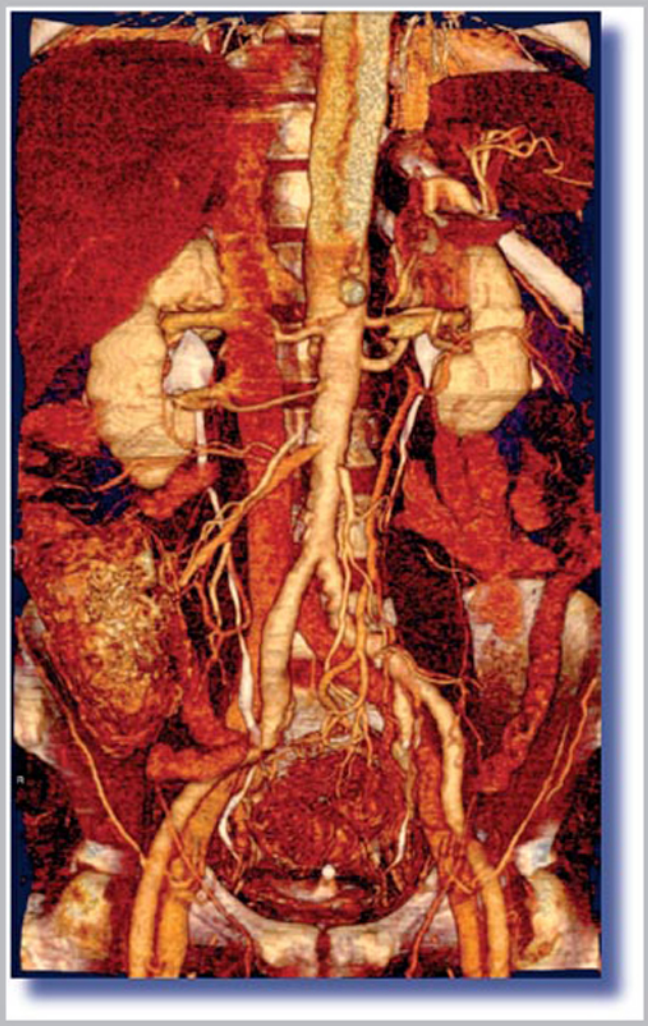

Thieme

Spiral and Multislice
Computed Tomography of the Body

Mathias Prokop, M.D.
Associate Professor of Radiology
Department of Diagnostic Radiology
University of Vienna
Vienna, Austria; *and*
Department of Radiology
University Medical Center Utrecht
Utrecht, The Netherlands

Michael Galanski, M.D.
Professor and Chairman
Department of Diagnostic Radiology
Hanover Medical School
Hanover, Germany

Co-editors:

Aart J. van der Molen, M.D.
Department of Radiology
Leiden University Medical Center
Leiden, The Netherlands

Cornelia Schaefer-Prokop, M.D.
Associate Professor of Radiology
Department of Diagnostic Radiology
University of Vienna
Vienna, Austria

With contributions by
C. Engelke, M. Jörgensen, K.J. Lehmann, A. Leppert, U. von Smekal

1972 Illustrations
332 Tables

Thieme
Stuttgart · New York

Library of Congress Cataloging-in-Publication Data
is available from the publisher

Parts of this book are an authorized translation of the German edition *Ganzkörper Computertomographie,* edited by M. Galanski and M. Prokop, published and copyrighted 1998 by Georg Thieme Verlag, Stuttgart, Germany

Parts translated by Terry C. Telger, Forth Worth, TX, USA

Contributors' addresses:

Christoph Engelke, M.D.
Department of Radiology
Klinikum der Technischen Universität Munich
Munich, Germany

Maik Jörgensen, M.D.
MR and CT Fleethof
Private Practice
Hamburg, Germany

Karl Juergen Lehmann, M.D.
Professor and Chairman
Department of Diagnostic and
Interventional Radiology
St. Vincentius Hospital
Karlsruhe, Germany

Andreas Leppert, M.D.
Department of Diagnostic Radiology
Hanover Medical School
Hanover, Germany

Ulrich von Smekal, M.D.
Institute for Diagnostic Radiology
and Neuroradiology
University Hospital
Cologne, Germany

Cover design: Thieme Marketing
Typesetting by: Druckhaus Götz GmbH,
D-71636, Ludwigsburg, Germany
Printed in Germany by: Druckhaus Götz GmbH,
D-71636, Ludwigsburg, Germany

ISBN 3-13-116481-6
ISBN 0-86577-870-1 2 3 4 5

Foreword

Although in its third decade, CT scanning remains a highly dynamic field. Rapid developments in CT technology, particularly over the past 5 years, have challenged radiologists to transform organ- and disease-specific CT acquisition protocols to take full advantage of the capabilities of 4-, 8-, and 16-row CT scanners. At no time in the past 3 decades has there been a greater diversity in CT scanner capabilities amongst those currently in clinical use. Further challenging radiologists are the new applications made possible by these technologic improvements. CT angiography and cardiac CT, as well as evolving post-processing technologies are among the newest and most dynamic areas of CT practice.

As challenging as the incorporation of rapidly evolving CT techniques and applications is to the practicing radiologist, the process of learning the practice of body CT as a resident seems particularly challenging. When I performed my first rotation in body CT as a resident in 1990, CT was a "mature" technology. We acquired almost all body CT scans with contiguous 10-mm thick acquisitions regardless of anatomic region or disease in question. My education focused squarely on the development of a working knowledge of transverse cross-sectional anatomy, CT manifestations of disease processes, and the development of cogent differential diagnoses. While these specifics of CT education of 1990 still represent the cornerstones of CT education in 2003, there is simply far more to be learned today.

This book by Mathias Prokop, Michael Galanski, Aart van der Molen, and Cornelia Schaefer-Prokop is perfectly suited to the task of helping residents achieve the needed competencies in body CT scanning to practice CT at its highest level. The authors are CT experts, who have established their reputations by embracing the technical developments of spiral and multi-row CT and using them to refine existing and develop new CT applications. This excellent text embodies the fresh perspective that they bring to a book on body CT. It is a terrific balance of CT techniques and interpretation in a comfortably paced, richly illustrated, comprehensive, and current textbook. After seven lucid chapters encompassing all aspects of CT principles and techniques, 18 organ-focused chapters cover the body from the neck through the musculoskeletal system. The authors have included clinically relevant CT anatomy, anatomic and disease-adapted techniques using single, 4- and 16-row CT scanners, disease manifestations, and image interpretation and have put special attention to new and advanced applications such as image processing, CT angiography and cardiac CT.

In an era of increasingly subspecialty-focused CT books, it is nice to see a manageable volume that encompasses the full spectrum of body CT. Both trainees in radiology as well as practicing radiologists wishing to bring their knowledge up-to-date will benefit greatly from this outstanding textbook.

Geoffrey D. Rubin, M.D.
Stanford University School of Medicine
Stanford, California

Preface

With the introduction of spiral scanning, and more recently, multislice technology, computed tomography has seen rapid technical advances and a growing number of new applications. The new technologies allow CT to defend its leading position as the cross-sectional imaging technique of choice for many indications. Multislice scanning, in particular, has transformed CT from a transaxial cross-sectional modality into a three-dimensional imaging tool.

The technical advances have yielded a substantial increase in diagnostic capabilities, improved accuracy and diagnostic confidence. Many indications that used to be the domain of projection radiography have been taken over by CT, among them diagnostic GI tests, skeletal tomography, and most intraarterial angiographic procedures. Improved 3D capabilities enable better guidance of surgical or interventional procedures, and have revolutionized the way we analyze disease processes.

At the same time, examinations have become more complex and demanding. The number of variable parameters has grown, and for each organ system the examination must be carefully adapted to the clinical question to obtain optimum results. New types of artifacts arise. Radiation exposure is gaining increased attention because the new techniques harbor the possibility both for dose reduction and for substantial dose increase. Knowledge of the underlying principles of image acquisition is essential for making choices appropriate for individual patients.

Given this background, a new book on body computed tomography was needed that would pay tribute to the new opportunities and demands and that reflects the current state of spiral and multislice technology, without neglecting the foundation of decades of experience in image analysis. This book reflects the current state of knowledge at the time of print, including scanning technique with 16-slice scanners. Technical principles and image interpretation take up a large portion of this book: they are the prerequisite for taking full advantage of the technique while at the same time preventing mistakes. The suggested scan parameters form a sensible compromise between image quality, diagnostic yield, and radiation exposure.

The organ chapters are subdivided into pathologic entities, discussing the indications for CT in the context of other imaging modalities. CT anatomy is reduced to the most important features necessary for correct diagnostic evaluation of the images. Special emphasis was placed on the organ- and indication-specific choice of examination technique, interpretation criteria and organ-specific pathology. New or improved applications such as CT colonography, cardiac CT, and CT angiography are introduced; however, we elected not to enter the heated debate on CT screening, in particular whole body screening, as the body of evidence to support such practice is presently insufficient.

To optimize readability, an up-to-date section with suggestions for further reading was placed at the end of the book. This does not cover the long history of CT literature but focuses on newer literature dealing with spiral and multislice technology. A more extensive list is available on the product information page at the publisher's website (www.thieme.com; search for "Prokop").

Since its inception, CT has been a cornerstone in radiology. We believe that the concept of this book, with its emphasis on both diagnostic and technical aspects, pays tribute to the future challenges of our discipline. We hope to have contributed to a better understanding of this intellectually stimulating and powerful technique, and that this book will become a constant companion in the daily work of radiologists worldwide.

M. Prokop
C. Schaefer-Prokop
M. Galanski
A. J. van der Molen

Abbreviations

Abbreviation	Meaning
AAA	abdominal aortic aneurysm
AAO–HNS	American Academy of Otolaryngology–Head Neck Surgery
AAST	American Association for the Surgery of Trauma
ABPA	allergic bronchopulmonary aspergillosis
ACC	*N*-acetylcysteine
ACE	acetylcholinesterase
ACKD	acquired cystic kidney disease
ACS	anterior cervical space
ACTH	adenocorticotropic hormone
ACVB	aortocoronary venous bypass graft
AFLP	acute fatty liver of pregnancy
AFP	alpha-fetoprotein
AGS	adrenogenital syndrome
AHA	American Heart Association
AIP	acute interstitial pneumonia
AJCC	American Joint Committee on Cancer
ALL	acute lymphocytic leukemia
AML	acute myeloic leukemia
APKD	acquired polycystic kidney disease
APUD	amine precursor uptake and decarboxylation (cell line)
ARDS	adult respiratory distress syndrome
ASD	atrial septal defect
ASH	asymmetric septal hypertrophy
ASNR	American Society of Neuroradiology
ASSR	American Society of Spine Radiology
ATAI	acute traumatic aortic injury
ATS	American Thoracic Society
AUA	American Urological Association
AUSPV	anomalous unilateral single pulmonary vein
AV	atrioventricular
AVM	arteriovenous malformation
BAL	bronchoalveolar lavage
BALT	bronchus-associated lymphoid tissue
BIP	bronchiolitis obliterans interstitial pneumonia
BMT	bone marrow transplant
BO	bronchiolitis obliterans
BOOP	bronchiolitis obliterans with organizing pneumonia
BPH	benign prostatic hyperplasia
bpm	beats per minute
BS	buccal space
CAD	coronary artery disease
CBV	cerebral blood volume
CCC	cholangiocellular carcinoma
CCD	charge couplet device
CHF	chronic heart failure
CLL	chronic lymphatic leukemia
CM	contrast medium
CML	chronic myeloid leukemia
CMN	contrast medium nephropathy
CMP	cardiomyopathy
CMV	cytomegalovirus
COP	cryptogenic organizing pneumonia [= BOOP]
COPD	chronic obstructive pulmonary disease
CPR	curved-planar reformation
CRP	C-reactive protein
CS	carotid space
CSF	cerebrospinal fluid
CT	computed tomography
CTA	CT angiography
CTAP	CT during arterial portography
CTC	CT cholangiography
CTDI	CT dose index
CTEPH	chronic thromboembolic pulmonary hypertension
CTHA	CT hepatic arteriography
CTP	CT perfusion imaging
CTSI	CT severity index
CUP	carcinoma of unknown primary

CVS	calcium volume score
CVS	continuous volume scanning (EBCT)
CWP	coal worker's pneumoconiosis
DAD	diffuse alveolar damage
DCF	deep cervical fascia
DEQCT	dual-energy QCT
DES	diethylstilbestrol
DIP	desquamative interstitial pneumonia
DLDCF	deep layer of the deep cervical fascia
DLP	dose – length product
DORV	double outlet right ventricle
DPB	diffuse panbronchiolitis
DRE	digital rectal examination
DSA	digital subtraction angiography
D-TGA	complete transposition of the great arteries
DVT	deep venous thrombosis
EAA	extrinsic allergic alveolitis
EAP	early arterial phase
EBCT	electron beam CT [= EBT]
EBT	electron beam tomography
ECA	external carotid artery
ECG	electrocardiogram
ECST	European Carotid Surgery Trial
EHE	epithelioid hemangioendothelioma
ELCAP	Early Lung Cancer Action Project
EMLA	eutectic mixture of local anesthesia
ERC	endoscopic retrograde cholangiography
ERCP	endoscopic retrograde cholangiopancreatography
ESR	erythrocyte sedimentation rate
FBI	fat – blood interface
FBSS	failed back surgery syndrome
FDG	fluorodeoxyglucose
FIGO	Fédération Internationale de Gynécologie et d'Obstétrique
FLC	fibrolamellar carcinoma
FNAC	fine needle aspiration cytology
FNH	focal nodular hyperplasia
FOV	field of view
FSH	follicle-stimulating hormone
FWHM	full width at half maximum
FWTA	full width at tenth area
Gd-MRA	Gadolinium-enhanced MRA
GFR	glomerular filtration rate
GI	gastrointestinal
GIP	giant cell interstitial pneumonia
GIST	gastrointestinal stromal tumor
GRE	gradient echo
GTD	gestational trophoblastic disease
HAE	hepatic alveolar echinococcosis
HAP	hepatic arterial phase
HBV	hepatitis B virus
HCA	hepatocellular adenoma
HCC	hepatocellular carcinoma
HD	Hodgkin's disease [= HL]
HDL	high density lipoproteins
HELLP	hemolysis, elevated liver enzymes, low platelets (syndrome)
HIV	human immunodeficiency virus
HL	Hodgkin's lymphoma [= HD]
HMG-CoA	hydroxymethylglutaryl coenzyme A
HNP	herniated nucleus pulposus
Ho:YAG	holmium:yttrium-aluminum-garnet
HOCM	hypertrophic obstructive cardiomyopathy
HRCT	high-resolution CT
HSV	herpes simplex virus
HVP	hepatic venous phase
ICA	internal carotid artery
ICFT	intracavitary fibrinolytic therapy
ICU	intensive care unit
IGCCCG	International Germ Cell Cancer Collaborative Group
IHE	infantile hemangioendothelioma
IHSS	idiopathic hypertrophic subaortic stenosis
IIAC	idiopathic infantile arterial calcification
ILP	interstitial laser photocoagulation
IMA	inferior mesenteric artery
INR	international normal ratio
IPF	idiopathic pulmonary fibrosis
IPH	idiopathic pulmonary hemosiderosis
IPMT	intraductal papillary mucinous tumor
IV	intravenous
IVC	inferior vena cava
IVF	*in vitro* fertilization
IVP	intravenous pyelogram
KUB	kidney ureters bladder (plain abdominal radiograph)
LA	left atrium
LAA	left atrial appendage
LAD	left anterior descending coronary artery

LAM	lymphangioleiomyomatosis
LAO	left anterior oblique
LAP	late arterial phase
LCA	left coronary artery
LCX	left circumflex [coronary artery]
LDH	lactate dehydrogenase
LDL	low density lipoproteins
LH	luteinizing hormone
LHA	left hepatic artery
LHV	left hepatic vein
LI	linear interpolation
LIMA	left internal mammary artery
LIP	lymphocytic interstitial pneumonia
LITT	laser-induced thermotherapy
LOCM	low-osmolar contrast media
LPV	left portal vein
L-TGA	corrected transposition of the great arteries
LV	left ventricle
MAC	*Mycobacterium avium* complex
MALT	mucosa-associated lymphoid tissue
MEN	multiple endocrine neoplasia
MFH	malignant fibrous histiocytoma
MHV	middle hepatic vein
MIBG	meta-iodobenzylguanidine
MinIP	minimum intensity projection
mIP	minimum intensity projection
MIP	maximum intensity projection
MLDCF	middle layer of the deep cervical fascia
MLI	multislice linear interpolation
mLV	morphologic left ventricle
Mn-DPDP	mangafodipir-trisodium
MPNST	malignant peripheral nerve sheath tumor
MPR	multiplanar reformation
MRA	magnetic resonance angiography
MRCP	magnetic resonance cholangiopancreatography
MRI	magnetic resonance imaging
mRV	morphologic right ventricle
MS	masticator space
MSAD	multiple slice average dose
MTF	modulation transfer function
MTT	mean transit time
NASCET	North American Symptomatic Endarterectomy Trial
NASH	nonalcoholic steatohepatitis
NASS	North American Spine Society
Nd:YAG	neodymium: yttrium-aluminum-garnet
NHL	non-Hodgkin's lymphoma
NIPF	nonspecific interstitial pneumonia and fibrosis
n.p.o.	nothing by mouth (*nil per os*)
nr-MIP	noise-reduced MIP
NSCLC	non-small cell lung cancer
NSIP	nonspecific interstitial pneumonia
OLT	orthotopic liver transplantation
OM	obtuse marginal branch
OO	osteoid osteoma
OP	organizing pneumonia
OR	operating room
PA	posteroanterior
PACS	picture archiving and communication system
PAI-1	plasminogen activator inhibitor-1
PAN	polyarteritis nodosa
PAP	pulmonary alveolar proteinosis
PAPVR	partial anomalous pulmonary venous return
PCP	*Pneumocystis carinii* pneumonia
PCS	posterior cervical space
PDA	patent ductus arteriosus
PDA	posterior descending coronary artery
PDV	pancreaticoduodenal vein
PE	pulmonary embolism
PEEP	positive end-expiratory pressure
PEI	percutaneous ethanol injection
PET	positron emission tomography
p.i.	post injection
PID	pelvic inflammatory disease
PIE	pulmonary interstitial emphysema
PLC	pulmonary lymphangitis carcinomatosa
PLDD	percutaneous laser disk decompression
PMF	progressive massive fibrosis
PMMA	polymethylmethacrylate
PMS	pharyngeal mucosal space
PNH	paroxysmal nocturnal hemoglobinuria
PPH	primary pulmonary hypertension
PPS	parapharyngeal space
PS	parotid space
PSA	prostate specific antigen
PT	prothrombin time
PTA	percutaneous transluminal angioplasty
PTC	percutaneous transhepatic cholangiography

PTCA	percutaneous transluminal coronary angioplasty
PTLD	post-transplantation lymphoproliferative disorder
PTT	partial thromboplastin time
PV	portal vein
PVOD	pulmonary veno-occlusive disease
PVP	portal venous phase
PVP	percutaneous vertebroplasty
PVS	prevertebral space
QCT	quantitative CT
RA	right atrium
RAO	right anterior oblique
RAS	renal artery stenosis
RBF	regional blood flow
RB-ILD	respiratory bronchiolitis associated interstitial lung disease
RBV	regional blood volume
RCA	right coronary artery
RCC	renal cell carcinoma
REAL	Revised European–American Lymphoma (classification)
RF	radiofrequency
RHA	right hepatic artery
RHV	right hepatic vein
RIMA	right internal mammary artery
RLD	right lateral decubitus
RN	regenerative nodule
ROI	region of interest
RPS	retropharyngeal space
RPV	right portal vein
RSV	respiratory syncytial virus
RV	right ventricle
RVOT	right ventricular outflow tract
SAPHO	synovistis-acne-pustulosis-hyperostosis-osteitis (syndrome)
SBO	small bowel obstruction
SC	slice collimation
SCCa	squamous cell carcinoma
SCF	superficial cervical fascia
SCLC	small cell lung cancer
SEQCT	single-energy QCT
SFOV	scan field of view
SI	sacroiliac
SLAP	superior labral anterior – posterior (tear)
SLDCF	superficial layer of the deep cervical fascia
SLE	systemic lupus erythematosus
SLS	sublingual space
SMA	superior mesenteric artery
SMS	submandibular space
SMV	superior mesenteric vein
SPECT	single photon emission computed tomography
SPIO	superparamagnetic iron oxide (particles)
SSD	shaded surface displays
SSP	section sensitivity profile
STT	scaphoid – trapezium – trapezoideum
SVC	superior vena cava
SVS	step volume scanning (EBCT)
TACE	transcatheter arterial chemoembolization
T-ALL	T-cell acute lymphoblastic leukemia
Tbc	tuberculosis
TEE	transesophageal echocardiography
TF	table feed
TGA	transposition of the great arteries
THAD	transient hepatic attenuation differences
THPE	transient hepatic parenchymal enhancement
TIA	transient ischemic attack
TIPS	transjugular intrahepatic portosystemic shunt
TNB	transthoracic needle biopsy
TNM	tumor, node, metastasis (staging classification
TNMS	tumor, node, metastasis, serum (staging classification)
TOA	tubo-ovarian abscess
TRUS	transrectal ultrasound
TSH	thyroid stimulating hormone
TTP	time to peak
TUR	transurethral resection
UFCT	ultrafast CT [= EBT = EBCT]
UICC	Union Internationale Contre le Cancer
UIP	usual interstitial pneumonia
UPJ	ureteropelvic junction
US	ultrasound
USPIO	ultrasmall superparamagnatic iron oxide (particles)
V/Q scanning	ventilation-perfusion scintigraphy
VATS	video-assisted thoracic surgery
VOI	volume of interest
VRT	volume rendering technique
VS	visceral space
VSD	ventricular septal defect
WHO	World Health Organization
ZEEP	zero end-expiratory pressure
β-hCG	β-human chorionic gonadotropin

Contents

Acknowledgements

We would like to gratefully acknowledge all who have made this book project possible.

Several friends and colleagues have been so kind as to review one or more of the chapters of this book. In particular, we thank Cynthia McCullough (Rochester, MN) for revising the chapter on radiation exposure, and Koos Geleijns (Leiden, The Netherlands) and Peter Homolka (Vienna, Austria) for providing critical comments and up-to-date numbers within this chapter. We are gratefully indebted to Frans Zonneveld (Utrecht, The Netherlands), who has meticulously checked the first five chapters on technical aspects. We thank Stanley Fox from GE, Leon de Vries from Philips, Thomas Flohr and Stefan Schaller from Siemens, as well as Arie Munne and Luc Bouwman from Toshiba for their willingness to share the newest information about their equipment and critically reviewing the vendor-specific sections in the chapters on Principles of CT and Scanning Technique. Jonas Castelijns (Amsterdam, The Netherlands) and Suresh Mukherji (Ann Arbor, MI) have reviewed the Neck chapter and Maarten van Leeuwen (Utrecht, The Netherlands) has given his critical remarks on the Liver chapter. We are grateful for their efforts.

We would like to acknowledge the excellent technical staff at our institutions, in particular Michaela Kinze and Frank Socko from Hanover Medical School, who have introduced many new and complex techniques into clinical practice at a time when spiral scanning was still in its infancy. Dominique Sandner-Porkristl and her dedicated team have facilitated implementing and standardizing advanced multislice techniques and helped establish a successful 3 D lab in Vienna, without which many of our images would not have been possible. The dedication of Maria Zeidabadi, Uschi Brehmer, Christine Jaeger-Radkofsky and Susanne Huber has ensured constantly high image quality and a high level of patient care.

The authors are deeply indebted to those colleagues who opened their image archives and helped provide particularly instructive or rare cases for this book. We cordially thank Ahmet Ba-Ssalamah (Vienna), Patrick Brouwer (Leiden), Benedikt Czermak (Zürich), Christian Czerny (Vienna), Rainer Erlemann (Duisburg), Ulrich Fink (Villingen-Schwenningen), Dominik Fleischmann (Vienna), Thomas Flohr (Forchheim), Tomas Franquet (Barcelona), Andrea Guidotti (Chieti), Gertraud Heinz (Vienna), Christian Herold (Vienna), Martin Hofmann (Ulm), Willi Kalender (Erlangen), Matthias König (Bochum), Rainer Köster (Neuss), Soeren Kreuzer (Vienna), Gerhard Lechner (Vienna), Wolfgang Lemmen (Wuppertal), Thomas Mang (Vienna), Ulrich Mödder (Düsseldorf), Milan Pijl (Groningen), Andreas Neuhold (Vienna), Lino Ramos (Utrecht), Martine Remy-Jardin (Lille), Götz Richter (Heidelberg), Patrik Rogalla (Berlin), Herbert Rosenthal (Hanover), Stefan Schaller (Forchheim), Wolfgang Schima (Vienna), Pierre Schnyder (Lausanne), Ewald Schober (Vienna), Martin Uffmann (Vienna), and Joachim-Ernst Wildberger (Aachen), Dag Wormanns (Münster), and Patrick Wunderbaldinger (Vienna).

The Publisher, Thieme, and in particular Clifford Bergman deserve great credit for their continuing support and willingness to expand the project from a mere translation of a German text to a totally new book that included not only single slice CT but also the newest developments in multislice scanning. Finally, we cordially thank Gert Krüger from Thieme for his patience, dedication and flexibility in assembling the material and allowing us to keep critical sections up-to-date until shortly before going to print. Without his expertise, producing the book in this form and quality would not have been possible.

1 Principles of CT, Spiral CT, and Multislice CT

M. Prokop

Computed tomography (CT) has been one of the biggest breakthroughs in diagnostic radiology. The first clinical CT scanner was developed by Godfrey N. Hounsfield for examinations of the head and was installed in 1971 at Atkinson-Morley's Hospital in Wimbledon, England. The first body CT scanner was installed in 1974, and before the end of the 1970s the basic technical evolution of CT was complete (Table 1.**1**). Technical details were refined during the 1980s, and CT technology remained on a plateau until the early 1990s, when the advent of spiral (helical) CT scanning sparked a further, rapid evolution leading to improved diagnostic capabilities, 3D imaging techniques, and CT angiography. The latest innovation is the introduction of multislice CT in 1998. This new technology is vastly expanding the performance of CT scanners: it truly transforms CT from a transaxial imaging modality to a 3D technique that yields high quality images in arbitrary planes and forms the basis for an expanding variety of 3D visualization techniques, including virtual endoscopy. In addition, these scanners have the potential to revolutionize cardiac imaging with CT.

Table 1.**1** Historical milestones in computed tomography

1924	Radon: basic mathematical principles
1963	Cormack: image reconstruction
1971	Hounsfield (EMI Laboratories): technology
1971	Head scanner (EMI Mark I)
1974	Whole-body scanner (ACTA)
1974	Third-generation scanner (Artronix)
1977	Fourth-generation scanner (AS&E scanner)
1979	Nobel Prize awarded to Hounsfield and Cormack
1980 s	Technical refinements
1983	Dynamic spatial reconstructor
1983	Electron beam CT scanning
1987	Scanners with a continuously rotating tube
1989	Spiral CT (helical CT)
1991	Dual-slice spiral CT (Elscint)
1991	CT angiography
1995	Real-time reconstruction (CT fluoroscopy)
1998	Multislice CT (4 detector rows)
1999	Multislice cardiac imaging
2001/2	Multislice CT (6/8/10/16 detector rows)
Future	Cone beam CT (≥ 256 detector rows)

Computed Tomography (CT)

Scanning Principle

Computed tomography is an x-ray tomographic technique in which an x-ray beam passes through a thin axial section of the patient from various directions (Fig. 1.**1**). Parallel collimation is used to shape the x-ray beam to a thin fan, which defines the thickness of the scan plane. Detectors measure the intensity of the attenuated radiation as it emerges from the body. A mathematical image reconstruction (inverse Radon transformation) calculates the local attenuation at each point within the CT section. These local attenuation coefficients are translated into "CT numbers" and are finally converted into shades of gray that are displayed as an image. With conventional CT scanners the volume of interest is scanned in a sequential fashion, usually proceeding one section at a time.

The first two generations of CT scanners (Table 1.**2**) were superseded in the late 1970s by third- and fourth-generation scanners, which are still in use today. In third-generation scan-

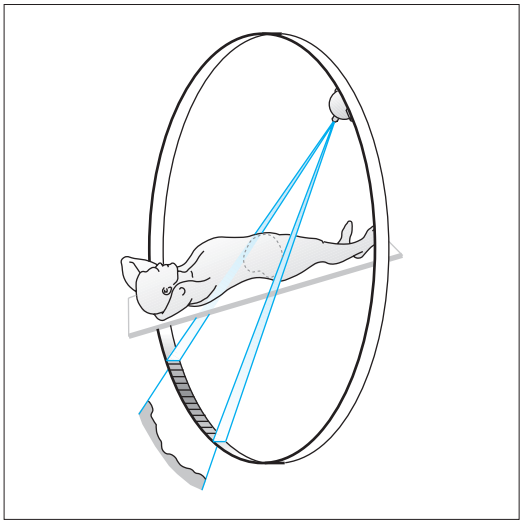

Fig. 1.**1** Principle of CT scanning.

Table 1.2 Comparison of CT scanner generations and types

Type	First generation	Second generation	Third generation	Fourth generation	Electron beam scanning
Principle	Translation-rotation		Rotation		Electron beam deflection
Detectors	Single	Series	Arc (30°–60°)	Ring (360°)	Semicircular (210°)
Active detector rows	2	1–2	1–16	1	4
Detector elements/row	1	3–52	256–1000	600–4000	432/864
Scan time	135–300 s	5–150 s	0.4–10 s	1–5 s	≥ 50 ms

ners, tube and detector array rotate synchronously around the patient. The detector array covers the full width of the fan beam (Fig. 1.**2**). In fourth-generation scanners, the detector elements cover a full circle around the scanner opening and remain stationary during the scan, while only the x-ray tube rotates around the patient (Fig. 1.**2**). Third-generation scanners, however, offer better scatter suppression and require less detector elements, which is the reason why all multislice CT scanners use third-generation technology.

Attempts to speed up the imaging process led to the development of a multi-tube CT scanner called the dynamic spatial reconstructor (the "Mayo monster" equipped with 28 tubes, able to scan up to 240 sections, each of 1 mm thickness, in one 360° rotation), electron beam CT scanning, spiral CT, and, recently, multislice CT. Of these procedures, only spiral and multislice CT have achieved large-scale clinical impact.

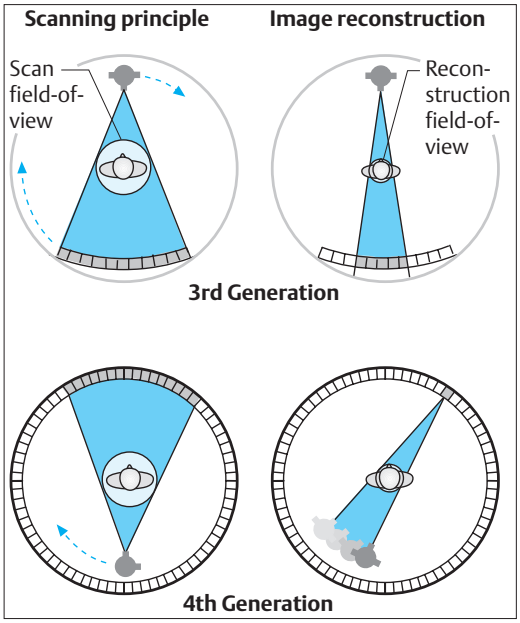

Fig. **1.2** Comparison of scanning principle and image reconstruction in third-generation (**a**, **b**) and fourth-generation CT scanners (**c**, **d**). The fourth generation uses a stationary detector ring, and the data acquired by one detector are assembled into a projection for the various tube positions.

Image Reconstruction

The detector signals registered during a scan are preprocessed to compensate for inhomogeneities in the detector system and to correct for beam-hardening effects within the patient. After various correction steps and transformation from signal intensities into x-ray attenuation values these data are called the *CT raw data* (Fig. 1.**3**). The raw data sets for third- and fourth-generation scanners each consist of the attenuation profiles of some 500 to 2300 projections for each 360° rotation of the x-ray tube. Each projection in turn is composed of some 500 to 900 single attenuation values. Image reconstruction from the raw data sets finally yields the image data set.

Image reconstruction starts with the selection of the desired field of view. Each ray from the tube to the detector that passes through this field of view is used for reconstruction. The attenuation coefficient for each image point is determined by averaging the attenuation values for all rays that cross this point (*back projection*). But this type of unfiltered back projection yields a very unsharp image with blurred edges, so multi-

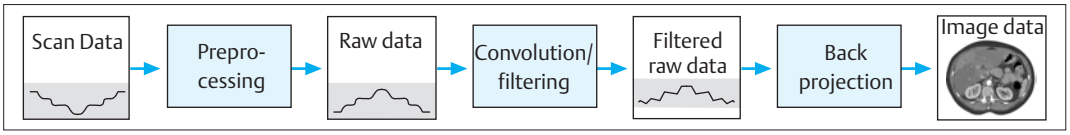

Fig. 1.3 Processes involved in CT image reconstruction.

ple rays are assembled into a projection, and the resulting attenuation profile is subjected to an edge-enhancing mathematical filtering (convolution) process. The so-called "convolution kernel" determines the type of filtering. Back projection of the filtered attenuation profiles then yields a sharp image. The *convolution kernel* (reconstruction algorithm) used for the *filtered back projection* determines the properties of the reconstructed CT sections in terms of spatial resolution and image noise, and can vary from soft or smooth to sharp or edge-enhancing (Fig. 1.**4**).

Third and fourth-generation scanners differ in the way that the attenuation values are assembled into a fan-shaped projection. The third generation uses the fan from a single tube position to the detector, while the fourth generation takes the data acquired by a single detector for various tube positions and assembles them into a projection (Fig. 1.**2**).

Image Display and Documentation

Image Matrix and Field of View

A CT image is composed of a square image matrix that ranges in size from 256 × 256 to 1024 × 1024 picture elements, or *pixels*. Since a CT section has a finite thickness, each pixel actually represents a small volume element, or voxel. The size of this voxel depends on the matrix size, the selected field of view (FOV), and the section thickness (Fig. 1.**5**). In most CT examinations the voxel has a matchstick shape, i.e., the pixel size measured in the plane of the section, the x–y plane, is 10 to 20 times smaller than the section thickness, measured along the z-axis. This anisotropy (nonuniform shape) of the voxels can be decreased only by greatly reducing the section thickness. Only with multislice CT is it possible to obtain nearly isotropic (cube-shaped) voxels for larger body areas. (See also p. 46 for a more complete discussion of the issue.)

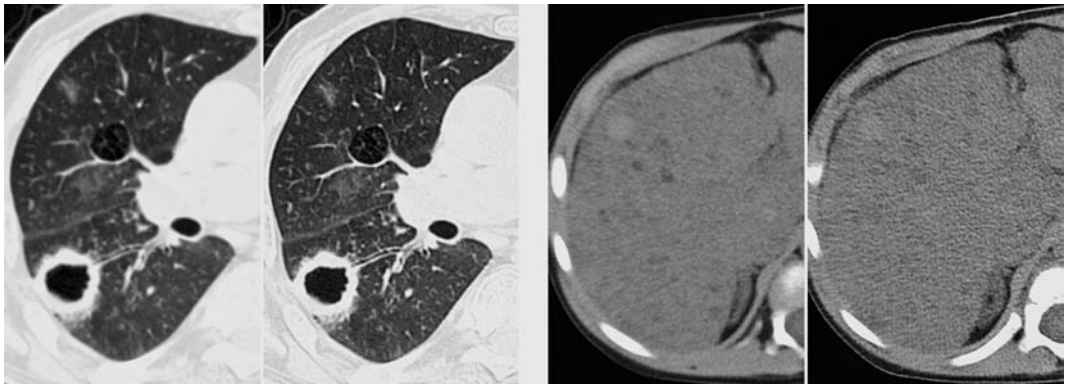

a **b** **c** **d**

Fig. 1.4 Effect of the convolution kernel on spatial resolution and image noise. In the lung parenchyma (high intrinsic contrast), the use of a sharp kernel (**b**) instead of a standard kernel (**a**) increases image sharpness. In the liver (low intrinsic contrast), a soft kernel (**c**) is preferable to a sharp kernel (**d**) because the increased noise could otherwise obscure low-contrast structures.

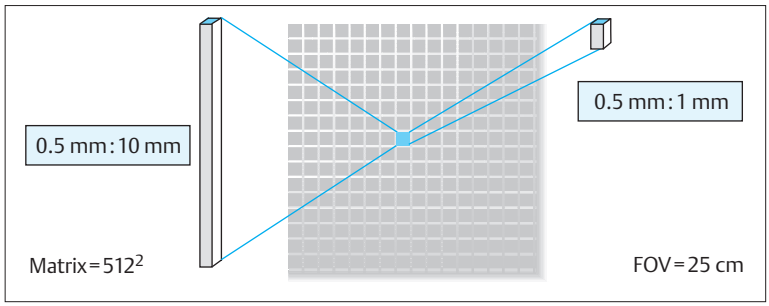

Fig. 1.5 The pixels in the CT matrix actually represent volume elements (voxels) in the scanned body region. Note that for a standard section thickness of 10 mm, each voxel has a matchstick shape.

There may be a difference between the actual *image matrix* that is reconstructed from the raw data and the *display matrix* that is shown on the viewing monitor or is printed out to film. Although the display matrix is usually identical to the image matrix, a larger display matrix may be selected (e.g., 1024×1024 instead of 512×512) to improve the image quality.

It is not usually necessary to use data from the entire body cross section for image reconstruction, and a *field of view* (FOV) of more restricted size can be reconstructed from the raw data. This field of view is characterized either by its size in mm or by the *zoom factor* relative to the maximum field of view possible on that scanner. Depending on the scanner it can either be round or square. Some manufacturers call this the *reconstruction field of view* (RFOV) to distinguish it from the *display field of view* (DFOV) that can be selected from that field and magnified for display on the monitor. Usually such a magnified image is less sharp than one directly reconstructed from the raw data because it uses only a portion of the image data rather than all the information contained in the raw data set.

The reconstruction and display field of view have to be distinguished from the *scan field of view* (SFOV) available on some scanners. The SFOV is a reduced, centrally located area from which data are acquired, which can increase the sampling rate and thus improve spatial resolution. Usually this technique is applied in examinations of the extremities (calcaneus), spine or in the head and neck region. Since a reduced SFOV uses a fan beam with a narrower angle, the technique also reduces radiation exposure to those portions of the patient that are outside the SFOV. For this reason, it is used on some scanners to reduce radiation exposure for cardiac multislice CT imaging.

CT Numbers

During image reconstruction, a numerical value (CT number) is assigned to each voxel according to the degree of x-ray attenuation in that voxel. To reduce dependence on the energy of the radiation and to obtain numerical values of convenient size, the CT number is defined as follows:

$$CT = 1000 \times (\mu - \mu_{water})/\mu_{water}$$

The unit for CT attenuation is called the Hounsfield unit (HU). The numbers are set on a scale in which –1000 represents the attenuation of air and 0 is the attenuation of water. Note that there is no upper limit to the scale. The available range of CT numbers varies between scanners and available bits per pixel (e.g., from –1024 to 3071 HU with 12 bits or up to 64,500 HU for 16 bits).

The scale of CT attenuation numbers is shown graphically in Fig. 1.**6**. Except for fat, low-protein fluids, and fresh blood, there are no "typical" values that would permit the specific characterization of soft tissues by their CT numbers (see also Fig. 7.**5**).

Window Settings

The human eye can distinguish only a limited number of gray levels (from about 40 to 100, depending on viewing conditions). Consequently, there is no point in assigning the complete diagnostic range of CT numbers (some 4000 HU) to the available range of gray levels (from white to black) because discrimination between structures with small differences in CT numbers would no longer be possible. It is therefore better to display just a portion of the CT scale. This so-called *window* is defined by its *width*, which affects image contrast, and by its *level* (center), which determines image brightness. Reducing

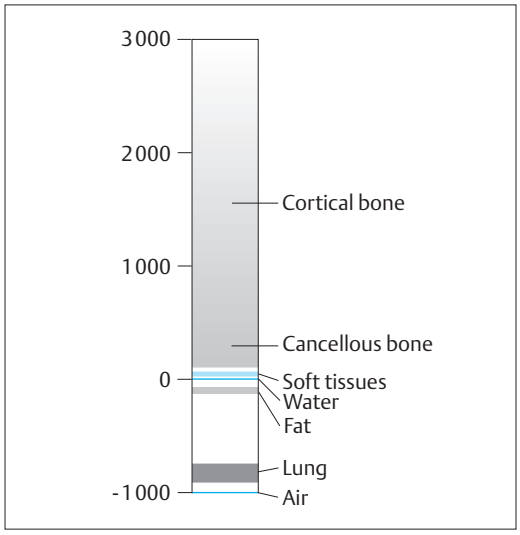

Fig. 1.**6** The scale of CT attenuation numbers is defined by the values for air (-1000 HU) and water (0 HU). Soft tissues occupy a narrow range around 50 HU.

the window width increases image contrast; lowering the window level brightens the image, and raising the window level darkens the image (Fig. 1.**7**). Examples of window settings are shown in Table 1.**3**.

Image Processing and Analysis

The software used in CT scanners provides various options for processing and manipulating the CT sections. The features of greatest practical importance are the measurement of lengths and angles and the analysis of CT numbers within a selected region of interest (ROI). This ROI may be selected interactively, allowing the operator to choose between predefined shapes (circle, ellipse, rectangle) or freely outlined regions of arbitrary shape. A computer program can then calculate mean CT numbers and standard deviations within the ROI and can generate histograms.

The scanned volume can also be manipulated to produce reformatted images in any secondary plane of section ("multiplanar reformation," MPR) and various types of three-dimensional reconstruction (see Chapter 2, Image Processing).

Documentation

CT images from conventional scanners are usually printed on film for image review. It is important to document all the window settings that are relevant for the examined body region. For example, chest scans should be documented in both the lung window and soft-tissue window settings. A bone window setting may be added to screen for skeletal metastases. Attempts to display two non-overlapping window settings simultaneously (e.g., mediastinum and lung) have been abandoned, because structures whose CT numbers lie between the two windows (e.g., pleural lesions) are too easily missed. This *dual window technique* is no longer used.

With modern spiral CT or multislice scanners, or with the introduction of picture archiv-

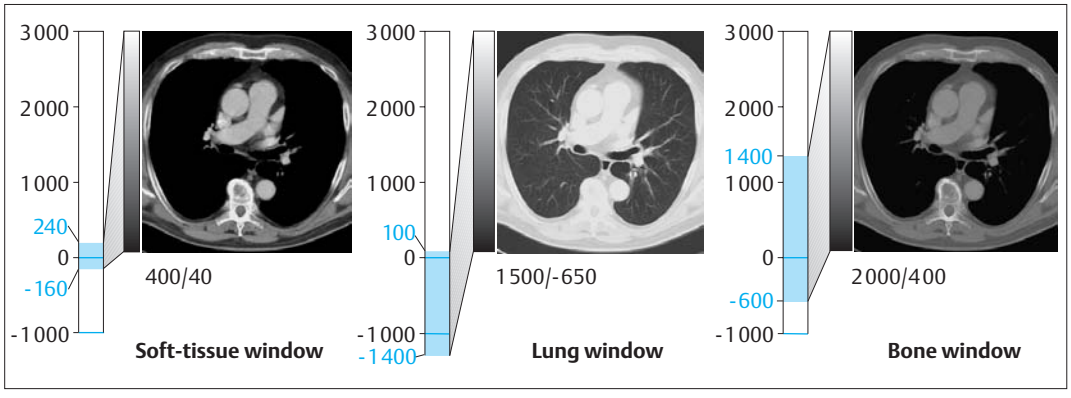

Fig. 1.**7** Window settings. For optimum contrast, the gray levels available for viewing or filming are assigned to a designated portion of the CT scale. The window is defined by its width, which determines contrast, and by its level, which determines brightness.

Table 1.3 Window settings

	Width	Level/center
Lung	1500	–650
Emphysema	800	–800
Soft tissues, noncontrast	400	40
Liver, noncontrast	200	40
Soft tissues + CM	400	70
Liver + CM	300	60–100
Neck + CM	300	50
CT Angiography	500	100–200
Bone	2000	500
Osteoporosis	1000–1500	300
Petrous bone	4000	700

CM = contrast medium

ing and communication systems (PACS), printing of CT images is increasingly abandoned in favor of direct viewing on CRT or flat screen monitors and storing image data in a digital archive.

Scanning Parameters

Gantry Angulation

The gantry, or frame that houses the scanning equipment, can be tilted about the x-axis to perform oblique scans. The range of gantry angulation may be ±30°, depending on the scanner. Gantry angulation is used mainly for scanning the head, neck, or spine. It is unnecessary for most other applications and is increasingly being abandoned with multislice scanning and reconstruction of tilted sections from a volume data set.

Section Thickness

Section Profile

The beam collimation setting determines the thickness of a CT section. But as in conventional radiography, the x-ray tube emits a conically divergent beam rather than parallel rays. To obtain sections of reasonably uniform thickness, it is necessary to use collimators located directly behind the tube. Some scanners use additional post-patient collimators in front of the detectors for further optimization of the section profile. Despite these measures, a truly plane-parallel section is never obtained in practice, and adjacent portions of the scanned object are always included. In addition, the finite size of the focus of the x-ray tube causes an area outside the primary beam to receive radiation of less intensity. This region is called the *penumbra* (Fig. 1.**8a**).

The effect on the acquired section can be described in terms of the *section sensitivity profile* (SSP) or *slice profile* (Fig. 1.**8**), which shows how much a point in the object contributes to the image as a function of its distance from the center of the section. The ideal section profile is a rectangle whose width equals the desired section thickness, so that all points outside the section contribute nothing to the measured attenuation while all points within the section contribute uniformly to the CT number. Real section profiles have rounded "edges", meaning that adjacent regions also contribute slightly to the image. While the profile of thick CT sections (7–10 mm) closely approximates to an ideal rectangular shape, thin sections exhibit a more bell-shaped profile (Fig. 1.**8b**).

In clinical practice, the increasingly large "tails" of thinner section profiles do not substantially affect image quality because the decreased width of the profile is more important and leads to improved resolution along the z-axis.

Effective Section Thickness

The width of the section sensitivity profile is usually quantified by measuring the width of the curve at 50% of its peak value, called the *full width at half maximum* (FWHM) (Fig. 1.**8c**). This value is also known as the *effective section thickness* or *section width* (SW). It is by definition equal to the *section collimation* (SC) or *nominal section thickness* in conventional CT. It should be noted, however, that the effective section thickness is not equivalent to the section collimation in spiral CT. It is the commonest measure for describing the spatial resolution along the patient axis (z-axis).

A more rigorous measure of the width of the section profile is the width that encompasses 90% of the area under the curve, called the *full width at tenth area* (FWTA). The FWTA indicates the width at which object elements located outside the section contribute just 10% to

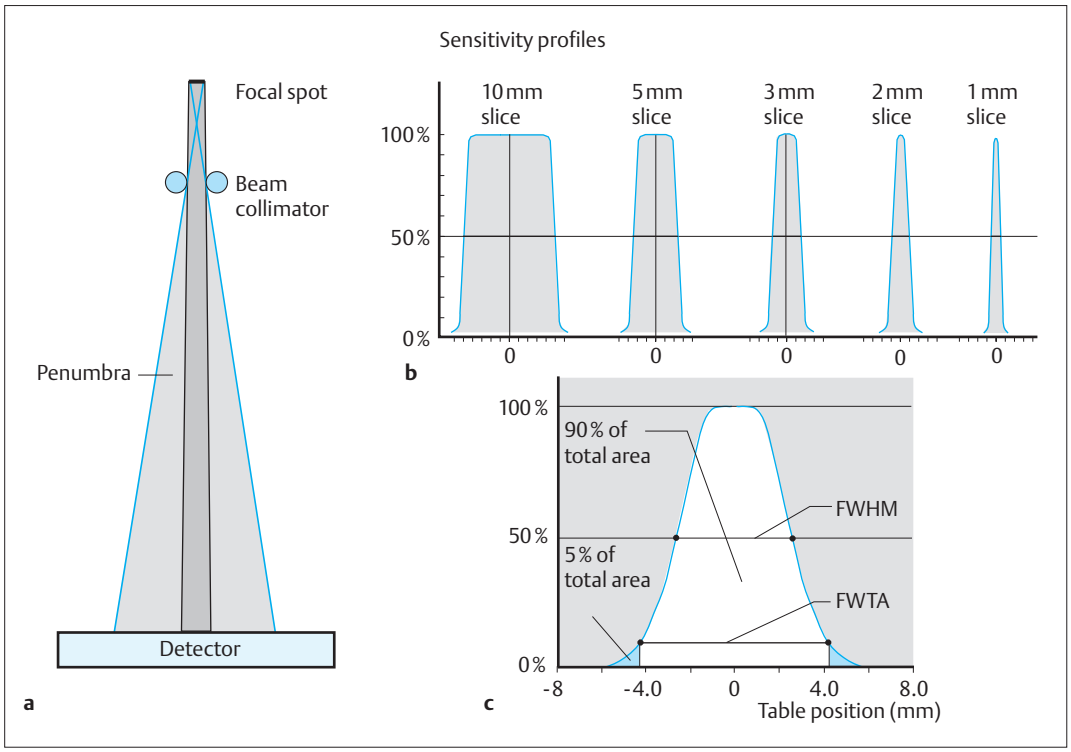

Fig. 1.**8** Because of the x-ray beam geometry, regions located outside the selected section thickness are included in the scan (**a**). This results in a rounded section sensitivity profile, which approximates to an ideal rectilinear shape only in thicker sections (**b**). The effective section thickness (= section width SW) can be measured by the width of the section profile at half of its peak value, called the full width at half maximum (FWHM), or the width that encompasses 90 % of the area under the curve, called the full width at tenth area (FWTA) (**c**).

the CT number. FWHM and FWTA yield similar values in conventional CT when thick sections are chosen, but they differ markedly in spiral CT and when thin collimation is used in conventional CT.

The *slice profile quality index* (SPQI) is another, more recent measure. It describes the percentage of the area under the section sensitivity profile that is bounded within an ideal rectangular profile of the same section width.

Partial Volume Effect

The CT number of a pixel is determined by the x-ray attenuation that occurs in the corresponding voxel. If tissues with different attenuation properties occupy the same voxel (e.g., blood vessels and lung), the resulting CT number will—with good approximation—represent the sum of the different attenuation values (*partial volume effect* or *partial volume averaging*):

$$CT = v_1 \times CT_1 + v_2 \times CT_2 + \ldots,$$

where the partial volume elements v_i add to 1.

Given the much greater extent of a voxel along the z-axis than in the x–y plane, the section collimation contributes a great deal more to this partial volume effect than the field of view or pixel size (Fig. 1.**9**).

Section Collimation

A number of anatomic structures (portions of the aorta, chest wall, or liver borders) are oriented parallel to the long axis of the body. The usual transaxial section orientation in CT means that the scan will cut the corresponding tissue boundaries at a perpendicular angle, which tends to minimize partial volume effects. For this reason, a section collimation of 7–10 mm is most commonly used in conventional body CT examinations.

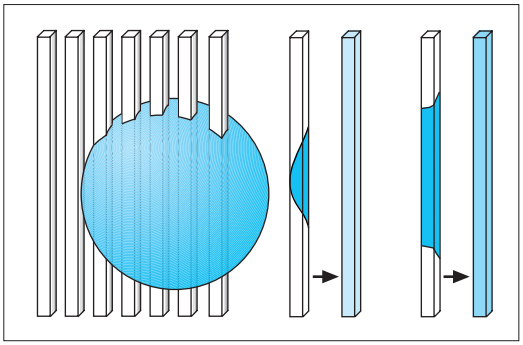

Fig. 1.**9** Partial volume effect. Because of the matchstick-like configuration of the voxels, the CT number of a voxel is affected not only by the object of interest (e.g., a round lesion) but also by adjacent structures (e.g., lung parenchyma). This creates an averaging effect that distorts the CT number of the voxel.

Partial volume effects are particularly troublesome in scans that are oblique or parallel in relation to tissue boundaries (diaphragm, apex of lung, pole of kidney) and in the evaluation of small structures (small vessels, bronchi, adrenals). A collimation of 3–5 mm can be used to evaluate structures that are parallel to the scan plane (e.g., the pancreas) or for evaluating small organs such as the adrenals. Thin collimation of 1–2 mm is preferred for the lung, where a detailed structural analysis is required for the diagnosis of interstitial lung disease. With multislice CT scanning thin collimations have become standard (see below).

Table Feed

In conventional CT, a tissue volume is scanned section-by-section. This is accomplished by moving the patient table by a designated amount, called the table feed (*table increment*), between consecutive scans. Contiguous imaging is generally performed, meaning that the section thickness and table feed are equal.

Overlapping Scans

Reducing the table feed produces an overlapping scan pattern that increases the radiation dose to the patient. While overlapping scans have been recommended to improve the 3D imaging of skeletal structures with conventional CT, the introduction of spiral scanning has made them obsolete.

Discontinuous Scanning

When the table feed is increased, intersection gaps are produced. This may be useful in selected cases where it is necessary only to search for gross pathologic changes that extend over larger ranges.

Respiratory Misregistration

Respiratory misregistration in CT occurs when structures that move with respiratory excursions are missed due to variations in the depth of respiration between sections. However large the efforts to reproduce a consistent depth of breath holding for 5 to 20 respiratory cycles, some gaps along the z-axis will generally occur. The thinner the collimation and the smaller the lesion, the greater the risk of respiratory misregistration will be (Fig. 1.**10**). This has only a moderate effect on the detection of hepatic lesions or the evaluation of the kidneys and adrenals, but it can seriously hamper the search for pulmonary metastases. To obtain seamless coverage, a section collimation of less than 5 mm should be avoided in areas that move with respiratory excursions. This creates conflicting demands in conventional CT, where it is *not* possible both to minimize partial volume effects and avoid respiratory misregistration in the same scan.

Reconstruction Algorithm (Convolution Kernel)

The convolution kernel used in reconstructing an image from the raw data determines the relationship between spatial resolution and image noise. Noise limits contrast resolution, and thus the ability to differentiate objects that show

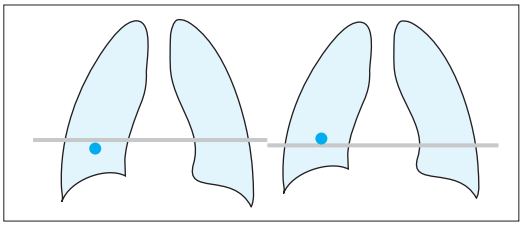

Fig. 1.**10** Respiratory misregistration: different depths of breath holding can cause a small lesion (e.g., a pulmonary nodule) to be missed in sequential scans.

very little attenuation difference from their surroundings. High *contrast resolution* is important for the detection of lesions in parenchymal organs like the liver and pancreas. High *spatial resolution* is necessary for the detection of very fine morphologic changes in lung or bone. High-resolution convolution kernels (*HR kernels*, *sharp kernels*) improve spatial resolution but disproportionately increase noise as well. Conversely, *soft* or *smooth kernels* lead to a concomitant reduction in noise and spatial resolution (Fig. 1.**11**). *Standard kernels* are designed as a compromise for good spatial resolution and reasonably low image noise for most body applications.

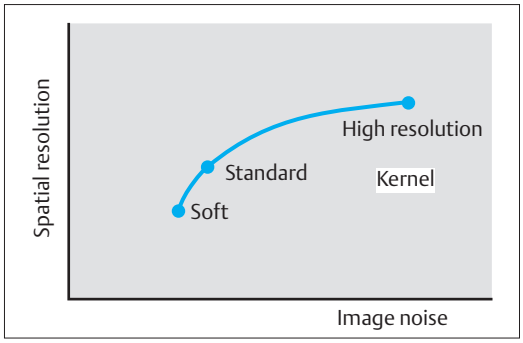

Fig. 1.**11** The use of higher-resolution convolution kernels can improve spatial resolution but leads to a disproportionate increase in image noise.

Partial Scan

Because attenuation of an x-ray beam is identical in both directions (from the tube to the detector and from the detector to the tube), enough data for reconstructing a CT image can be obtained from less than a full 360° rotation. Instead, data from a partial rotation of 180° plus the fan angle of the x-ray beam (usually some 60°) is sufficient for this purpose. This partial scan or half scan reconstruction can be used to reduce the scan time per CT section and thus reduce motion artifacts. In particular, it is employed for cardiac imaging using electron beam CT or multislice CT, when temporal resolution is of utmost importance.

Spiral (Helical) CT

During the past decade, spiral (= helical) CT has become the standard technology for the majority of clinical indications for CT scanning.

Scanning Principle

Spiral CT requires a scanner with a continuously rotating x-ray tube. A tube with a large heat capacity is needed that can operate continuously for the duration of the scan. More than 100 seconds scan duration are available with current scanners. In contrast to conventional CT, the patient is not scanned section-by-section but is translated through the scan plane at a uniform table speed during acquisition of the raw data (Fig. 1.**12**). The technique is named spiral or helical CT after the spiral or helical pattern that is traced by the scan.

A CT image can be generated from any segment within the scanned volume, so the table feed is unrelated to the site of image reconstruction. Sectional images can be produced at arbitrary levels, and individual images can be overlapped as desired without increasing radiation exposure. The spacing between the reconstructed sections is called the *reconstruction interval*, *increment* or *index*.

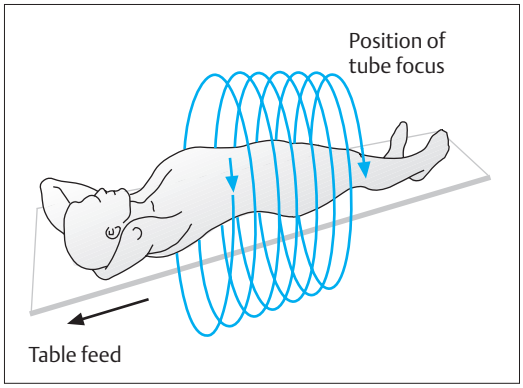

Fig. 1.**12** Principle of spiral CT.

The section collimation (nominal section thickness) and table feed can be varied independently of each other in spiral CT. The *pitch* defines the ratio of the *table feed* (table increment) per gantry rotation to the *section collimation* (see Fig. 1.**15**). The higher the pitch, the lower the radiation dose to the patient and the greater the available range of scan coverage.

Advantages

The advantages of spiral CT arise from continuous data acquisition and short total scanning time.

With conventional CT, small lesions such as pulmonary or hepatic metastases may be missed due to respiratory misregistration (see Fig. 1.**10**). But spiral CT can acquire data in a seamless volume during one breath hold, eliminating respiratory motion and interscan gaps. The use of overlapping reconstruction intervals allows for optimum visualization of small lesions while eliminating partial volume effects. When thin collimation is used, 2 D reformatted images can be generated in arbitrary planes of section, and 3D reconstructions of good quality can be produced.

Owing to the short scan time, most spiral examinations can be performed during a single breath hold. Intravascular contrast medium can be used more effectively, providing either higher contrast or a reduction in the volume of contrast material. Arterial phase imaging has become available only with spiral scanning. These advantages can significantly improve the detection of hepatic and pancreatic lesions compared with conventional scanning.

High vascular contrast is the foundation for CT angiography (CTA), which is a technique that is not available with conventional CT. Volume acquisition and short scan times are utilized in this technique to capture the arterial enhancement and generate angiogram-like vascular images (see Chapter 24).

Disadvantages

Most disadvantages of spiral CT result from the use of older scanners. In these scanners the continuous tube operation necessitates a lower radiation dose per rotation and may lead to a marked increase in image noise. Modern scanners employ an improved tube technology, so noise is no longer a limiting factor.

While the scan duration is shorter with spiral CT, there are more sections to be processed. This may increase the time required for image reconstruction, especially when overlapping sections are used. While this was a time-consuming process with older scanners, new scanners provide fast reconstruction and often require less than one second per image. An increased number of images needs to be viewed, documented and archived, which again may increase time and costs.

There is a basic tradeoff in spiral CT between a large scan volume and a high spatial resolution in the z-direction. Short scan ranges, such as the inner ear, can be covered with thin collimation but long ranges, such as in thoracoabdominal CT examinations, require a thicker collimation.

The short scan time also complicates the administration of contrast medium, and new types of artifact may occur. A faulty contrast technique can lead to suboptimum examinations or misleading findings (see Figs. 7.**39**–7.**41**).

Image Reconstruction

Interpolation Algorithm and Section Profile

The table movement during the scan will produce motion artifacts if the raw data acquired during a 360° rotation are used directly for image reconstruction. This is because the first and last projections in the 360° rotation sample different data (due to the table motion during tube rotation). To avoid these artifacts, interpolation of the raw data before image reconstruction is required. The goal of the interpolation is to obtain a complete set (360°) of projections at the desired z-axis position in the scanned volume.

The simplest *linear interpolation* of the projection data is called *360° LI* (Fig. 1.**13 a**). At every angular position of a 360° rotation it interpolates between the two projections in the spiral data set that are closest to the chosen position along the z-axis. This interpolation from 720° of data results in a complete (360°) set of projections for the chosen z-position. The 360° LI interpolation provides the least image noise but substantially broadens the section profile (Fig. 1.**13 b**).

More advanced interpolation algorithms exploit the fact that x-ray attenuation is independent of direction, i.e., the attenuation along

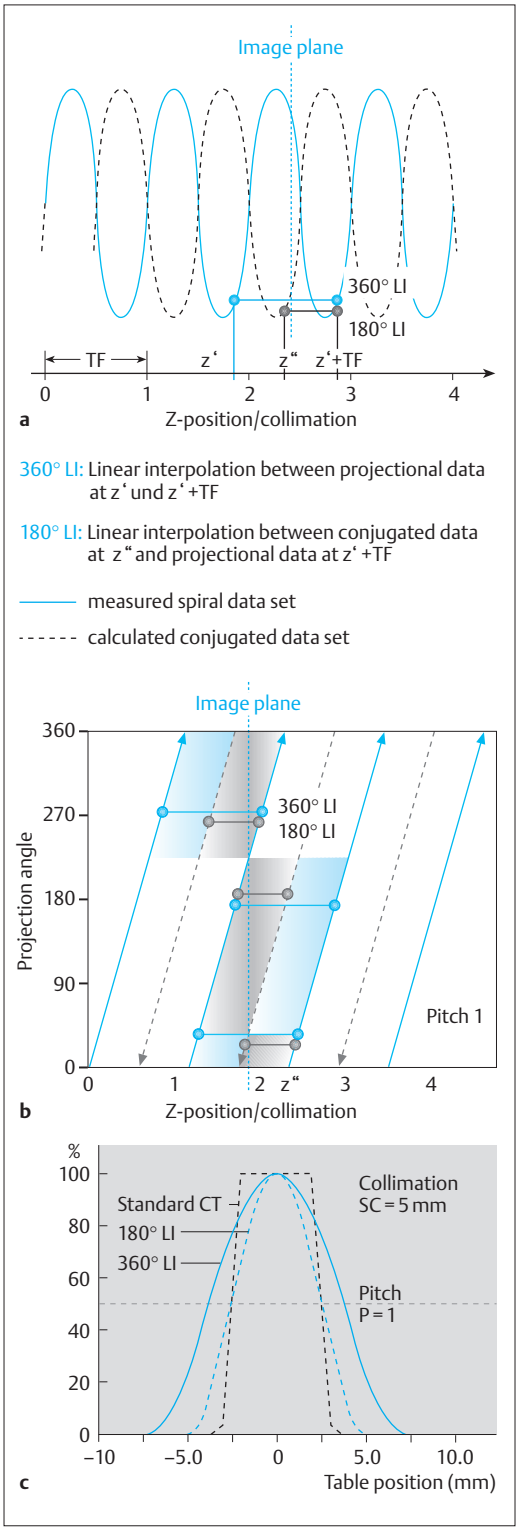

a ray between the tube and detector is equal in both directions. This makes it possible to compute a virtual second spiral (conjugated data) for the attenuation values along a ray from the detector to the tube, and to interpolate the projections at corresponding angles between the real and virtual spiral. This algorithm is called *180° LI* (Fig. 1.**13 a**) but actually uses data from 360° plus the fan angle of the x-ray beam. The resulting section profile is substantially narrower (Fig. 1.**13 b**) because the distances between corresponding projections in the real and virtual spirals are less than between corresponding projections in the real spiral alone. Differences between the 360° and 180° interpolations are best appreciated in multiplanar reformations and are most pronounced when pitch factors >1 are used (Fig. 1.**14**). The 180° LI algorithm, however, results in a larger *image noise* since only half the data are used for interpolation as compared to 360° LI. In fact, the noise with 180° LI is as high as it would be with a 360° LI and half the exposure dose.

Higher-order interpolation algorithms use not only two points from adjacent (real or virtual) spirals but instead, apply a more complex weighting function (*longitudinal filtration*, *z-filtering*) to the spiral projection raw data. This z-filter function defines how much each projection contributes to the final image depending on its distance to the reconstructed section. Such algorithms can be optimized to obtain more rectangular section profiles at the cost of more image noise (e.g., 180° HI), or they can reduce noise (and thus dose requirements) at the expense of a slightly broadened section profile (e.g., HRLF-10, *SmartHelical,* GE).

Effective Section Thickness (Section Width)

While the width of the section profile in conventional CT is equal to the section collimation (*nominal section thickness*), the bell-shaped section profile in spiral scanning must be described in terms of the *effective section thickness* or *section width* (SW). The effective section thickness depends on the section collimation and a num-

◀ Fig. 1.**13** Principle of raw data interpolation. (**a**) Conventional diagram, (**b**) angluar diagram, (**c**) comparison of section profiles for 360° and 180° linear interpolation (LI).

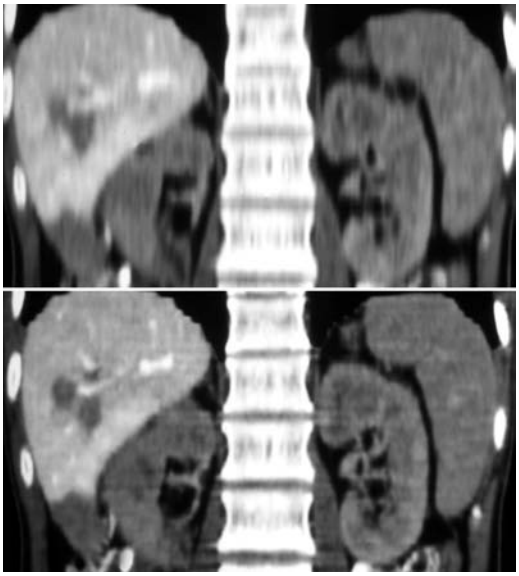

Fig. 1.**14** Quality comparison of coronal reformatted images using 360° LI (**a**) and 180° LI (**b**). The examination was performed with 3 mm collimation, 6 mm table feed, and a 2 mm reconstruction increment.

ber of other factors that include the table feed and interpolation algorithm. The most frequently used measure for the effective section thickness is the full width at half maximum (FWHM), i.e., the width of the profile at one-half of its peak value.

For a pitch of 1 the section width, given as FWHM, is identical to the section collimation if a 180° LI interpolation is used (see Fig. 1.**13 b**). With a 360° LI interpolation, the section width is 28% larger. The same 28% larger section width is obtained if a 180° LI interpolation with a pitch of 2 is used (see Fig. 1.**15 b**).

Image Noise

Image interpolation always includes a projection whose position corresponds precisely to the center of the section (Fig. 1.**13 a**). This projection is not interpolated in the algorithms described, whereas its 180° counterpart undergoes maximum interpolation. This leads to a position-dependent discrepancy of spatial resolution and noise in the scan plane, as image areas near the tube show slightly better sharpness due to the lack of interpolation while opposite image areas show a reduction in noise (see Fig. 7.**48**). Newer interpolation algorithms (e.g., 180° adaptive interpolation) can correct for these discrepancies.

As mentioned above, a comparison of 360° LI and 180° LI interpolation shows that 360° LI yields a 28% larger section width (less spatial resolution along the z-axis) and a 29% reduced image noise. Variants such as SmartHelical (GE) lead to a 10% wider section profile than 180° LI but only suffer from 8–16% less noise (depending on the pitch).

Scanning Parameters

The variable scan parameters in spiral CT examinations are reviewed in Table 1.**4**. Three *basic parameters* for spiral CT scanning are user-selectable. In most scanners these are section collimation (SC), table feed per rotation (TF), and reconstruction interval (RI). In some scanners the table feed TF is substituted by the pitch factor P. All the other parameters are varied only in exceptional cases. For this reason, the basic scanning parameters provide an excellent idea of how a spiral CT scan was performed. In this book, we use a triplet of numbers (*SC/TF/RI*) to describe these basic parameters.

Section collimation, *table feed* and *pitch* are the most important acquisition parameters, while the *reconstruction increment* is the most important parameter for image reconstruction.

Acquisition Parameters

Section Collimation

The section collimation (SC) determines the spatial resolution that is achieved along the z-axis (the direction of table travel). SC can be varied in fixed increments, depending on the scanner. Usually the manufacturer predefines these increments, but with some scanner units they can be modified at installation. The following settings can be recommended as a good compromise between clinical requirements and number of collimation settings:

SC = 0.5 mm, 1 mm, 2 mm, 3 mm, 5 mm, 7 mm, or 10 mm.

Table Feed and Pitch

The table feed per tube rotation (TF), also called the table increment, can be selected independently of the section collimation in spiral scan-

Table 1.4 Scan parameters in spiral and multislice CT

Acquisition parameters	
SC = Slice collimation (mm)	= nominal section thickness
TF = Table feed/tube rotation (mm)	= N × P × SC = P* × SC
P = Pitch	= TF/[N × SC] = beam pitch
P* = Volume pitch	= TF/SC = N × P = slice pitch
L = Scan length (cm)	= TI × TS = TI × N × P × SC/RT
Reconstruction parameters	
SW = Section width (mm)	= effective section thickness
RI = Reconstruction increment (mm)	= reconstruction interval
Derivative parameters	
TS = Table speed (mm/s)	= TF/RT
TI = Scan time (s)	= scan duration = L/TS = (L × RT)/(N × P × SC)
Equipment parameters	
RT = Rotation time (s)	= duration of one tube rotation
N = Number of detector rows	Single slice: N = 1; dual slice: N = 2; multislice: N = 4 – 16

ning. *Pitch* (P) is defined as the ratio of the table feed per tube rotation to the collimation (Fig. 1.**15**). The following rules should be noted.

Scanning at a pitch less than 1 produces an overlapping scan pattern that increases the radiation dose to the patient. Overlapping scans may offer slight advantages for the 3D reconstruction of contours that are roughly parallel to the scan plane (e.g., the calvaria), but there are very few indications in which the minimal improvement of image quality justifies the increased exposure. Moreover, there is little if any effect on image noise, and the higher radiation dose essentially goes unutilized. The only exceptions are scanners with dual detectors (see below, p. 20), which have special z-filtering algorithms that can utilize the higher applied dose to improve image quality (useful in examinations of the intervertebral disks, for example).

If the pitch is greater than 2, the volume of interest will be under-sampled, leading inevitably to artifacts. This may be acceptable in some instances, such as trauma cases where priority is placed on the rapid assessment of large volumes rather than on high image quality. But as a general rule, it is better to avoid scanning at pitch values greater than 2. One exception is scanning with very thin collimation, where even conventional CT sections have a bell-shaped profile. Due to broadening of the section profile, a pitch as high as 3 can be used without causing serious artifacts if the collimation is 1 mm or less (Fig. 1.**16**).

Effective Section Thickness and Pitch

The most widely used interpolation algorithms at present (180° LI) do not increase the section width (effective section thickness) over the section collimation when a pitch of 1 is used (Fig. 1.**15 b**). Increasing the pitch to 2 reduces the radiation dose by half and doubles the scan length but does not increase the effective section thickness to a proportionate degree. The section profile obtained with 180° LI and a pitch of 2 equals the profile obtained with 360° LI and a pitch of 1, i.e., the scan length is increased and radiation exposure reduced, each by a factor of 2, with identical resolution along the z-axis (Fig. 1.**15 b**).

Increasing the pitch may produce an increase or decrease in the section width. If the section collimation is kept constant while the table feed is increased, the section width increases (Figs. 1.**15 a, b**). Conversely, the section width is reduced if the section collimation is decreased while the table feed remains unchanged (Figs. 1.**15 c, d**).

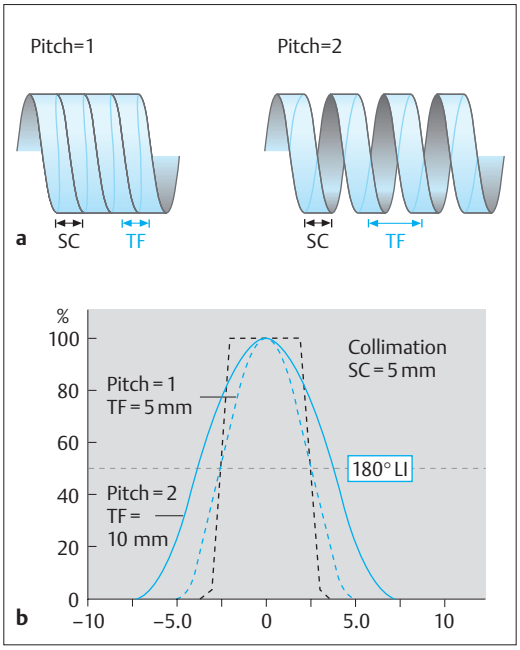

Fig. 1.**15** Increasing the pitch while keeping the section collimation SC constant has the effect of stretching out the spiral (**a**). This widens the section profile (**b**). The resulting profile with 180° LI at pitch 2 is identical to the section profile with 360° LI at pitch 1 (compare Fig. 1.**13 c**). Thus, using a pitch of 2 instead of 1 will yield an only 30% wider section width but cover twice the scan length. Increasing the pitch by reducing the section collimation SC covers the same scan length (**c**). With 180° LI, this leads to a 35% narrower section width than with a pitch of 1 (**d**).

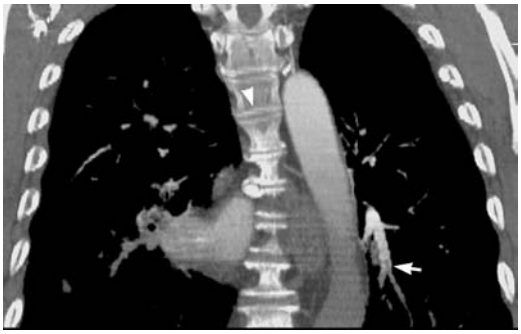

Fig. 1.**16** For narrow collimation, the pitch can be increased to 3 without markedly compromising image quality. Note the excellent quality of multiplanar reformations with a SC/TF/RI = 1/3/1 protocol for visualization of subsegmental pulmonary emboli (arrow). Note that the vertebral end plates are well delineated but suffer from minor horizontal interpolation artifacts (arrow head).

In clinical practice, the length L of the scan range and the available scan duration TI (usually a maximum of 30 seconds for breath-hold scanning) determine the selection of the table feed (see formula in Table 1.**4**). In this situation it is generally best to use a pitch greater than 1 to maximize the spatial resolution along the z-axis for a given scan length (Table 1.**5**). This not only reduces the radiation dose but also keeps the effective section thickness as small as possible. A pitch of 2 would be most favorable on theoretical grounds but is more vulnerable to motion and spiral artifacts.

A pitch between 1.5 and 2 is the most reasonable tradeoff for most clinical investigations.

Rotation Time

The rotation time (RT) of the x-ray tube (duration of one revolution) is 1 second in most scanners but can vary from 0.4 to 2 seconds, depend-

Table 1.5 Effect of pitch on z-axis resolution (effective slice thickness) for a constant table feed

Scan parameters			Section width (FWHM)	
SC	TF	Pitch	180° LI	360° LI
3 mm	6 mm	2.0	3.9 mm	6.9 mm
4 mm	6 mm	1.5	4.6 mm	7.2 mm
5 mm	6 mm	1.2	5.3 mm	7.5 mm
6 mm	6 mm	1.0	6.0 mm	7.8 mm

SC = slice collimation, TF = table feed, FWHM = full width of section profile at half maximum

ing on the scanner type. The table speed (TS), or scan length per unit time, can be calculated by dividing the table feed TF by the rotation time (see formula in Table 1.4). The TS is one-third higher in 0.75 second scanners and one-third lower in 1.5 second scanners than in standard 1 second scanners. With a shorter rotation time, the z-axis coverage within a given scan time can be increased.

All scanning protocols (basic parameters) for spiral CT presented in this book are based on scanners with a rotation period of 1 second.

To achieve the same coverage with a slower scanner, the scan time must be increased by the factor RT compared with a 1 second scanner. This is feasible only in regions that do not show respiratory motion (usually skeletal examinations). In all other cases, slower scanners require wider section collimation. Conversely, faster scanners can apply narrower collimation.

Because of the detector properties in some scanners, the number of projections available for image reconstruction must be reduced at the shortest rotation time available with these scanners. This leads to a degradation of image quality (loss of sharpness) in the scan plane. If the rotation time is user-selectable (not available in all scanners), it is advantageous to select a longer rotation time for studies that require higher in-plane spatial resolution (e.g., high resolution lung or skeletal examinations).

Scan Time

The maximum scan time (scan duration) available in a spiral scanner depends on the x-ray tube. The higher the dose requirement, the shorter the available scan time will be. Old scanners were limited to a scan time of 24 seconds, but current units can achieve scan times up to 100 seconds.

In practice, scan times longer than 30 seconds are feasible only for body regions that can be examined without breath holding—the neck, the musculoskeletal system, and in some cases the pelvis. Thoracic and abdominal examinations generally require breath holding to ensure optimum image quality. In some regions (e.g., the lower abdomen), scanning can proceed while the patient slowly exhales after holding his or her breath and continues breathing shallowly. This will cause no substantial loss of quality and will enable scan times longer than 30 seconds.

Reconstruction Parameters

Raw Data Interpolation

Most modern scanners use the 180° LI raw data interpolation algorithm, but there are variants available among different units (e.g., SmartHelical on GE scanners, slim2 on Siemens scanners). Fourth-generation scanners (Marconi/Philips) use an interpolation (z-filtering) in which the effective section thickness is largely independent of the pitch (for a constant collimation), but image noise increases with the pitch. This differs from standard interpolations (360° LI, 180° LI), in which image noise is independent of pitch for a given collimation.

Reconstruction Algorithm (Convolution Kernel)

The convolution kernels in spiral CT are no different from those in conventional CT (see above).

Reconstruction Increment

One of the main advantages of spiral scanning is the continuous acquisition of data, which makes it possible to generate axial CT sections retrospectively at arbitrary z-positions within the scanned volume. The reconstruction increment (RI) defines the spacing of the reconstructed images.

The reconstruction increment has nothing to do with section collimation or section width. Rather, it defines the degree of *overlap* between the axial sections.

For the detection of small structures (e.g., pulmonary nodules) it is important to choose RI so that at least a 30% section overlap is generated. For optimum multiplanar reformations or 3D reconstructions, the reconstruction increment should not exceed half the section width (effective section thickness). This provides a 50% degree of section overlap and generates more than twice as many CT images as conventional scanning. Non-overlapping reconstruction wastes an important advantage of spiral CT, and small lesions located at the boundary between two sections may be missed due to partial volume effects. Overlapping reconstruction ensures optimum lesion display.

The theoretic optimum for RI is even smaller than half the section width (see Chapter 4, p. 124), but the added value in clinical practice is generally low.

Image Review, Display and Documentation

Axial CT Images

Spiral CT images differ very little in appearance from conventional CT sections obtained with a similar radiation exposure, an identical convolution kernel, and an identical number of projections. This is because the raw data interpolation eliminates image artifacts, and the spatial resolution in the axial scan plane corresponds to the spatial resolution of conventional CT images. Compared with conventional CT, however, the image noise for the same scan dose may be 18% lower (360° LI) or 15% higher (180° LI), depending on the type of interpolation algorithm used.

Spiral CT with a small reconstruction increment generates a large number of images. For example, spiral CT of the abdomen with 1 s rotation time, a table feed of 8 mm, a scan time of 30 seconds, and image reconstruction at 2 mm intervals (as in CT angiography) will generate (30 s × 8 mm/s / 2 mm =) 120 images. This large number of images cannot be conveniently documented and reviewed with traditional methods.

Cine Mode and Image Documentation

As a rule, not all images can be documented on *film*. One solution is to document every second to fourth image on film, depending on the type of examination. Abnormalities must be adequately documented, however, and a suspicious or abnormal finding must be reproducible. For this reason, selected overlapping sections or multiplanar reformations (MPRs) should also be documented if required.

Image quality (noise) can be improved by retrospectively increasing the section width (approximately 7–10 mm) for documentation instead of using the original sections. In some scanners, this can be done directly from the raw data by fusing projections from multiple tube rotations (similarly to multislice CT). These thicker sections reduce noise, which is particularly beneficial in scans taken with a low dose or a thin collimation. If this option is not available, thicker sections can be produced by averaging the data from several overlapping images (e.g., using *thick axial reformations*). This is usually too time-consuming for routine examinations but may be appropriate in selected cases where image noise is excessive. It is, however, the preferred technique for image documentation in almost all multislice CT applications.

If not all the reconstructed images are printed, all available images should be viewed in an interactive *cine display* so that an accurate evaluation can be made. This mode displays the individual images in the scanned volume on the monitor in a movie-like sequence, providing a three-dimensional impression of complex, nonlinear structures that have multiple intersections with the image plane. The radiologist can control the speed and direction of the image display sequence interactively by manipulating a computer mouse or trackball.

Image Processing

A data set composed of overlapping axial spiral CT images is well suited for generating multiplanar reformatted images (MPRs) in arbitrary sectional planes through the scanned volume (see pp. 48). In cases with equivocal findings, MPRs can assist the diagnosis by providing information in an extra viewing plane. When thin sections have been used, reformatted images of good quality can be produced.

Three-dimensional images (see pp. 60) of the skeleton or vascular system improve anatomic orientation and can enhance the presentation of findings to referring colleagues.

Multislice CT

Multislice CT, or multidetector-row CT, multidetector CT, or volume CT, as it is also called, represents the next breakthrough in CT technology. Multislice CT scanners provide a huge gain in performance that can be used to reduce scan time, reduce section collimation, or to increase scan length substantially. Multislice CT transforms CT from a transaxial into a truly three-dimensional imaging technique.

Multislice CT has gained a rapid acceptance by the radiological community. There is an almost exponential growth of the number of scanners: in 1998 there were 10 scanners installed, in 1999 it was 100 by the middle of the year, and by the end of 2000, over 1000 scanners were installed worldwide.

Scanning Principle

Unlike standard systems that use a single detector arc or detector ring, multislice CT systems are equipped with two or more parallel detector arrays and always utilize a third-generation technology with synchronously rotating tube and detector array as well as solid state detectors (Fig. 1.**17**). Although the very first CT scanners in the 1970s also employed a split detector, the first dual or split detector systems with continuously rotating tubes became available only in the early 1990s. Systems with four active detector arrays were introduced in 1998, and systems with 6, 8, 10 or 16 active detector arrays are now available.

The performance of many of these systems is further improved by a faster rotation time. As a result, a four-detector-row scanner with 0.5 s rotation has an about 8 times higher performance than a conventional 1 s single-detector-row scanner.

Multislice CT does not always involve *spiral data acquisition*, although spiral acquisition is implied in this book unless stated otherwise. A *sequential mode* (step-by-step scanning) as in conventional CT with possibilities of image fusion is also available, although it will be used only in a minority of applications, such as HRCT of the lungs or interventional procedures.

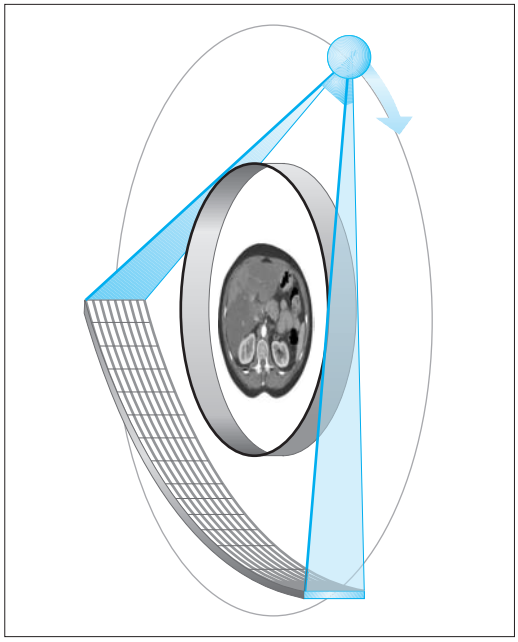

Fig. 1.**17** Principle of multislice CT scanning. More than two detector rows are exposed simultaneously.

Advantages

The performance of multislice CT is at least 4 times, with modern scanners 8–20 times higher than that of a conventional spiral CT scanner. This enormous increase in performance can be used for shorter scan duration, longer scan ranges, and thinner sections (Table 1.**6**). In general, the performance gain will be used to improve all of the above to a substantial amount. In consequence, multislice CT has overcome one of the most severe limitations of spiral CT, namely the inverse relation between scanning range and section collimation.

Shorter scan duration will reduce the danger of motion artifacts, especially in children or critically ill patients. Marked improvements can be seen for trauma patients or in dyspneic individuals with suspected pulmonary embolism. Shorter scan duration also will allow for scanning of the liver or other parenchymal organs in a more well-defined phase of contrast enhancement, which again improves lesion detection and characterization. Shorter scans will

Table 1.6 Advantages of higher scanner performance with multislice CT or subsecond spiral CT

Shorter scan duration
Reduced motion artifacts: • Children • Trauma patients • Acutely ill patients
Improved scanning of parenchymal organs • Well-defined phase of contrast enhancement
Reduced volume of contrast medium
Perfusion imaging
Longer scan ranges
Trauma • Thoraco-abdominal spine/blunt trauma
CT angiography: • Aorta and peripheral run-off • Thoraco-abdominal aorta • Carotids from arch to intracerebral circulation
Thinner sections
Near-isotropic imaging: • Temporal bone imaging • Musculoskeletal imaging • Arbitrary imaging planes • Multiplanar reformats • 3D rendering

also allow for substantial reduction of the volume of contrast material to be administered as long as only an arterial phase of contrast enhancement is required.

Longer scan ranges are especially important for CT angiography. CTA-examinations become feasible that include the abdominal aorta and the peripheral run-off vessels down to the feet. Alternatively, the whole aorta can be scanned with high spatial resolution, or the carotids can be examined form the aortic arch to the intracranial circulation. Long scan ranges such as in thoraco-abdominal studies no longer pose a problem, even for indications that require a high spatial resolution.

Finally, *thinner sections* and even isotropic imaging will become feasible yielding almost identical spatial resolution in all directions. This makes near-isotropic multiplanar imaging possible with a spatial resolution in any arbitrary plane that equals, or often exceeds, the resolution of MRI.

Disadvantages

The downside is a markedly increased *data load*, especially if near-isotropic imaging is performed. A scan of the chest and abdomen (60 cm) can be performed with a 4×1 mm collimation in 50 s and produces up to 500–800 images, depending on the degree of overlap. A chest scan with an identical collimation will produce as many images if reconstructed in a smoothing convolution kernel for the mediastinum and an edge-enhancing kernel for the lungs. A CTA of the aorta and peripheral arteries may produce 1000 images and more.

The only way to avoid this enormous amount of data is to (acquire and) reconstruct thicker sections. This, however, will forgo many of the advantages of multislice CT. Current *scanning protocols* frequently are modified versions of standard spiral CT protocols with a somewhat thinner section collimation. Most present scanners and workstations can easily handle the data created by such protocols. However, if near-isotropic imaging is performed, image reconstruction speed and data handling become limiting factors for some of the present scanners and workstations and make this technique cumbersome for clinical routine use. There is not yet an in-depth experience with near-isotropic imaging, nor do standardized protocols exist. This book suggests protocols optimized for clinical routine work as well as specialized protocols for more advanced applications and multiplanar imaging.

Image processing adds to the increased time requirements for data analysis if a full-resolution scan is performed. No standardized protocols are available yet but manufacturers are working on techniques to include 3D processing in the standard workflow.

Image noise grows as section collimation is reduced. For this reason, it is important to reconstruct thicker sections (MPR or axial sections) to keep image noise low. With very thin collimation the geometric efficiency of the detector deteriorates (see Fig. 5.**5**). It varies between manufacturers and depends on scanner geometry, the implementation of beam collimation and image interpolation algorithms. With 16-slice scanners, the geometric efficiency approaches that of single slice CT.

An increase in *patient dose* is only necessary if thin-section images of high quality are re-

quired. In all other cases, multislice CT requires less dose than conventional CT or a similar dose as spiral CT with a pitch of 2.

Detector Types

Dual Detector Systems

Dual or *split detector systems* are based on a detector array that is twice as wide as a conventional CT detector and is split in half (Fig. 1.**18**). Elscint was the first company to use this concept on a spiral CT system (Elscint Twin). Now, most vendors offer such dual-slice systems.

Multidetector-row Systems

True multidetector-row or *multislice systems* are able to acquire at least four simultaneous sections. To be able to choose between various section collimations, the detector arrays have to be subdivided into multiple detector rows. Data from each of the scanned sections is recorded by a *data acquisition system* (DAS), which consists of one detector row or a combination of detector rows, depending on the chosen section collimation (Figs. 1.**19**–1.**21**). The basic types of detectors available are described below. The width of each detector row is not given as its real width but instead as the width of the corresponding x-ray beam at the center of the scan field.

Matrix Detector

Matrix detectors consist of multiple detector rows of identical width (Fig. 1.**19 a**). The GE matrix detector is a typical example. It uses 16 parallel detector arrays with a width of 1.25 mm each.

One has to note that the detector width mentioned in this text (as well as most publications) is not the "real" width of the detector elements but the width of the detector-row beam collimation, measured in the center of the scan field. The real width of the elements of the x-ray detector is about twice as large, depending on the scanner geometry and the distance from the center of the scan field to the actual detectors.

By exposing only the innermost four detector rows, a 4×1.25 mm collimation can be produced. For wider collimator settings the signals of groups of two or more adjacent detector rows have to be added to obtain 4×2.5 mm, 4×3.75 mm and 4×5 mm collimations (Fig. 1.**19 b**). By partially covering the innermost two detector rows, also 2×0.625 mm sections can be generated.

The same principle of grouping adjacent arrays holds true with 8-detector-row scanners, which will allow for 8×1.25 mm and 8×2.5 mm section collimation (Fig. 1.**19 c**). The total collimation (e.g., 8×1.25 mm = 10 mm, or 8×2.5 mm = 20 mm) is limited by the total width of the detector array.

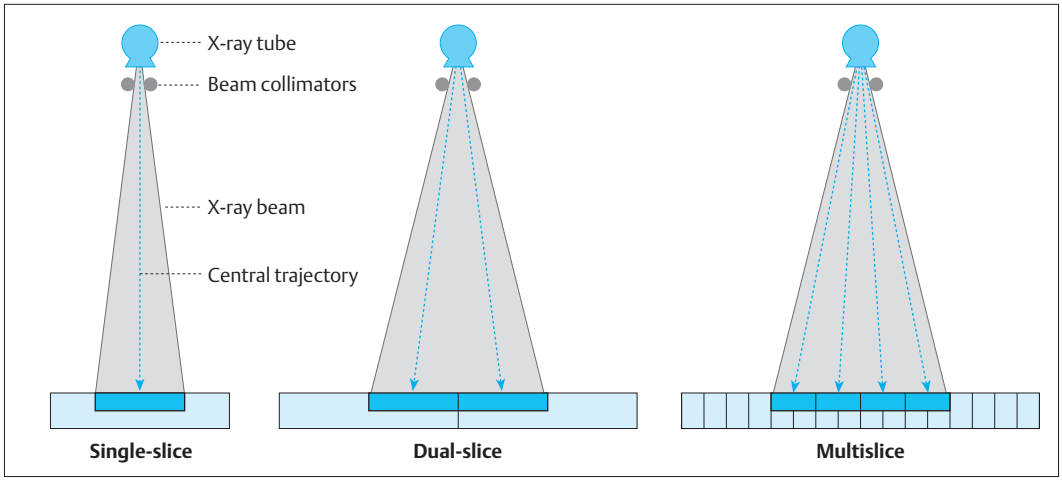

Fig. 1.**18** Comparison of single and dual (split) detector systems.

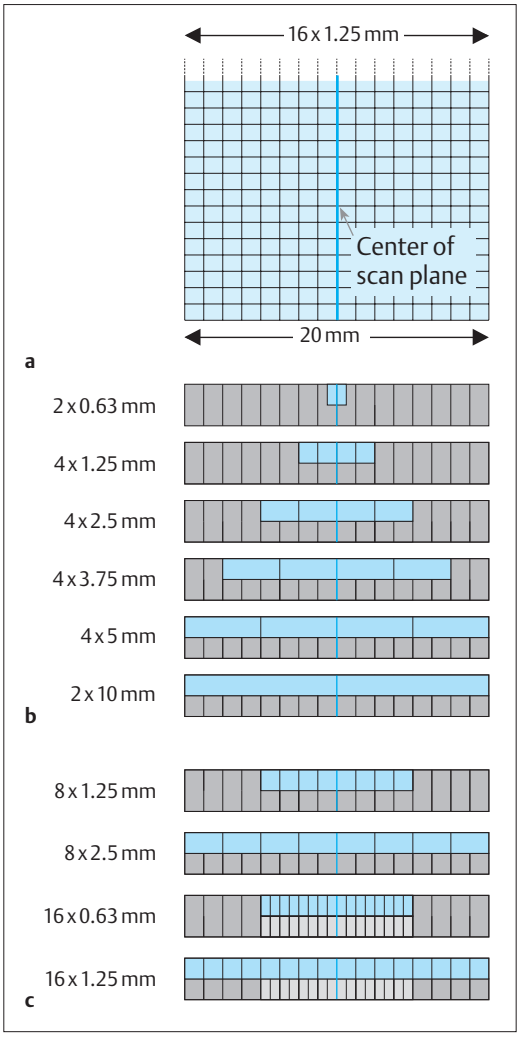

Fig. 1.**19** Matrix detectors consist of detector rows of identical widths. For the GE HiLight detector this width is chosen so that each detector row covers a 1.25 mm-thick section in the center of the scan field (**a**). Collimating the x-ray beam, or combining the signal from adjacent detector rows, or both, will yield various section collimations (**b**). An 8-slice scanner provides 8 × 1.25 mm and 8 × 2.5 mm collimation. The 16-slice scanner uses a hybrid detector with 16 × 0.63 mm and 16 × 1.25 mm collimation (**c**).

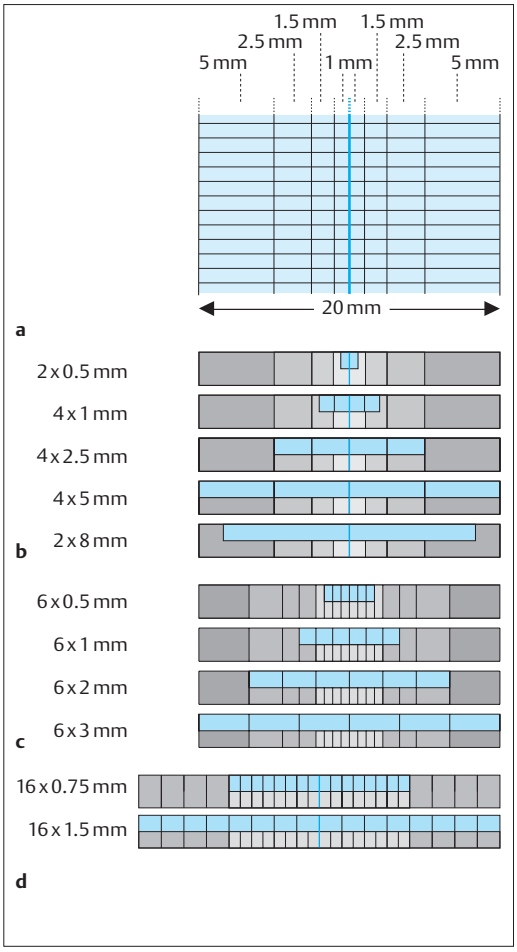

Fig. 1.**20** Adaptive array detectors have outer detector rows that are wider than the innermost detector rows (**a**). The detector used by Philips and Siemens covers a total section width of 20 mm and allows for section collimations ranging from 2 × 0.5 mm to 4 × 5 mm (**b**). A new detector configuration is chosen for the Siemens 6-row scanner (**c**). The 16-slice scanners of both manufacturers provide 16 × 0.75 mm and 16 × 1.5 mm collimation (**d**). The Philips 6-slice and the 10-slice scanners of both manufacturers open only part of this detector.

Adaptive Array Detector

Adaptive array detectors consist of detector rows that grow in width from the center of the section to the periphery (Fig. 1.**20 a**). Philips (Asymmetrix detector) and Siemens (AAD) have adopted this concept and use the same detector in their scanners.

By collimating half of the two innermost 1 mm-wide detector arrays of 4-detector-row scanners, a section collimation of 2 × 0.5 mm can be obtained. By partially collimating the next arrays, 4 × 1 mm sections can be gained. Adding the innermost two detector rows will yield 4 × 2.5 mm collimation (Fig. 1.**20 b**).

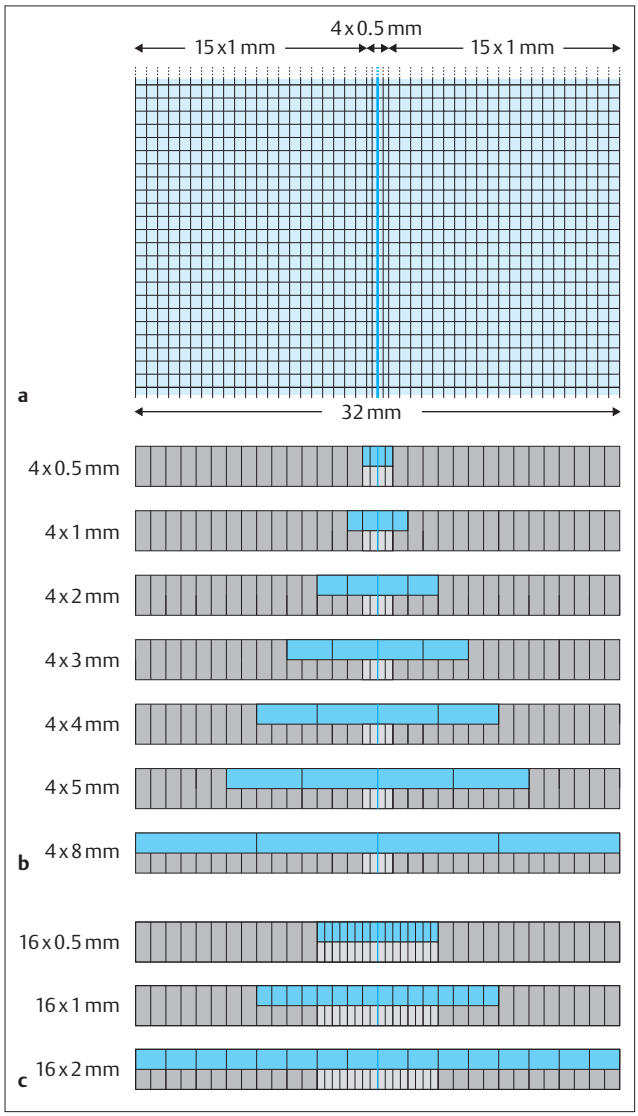

Fig. 1.**21** Hybrid detectors are matrix detectors with thinner innermost detector rows (**a**). Toshiba uses a detector that covers 32 mm and allows for 4 × 0.5 mm to 4 × 8 mm collimation (**b**). The detector configuration for the 16-slice scanner provides 16 × 0.5 mm to 16 × 2 mm collimation (**c**).

The rationale behind this approach is based on the fact that the x-ray beam hits the more peripheral detectors at an oblique angle. Any perpendicular septa in the more peripheral portions of the detector will block some of these oblique rays and will thus decrease the detection efficiency. Reducing the number of septa in the peripheral regions of the detector array should thus increase geometric dose efficiency. Indeed, the detector has a dose efficiency that is only slightly less than that of a single-slice scanner, if a section collimation ≥ 2.5 mm is used (for more details see Chapter 5 and Fig. 5.**5**).

The detector geometry is optimized only for a particular number of active detector rows. A new detector configuration is needed as the number of detector rows progresses from 4 to 6 (Fig. 1.**20 c**). With more rows, also more septa have to be added.

Hybrid Detectors

Hybrid detectors are similar to matrix detectors with the exception that the innermost detector rows are thinner than the outer ones (Fig. 1.**21 a**). This concept is embraced by Toshiba (selectable slice-thickness multirow detector, SSMD).

These hybrid detectors are based on a detector array of a total width of 32 mm that consists of 1 mm-wide detector rows. With 4-slice scanners the innermost 2 mm of this array are further subdivided into four 0.5 mm wide detector rows. With this detector configuration there is a multitude of possible collimations, ranging from 4×0.5 mm up to 4×8 mm (Fig. 1.**21 b**; Table 1.**7**). With 8- and 16-slice scanners the innermost 8 or 16 rows of the 32 mm-wide detector array have a width of 0.5 mm (Fig. 1.**21 c**).

The Toshiba detector uses dividers between the various detector rows that are opaque to the scintillation light produced by each detector element (thus avoiding cross-talk) but which are transparent to the incident radiation. This effect increases dose efficiency but also makes the detector slightly more vulnerable to scattered radiation.

The 16-slice scanners of all other vendors (Figs. 1.**19 c** and 1.**20 d**) also use thinner innermost detector rows and therefore should be considered hybrid detectors. The 10-slice systems are based on the same configuration as 16-slice scanners but open only parts of the detector.

Cone Beam Systems (Volumetric CT)

Future generations of CT scanners will be based on cone beam technology in which a wide x-ray beam is used to cover a large range along the z-axis. Prototypes by various vendors include a 256-row detector and a 1024^2 flat panel detector. Such scanners may provide enormous spatial resolution and high-speed data acquisition.

Cone beam systems that are already on the market are reserved for rotational angiography. They use image intensifiers or (CCD) flat panel detectors as the radiation receptor and require a number of seconds for acquiring one (single-rotation) data set. The present systems are only able to depict high-contrast structures such as vessels during intra-arterial contrast injection. The reason is the large amount of scattered radiation that is not blocked from hitting the detector—as opposed to multislice CT where the relatively narrow beam and the various septa between the detector rows achieve adequate scatter suppression. This scattered radiation destroys low-contrast resolution if no adequate scatter-reduction techniques are developed. So far, this major obstacle is only partially solved in the 256-row prototype but not in the flat panel detectors.

Another major problem with cone beam detectors is the bandwidth of the signal transmission system that has to transfer the various detector signals out of the gantry to the image reconstruction computer. The data throughput in these systems will become enormous and will grow by a factor of 64 relative to a 4-detector row scanner if 256-detector rows are employed. At present there is no system that can transmit and process the acquired data with sufficient speed.

The third and biggest problem is image noise, which will increase substantially. Image noise for isotropic resolution with voxels of a size of x^3 is theoretically proportional to $1/x^4$. This means that image noise will grow by a factor of $2^4 = 16$ if the size of an isotropic voxel is reduced from $(1\,\text{mm})^3$ to $(0.5\,\text{mm})^3$, and by $5^4 = 625$ if the voxel size is further decreased to $(0.2\,\text{mm})^3$. As a consequence, sophisticated noise suppression and data reconstruction techniques will be necessary to create clinically useful images.

For the reasons mentioned above, it will be several years until cone beam scanners become available for clinical use.

System Performance

The performance of multislice CT scanners increases with the number of active detector rows, the speed of x-ray tube rotation, and with the available pitch factor. This increased performance can be used to reduce scan time, reduce section collimation, or to increase scan length (Table 1.**6**). At the same time, increase in performance has to be counterbalanced by the amount of artifact induced and by increased image noise with thinner sections.

Rotation Speed

The rotation speed of the x-ray tube is commonly described by the time required for one tube revolution, the so-called rotation time RT. All multislice scanners have a rotation time of 0.8 seconds or less. Most high-end scanners even allow for a 0.5 s rotation. With the newest generation of scanners, rotation times of 0.375 s are available.

Pitch

There are two definitions of *pitch* factor available with multislice CT scanners, depending on whether a single *section collimation* SC or the *total collimation* of the detector array (N × SC) is chosen as the reference. To distinguish between them, an asterisk is used to indicate the definition used by most manufactures for 4-slice scanners (*volume pitch* P*, also called *slice pitch* or *detector pitch*), while P denotes the definition agreed upon internationally (IEC) and preferred by most physicists (*pitch* P), also called beam pitch:

$P = TF / (N \times SC)$	Pitch
$P^* = TF / SC$	Volume pitch

While P is independent of the number of detector rows, P* increases as the number of detector rows grows. As with single-slice spiral CT, the pitch P can be increased up to 2, independent of the number of detector rows N. In multislice scanners with four active detector rows this corresponds to $P^* = 8$. Some manufacturers have limited the maximum pitch P to 1.5 (corresponds to $P^* = 6$ for four-slice scanners).

Relative System Performance

System performance is proportional to the number of detector rows N and improves with a shorter rotation time RT of the x-ray tube. This concept can be applied to standard spiral CT as well as to dual detector scanners or multislice CT. Table 1.7 gives an overview of the relative performance of various scanner types and scanning protocols. It has to be noted that the quality of axial images may deteriorate when the highest possible pitch factors are chosen.

Image Reconstruction

Image reconstruction in 2- and 4-slice CT systems does not have to use sophisticated interpolation if a section-by-section mode is used, but even then, the cone beam geometry of the system will lead to artifacts for regions outside the center of the gantry. With spiral acquisition, the situation is becoming more complex because the trajectories of the various detector rows may overlap and yield "redundant" data, depending on the pitch factor employed. For this reason, more sophisticated raw data interpolation schemes have to be used.

Table 1.7 Examples of system performance relative to a 1 sec single-slice spiral CT scanner with pitch = 2

System	Rotation time (s)	Detector rows (N)	Pitch P	Pitch P*	Rel. performance
1 s-scanner	1 s	1	1	1	0.5
1 s-scanner	1 s	1	2	2	1
0.8 s-subsecond scanner	0.8 s	1	2	2	1.25
0.5 s-subsecond scanner	0.5 s	1	2	2	2
1 s-dual-slice scanner	1 s	2	2	4	2
0.5 s-dual-slice scanner	0.5 s	2	2	4	4
0.8 s-4-slice scanner	0.8 s	4	0.75	3	1.875
0.8 s-4-slice scanner	0.8 s	4	1.5	6	3.75
0.5 s-4-slice scanner	0.5 s	4	1.5	6	6
0.5 s-4-slice scanner	0.5 s	4	2	8	8
0.6 s-6-slice scanner	0.6 s	6	1.8	10.8	9
0.5 s-8-slice scanner	0.5 s	8	1.35	10.8	10.8
0.4 s-16-slice scanner	0.4 s	16	1.5	24	30

The Cone Beam Problem

Due to the nature of the x-ray beam, which arises from a small focal spot, all CT scanning relies on cone beam geometry. With single-slice CT these effects are hardly visible but they play a major role in multislice scanning because the same structure may be depicted on different detector rows during one revolution of the x-ray tube (Fig. 1.**22 a**). Only in the center of rotation are structures always captured by identical detector rows. The effect becomes more prominent the further a structure is from the isocenter (rotational axis), and the more detector rows are used (Fig. 1.**22 c**).

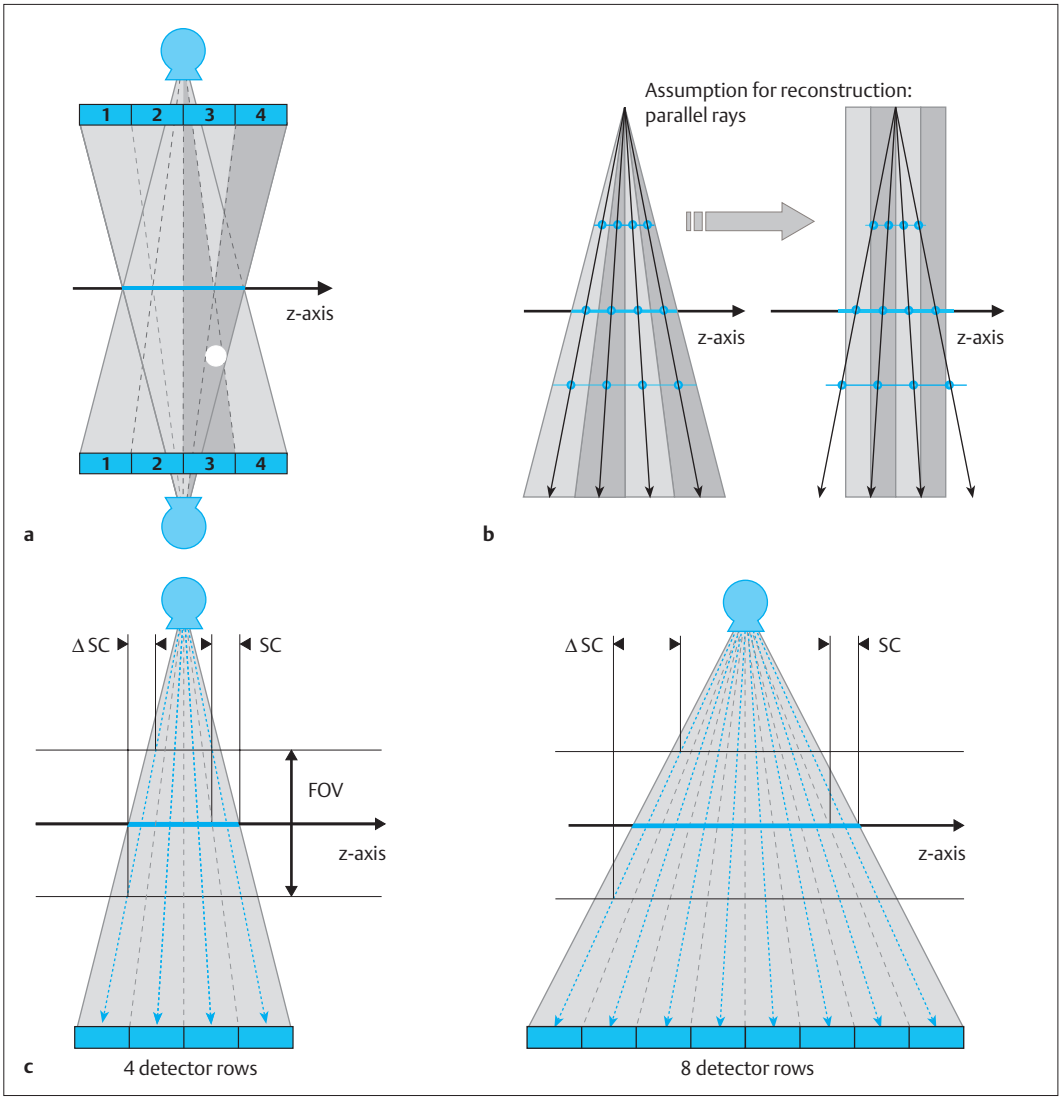

Fig. 1.**22** Cone beam geometry. Peripheral structures will be seen by different detector rows during one revolution of the x-ray tube (**a**). Simple raw data interpolation algorithms make the assumption that all beams are parallel like in convention spiral CT scanning (**b**). Such algorithms will fail with more than four detector rows because the cone beam effect will become more prominent when more detector rows are used (**c**). The distance ΔSC traveled by the outermost rays within the field-of-view (FOV) becomes larger than the section collimation SC and will cause artifacts in standard reconstructions.

Simple raw data interpolation algorithms make the assumption that all beams are parallel (Fig. 1.**22 b**), which yields reasonable results up to four active detector rows but fails with a higher number of rows. While adaptation for thin section and 8-slice scanners may still be possible, 16-slice scanners require more sophisticated cone beam algorithms for image reconstruction.

Multislice Linear Interpolation

Algorithms for 4-slice systems that are analogous to 180° LI and 360° LI from spiral CT are called 180° MLI (multislice linear interpolation) and 360° MLI (Fig. 1.**23**). For each projection angle, they use the projection data from the two detectors that are closest to the scanning pane (360° MLI only real trajectories, 180° MLI also virtual trajectories from the detector to the x-ray tube). Section profiles with these algorithms vary between those from conventional 180° LI and 360° LI spiral CT interpolation, but the dependence on the pitch factor is more complex because of the sampling patterns described below.

It is difficult to represent these effects using the standard diagrams for single-slice spiral CT. A diagram that displays the rotational angle of the x-ray tube for varying z-positions of each DAS channel (active detector row) is more suitable for this purpose (Fig. 1.**23 b**, compare also Fig. 1.**13 a**).

The Sampling Problem

Depending on the pitch factor, the spiral trajectory of the first detector row of a 4-slice scanner may overlap with that of the second, third or fourth row for P* = 1, 2, and 3, respectively

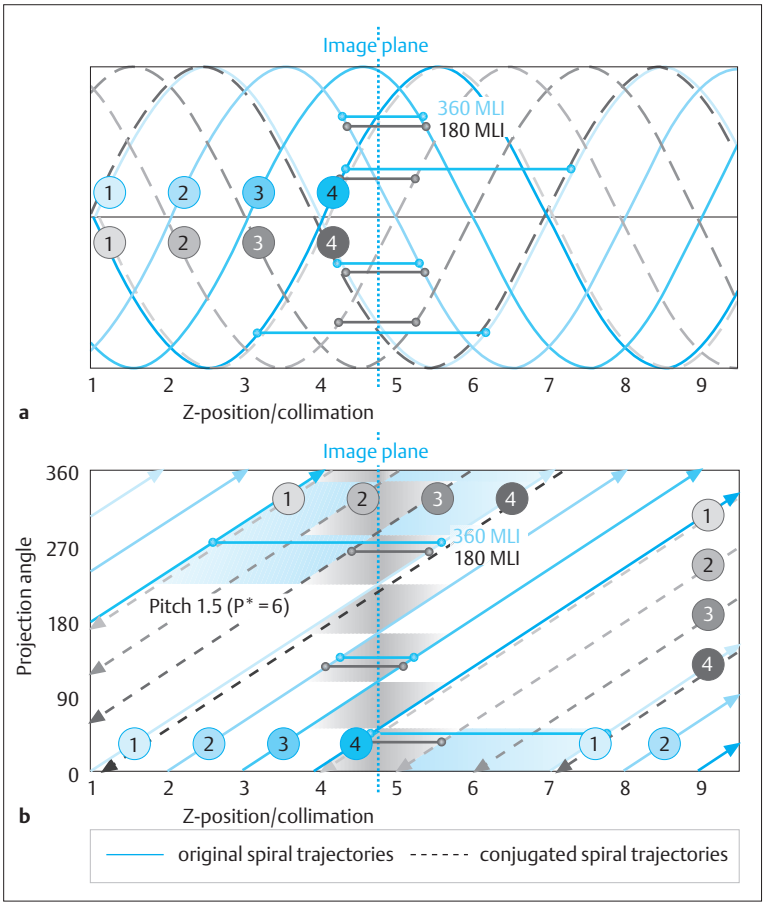

Fig. 1.**23** Multislice linear interpolation for a 4-slice scanner and a pitch P = 1.5 (volume pitch P* = 6). The conventional representation (**a**) and the angular diagram (**b**) are equivalent but the angular diagram provides a better overview. Note that there is a gap between the trajectories of the original spiral of detector rows 1 and 4 because of a pitch >1. At the same time, the trajectories of the original spiral (detector row 4) and the conjugated data (from detector row 1 to x-ray source) overlap. This causes substantial variations in distance between some of the interpolation partners with the 360 MLI algorithm, while there is a constantly narrow distance for the interpola tion partners with the 180 MLI algorithm.

(Fig. 1.**24**). For a pitch of 0.5 ($P^* = 2$), even the conjugate data from the virtual spiral overlap the real spiral at the isocenter (Fig. 1.**24 b**). This makes data sampling particularly inefficient and only allows for an interpolation between data samples that are one section collimation apart. As a consequence, the section width is widened similar to a 360° LI interpolation. Because of varying degrees of overlap with changing pitch factors, the sampling density and thus the section width varies (Fig. 1.**25**).

In principle this sampling problem applies also to 8- and 16-slice scanners but, because of the cone beam effect, the projection rays for the overlapping detector rows are not completely redundant outside the isocenter. Still, there are constellations in which the sampling is particularly advantageous or disadvantageous. While Philips and Siemens have made their interpolation algorithms independent of pitch, Toshiba and GE provide preferred pitch factors to ensure particularly advantageous data sampling for their 4-, 8- and 16-slice systems. Siemens has chosen another approach, in which a z-filtering for 4-slice systems and cone-beam reconstruction for 16-slice systems is chosen in a way that makes section width, image noise and radiation dose independent of the sampling pattern with varying pitch (see Figs. 1.**25 c** and 1.**28 c**).

Z-Filter Interpolation

Z-filter interpolation is reserved for 4- and 8-slice scanners uses a similar concept as higher-order interpolation algorithms for conventional spiral CT. Not only the two projections from the detectors that are closest to the scan plane are used but also adjacent projections (*multipoint interpolation*). These projections are weighted according to their distance from the scan plane (Fig. 1.**26**). This filter function may even contain negative portions that result in "edge enhancement" along the z-axis and thus can ensure that the section width is equal to the collimation even at unfavorable pitch factors. This, however, will come at an increased image noise. By using a wide filter function, noise is reduced and the section width becomes larger.

Z-filtering controls the width of the slice profile (section width SW) of the reconstructed images. While most manufacturers (Philips, Siemens, Toshiba) always display the correct section width SW on their user interface, GE has chosen to display only multiples of SC as potential section widths SW on their scanners. This is correct for the vast majority of parameter combinations. For the thinnest section widths at pitch $P > 1$, however, the true width of the section profile at half maximum (FWHM) is ap-

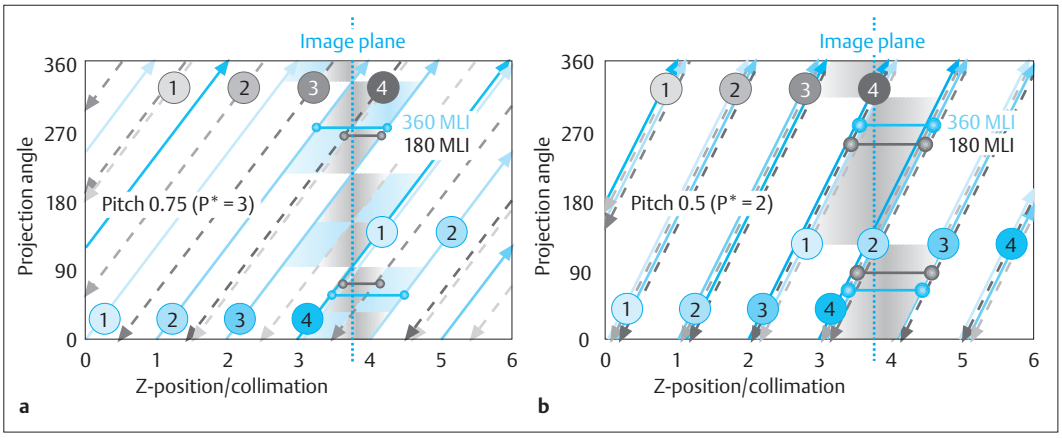

Fig. 1.**24** Overlapping data sampling occurs when the trajectory of one detector row superimposes on another, e.g. for a pitch of 0.75 ($P^* = 3$) (**a**). In the isocenter of rotation, even the conjugated data from the virtual spiral overlap the real spiral trajectory for a pitch of 0.5 ($P^* = 2$) (**b**). Note, however, that the cone beam geometry ameliorates this effect, especially for image points farther away from the isocenter.

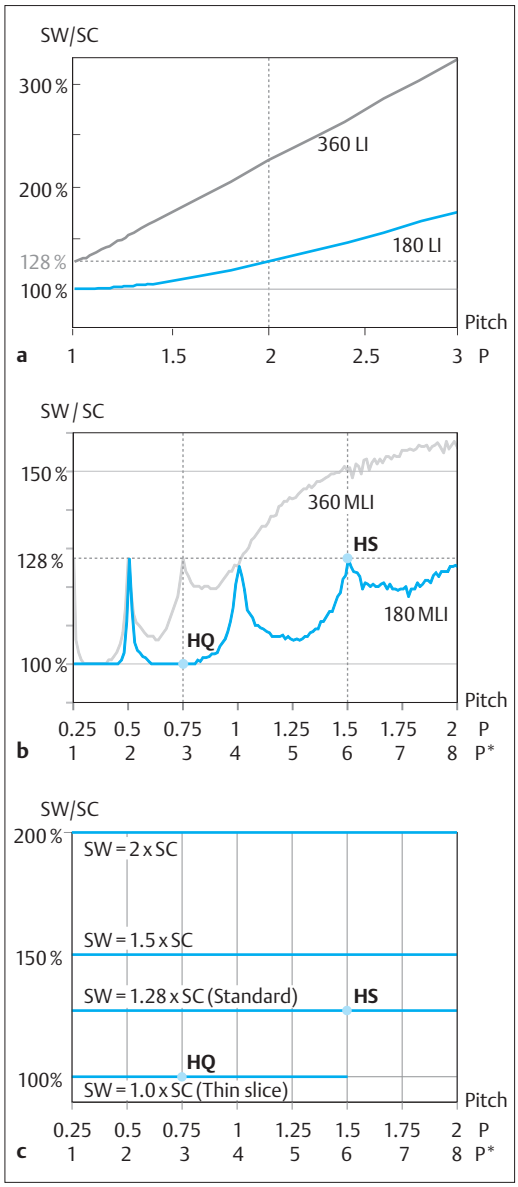

Fig. 1.**25** Effective section thickness (section width) as a function of pitch for 180° LI and 360° LI with single-detector-row CT (**a**) compared to 180° MLI and 360° MLI with 4-slice scanners (**b**). Adaptive interpolation schemes (**c**) keep section width independent of the pitch.
HQ = high quality mode, HS = high speed mode on GE scanners.

proximately 30% larger than SC (for 4- and 8-slice scanners but also for 16-slice units) and than the displayed value for SW. This widening of the section profile is also present with other manufactures but is correctly represented in the displayed section width SW.

Depending on the manufacturer, various combinations between chosen section collimation and reconstructed section width are available (Tables 1.**8**–1.**10**). In principle, the only restraint is that the section width must be larger than or equal to the collimation.

The main difference between manufacturers is how they treat the minimum available section width. If standard 180° MLI or 360° MLI algorithms (or variants) are used, the section width varies between 100% and 128% of the section collimation, depending on the pitch factor.

The minimum section width with the *GE* high speed mode ($P^* = 6$) on 4-slice scanners is some 30% wider than the collimation SC (see Table 1.**8**). It is only in this mode and in the UF ($P^* = 10.8$, $P = 1.35$) and US ($P^* = 13.4$, $P = 1.675$) modes in 8-slice scanners that the "reconstruction slice thickness' indicated on the user interface is not approximately equal to the section width.

Philips provides the real section width on their user interface. The available minimum numbers vary with pitch (between SC and SC + 30%).

Siemens varies their z-filter (adaptive array interpolation) with the pitch in such a way that section width, image noise, and dose requirements remain constant independent of pitch (Fig. 1.**25 c**). As a standard, they offer a section width that is some 30% wider than the section collimation. An edge-enhancing z-filter is also available for the 4×1 mm detector configuration that provides 1 mm section width independent of the pitch. The resulting images, however, suffer from a substantially higher noise (just like the difference between 180° LI and 360° LI in spiral CT).

Toshiba uses a z-filter of varying width (MUSCOT algorithm) that provides a given section width independent of the chosen pitch factor. The minimum section width is identical to the collimation and can be increased in steps of 0.5 mm. If SW is chosen equal to SC, the noise is substantially increased (like with all other vendors).

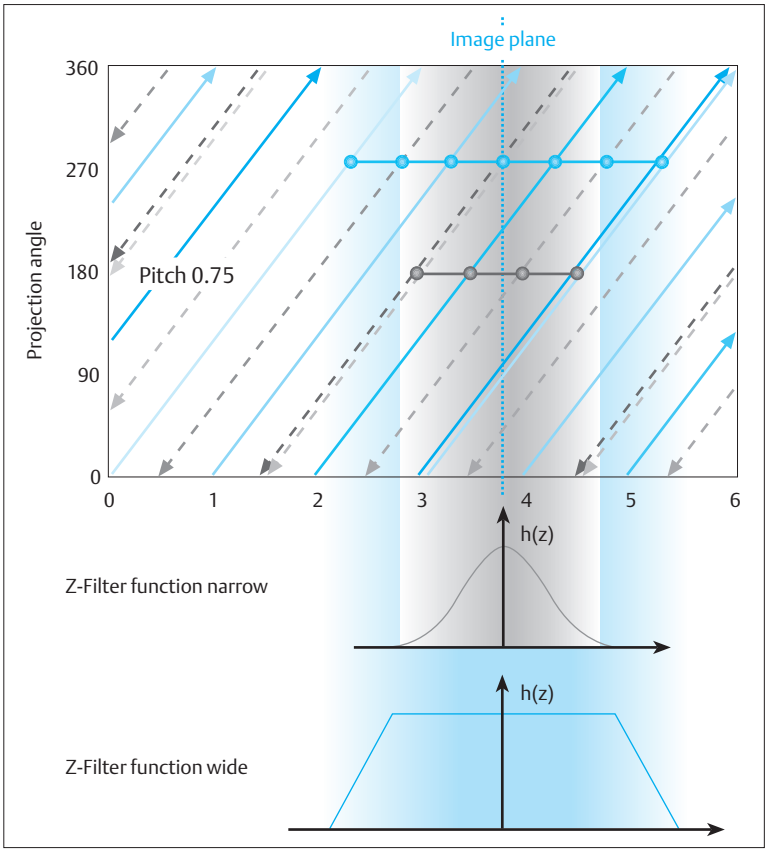

Fig. 1.**26** Z-filtering is a technique that weights projection data according to distance from the reconstructed imaging plane.

Cone Beam Interpolation

Z-filter interpolation still relies on the assumption that rays are parallel (Fig. 1.**22c**). Real cone beam corrections require more complex calculations. Such algorithms are mandatory with 16 or more detector rows because cone beam artifacts (see Fig. 7.**47**) increase substantially with wider detector arrays.

Most of these algorithms are still being refined, and use various types of compensation techniques for the cone beam geometry. Variants of 3D back projection (e.g., COBRA, Philips or TCOT, Toshiba) theoretically should yield the least artifacts. They rely on rebinning of projection data and back projection along the correct cone angles. The Adaptive Multiple Plane Reconstruction (AMPR, Siemens) shifts the plane of interpolation from an axial orientation to an oblique position with a maximum angulation determined by the cone angle (Fig. 1.**27**). As an intermediate step, this yields a set of oblique planes ("booklets") that rotate with different z-positions. Interpolation between these oblique planes then creates axial, coronal, or arbitrarily oriented sections of any desired section width without necessarily having to go through a real

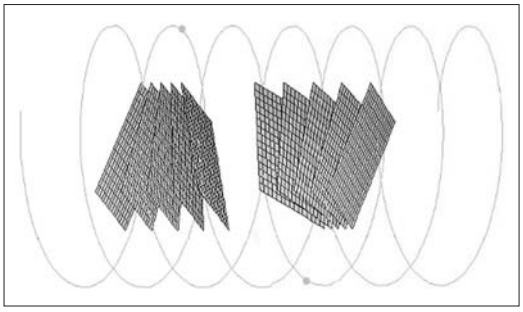

Fig. 1.**27** Cone beam interpolation by interpolating raw data to obtain multiple angulated imaging planes ("booklets") that are then interpolated to form a 3D volume.

reconstruction of an orthogonal 3D data set. In the future, Segmented Multiple Plane Reconstruction (SMPR) will use more planes ("pages") per booklet and is more suitable for larger cone angles. GE uses a combination of approaches (Crossbeam correction, Hyperplane and Conjugate Ray reconstruction) to address the various problems of cone-beam scanning, i.e. cone-beam artifact reduction and thin-slice, high-pitch scanning. At present, artifact behavior of these various algorithms has not yet been studied.

The cone beam interpolation used in the 16-slice scanners of Philips, Siemens and Toshiba allow for arbitrary pitch factors up to 1.5 to 2. However, Toshiba suggests preferred pitch values (at present P* = 11, 15 and 23; P = 0.6875, 0.9375, and 1.4375, respectively). Similar to their 4-slice and 8-slice systems, GE supports fixed pitch factors (P* = 9, 15, 22 and 28; P = 0.5625, 0.9375, 1.375 and 1.75, respectively), for which their cone beam algorithms have been specifically optimized.

Image Noise

Image noise in multislice CT depends on the z-filter (or cone beam algorithm) and the chosen section width. To understand how, we have to look back at conventional spiral CT.

There, the noise was independent of the pitch but varied with the chosen interpolation algorithm. In fact, it was much smaller with 360° LI as compared to 180° LI; for identical noise, the dose with 180° LI would have to be doubled. The 180° LI algorithm had an identical performance to the 360° LI only at a pitch of 2 and twice the mAs setting (same section profile, identical noise at identical dose). This should have made the 360° LI algorithm the interpolation of choice for low pitch factors, and is another argument for using 180° LI only in combination with high pitch factors. The effects becomes clear when the noise data are normalized to identical patient exposure (Fig. 1.**28 a**), which can be done by increasing the mAs setting proportional to the pitch so that the effective mAs (= mAs/Pitch) remain constant.

Multislice CT overcomes the limitation of single-slice spiral CT because of the higher number of detector rows and, thus, faster coverage. With 4-slice scanners, the 360° MLI algorithm has similar advantages in terms of image noise and dose requirements over 180° MLI as the corresponding algorithms from single-slice

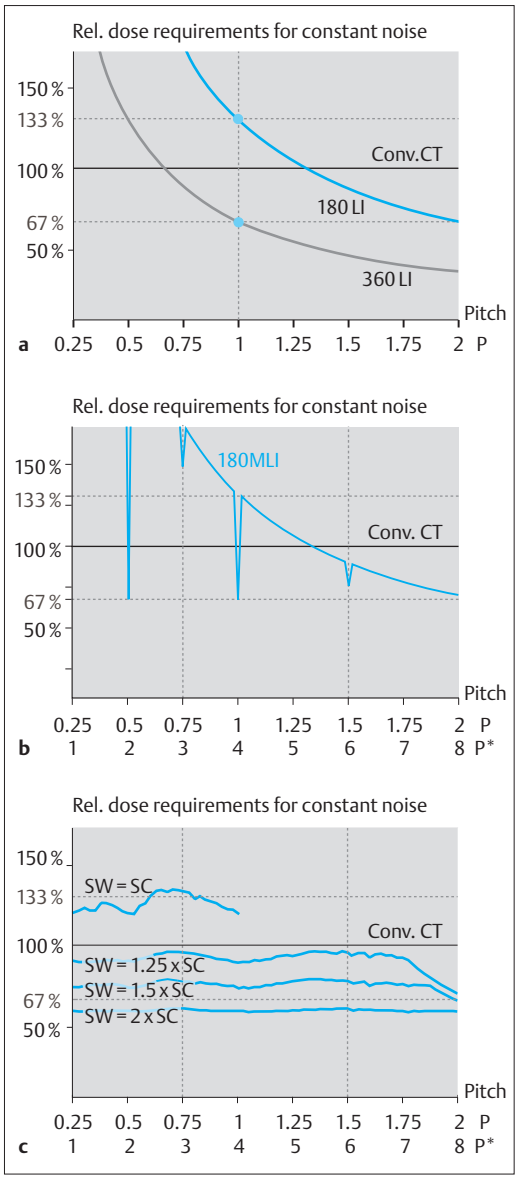

Fig. 1.**28** Relative dose requirements for constant image nois as a function of pitch. Comparison of 180° LI to 360° LI for single-slice CT (**a**), and 180° MLI for 4-slice CT (**b**). Adaptive interpolation keeps image noise fairly independent of the pitch (**c**).

CT. When considering the pitch-dependence of the section width (Fig. 1.**25**) and normalizing the noise behavior to identical patient exposure (Fig. 1.**28 b**), it becomes clear that a 360° MLI algorithm should be preferred for pitches up to 1

(slice pitch up to 4), and the 180° MLI algorithms should be used for pitches up to 2 (P* up to 8). Since a variant of 180° MLI is used for both the HQ (P* = 3) and HS (P* = 6) modes of GE scanners, the noise per dose is higher for the HQ mode than with the HS mode.

More complex z-filtering may improve the relation between noise and section width (e.g., SmartHelical) and can reduce the noise compared to a 180° LI algorithm (GE). Siemens use adaptive z-filtering to keep the noise and the section profile independent of the pitch at identical patient exposure (Figs. 1.**25 c** and 1.**28 c**). The noise with this algorithm is 12–16% lower than the noise with conventional CT but the section profile is always some 30% wider than the collimation (as with 360° LI). Since 4-slice CT allows for using very thin collimation (4 × 1 mm), this broadening (to 1.3 mm) is of little practical importance. With the Toshiba approach, the user selects a certain section width (in 0.5 mm steps) and the system chooses an appropriate z-filter width. Noise will increase substantially if the smallest section width (identical to the collimation) is used but decreases with the next larger section width.

When choosing an even wider section width, more data are included in the reconstruction and image noise decreases further.

The noise behavior with 16-slice scanners has not yet been published but in general, a similar behavior as 4-slice units can be expected. If the section width SW is chosen identical to the section collimation SC, image noise should be substantially increased, while it should rapidly diminish if at least a 30% wider section width is employed.

Overscanning

Overscanning refers to the extra rotations needed in helical scanning to be able to reconstruct images at the edges of the prescribed scan range. The number of extra rotations in single-slice CT was limited to 0.5 (180° LI) and 1.0 (360° LI) at the beginning and the end of the scan range and added little radiation dose to the patient. The image reconstruction algorithms in multislice CT require in total between 1.6 and 2.3 overscan rotations per scan, depending on pitch, cone beam correction and manufacturer. The additionally exposed area is at least equal to the number of overscan rotations × table feed TF. Especially for short scan ranges, wide total collimation and large table feed, overscanning will substantially increase effective patient dose.

Scanning Parameters

As with spiral CT scanning, section collimation (SC), table feed per rotation (TF), and pitch (P) are the most important *acquisition parameters* in multislice CT. In addition to the reconstruction increment (RI), however, there is the effective section thickness or section width (SW) of the reconstructed images that contributes to the most important *reconstruction parameters*. All the other parameters are varied only in exceptional cases. Together with the number of active detector rows N, the acquisition parameters can be given as (N × SC / TF), and the reconstruction parameters can be given as (SW / RI). Because more than one set of reconstructions is possible with multislice CT, it is reasonable to separate acquisition and reconstruction parameters.

Acquisition Parameters

As has been pointed out above, the section collimation is determined by the available detector configuration. In general, thinner sections (4 × 1 to 4 × 1.25 mm, and 8 × 1 to 8 × 1.25 mm) are used for near-isotropic *volumetric imaging* with the option to reconstruct arbitrary cut planes. Thicker sections (4 × 2 to 4 × 2.5 mm or more) are employed with *fast spiral scanning* for routine applications, and when data acquisition has to be particularly fast.

With 16-slice scanners, thin sections become standard even for routine *fast spiral* scanning. GE offers 16 × 1.25 mm, Philips and Siemens provide 16 × 1.5 mm, and Toshiba gives the choice between 16 × 1 mm and 16 × 2 mm for this purpose. For isotropic volumetric imaging, the scanners offer 16 × 0.625 mm (GE), 16 × 0.75 mm (Philips, Siemens), and 16 × 0.5 mm (Toshiba).

There is a continuing discussion as to whether to use a *high or low pitch factor*. Lower pitch factors (e.g., the HQ mode in a 4-slice GE scanner) yield axial images with less cone beam artifact, but good results of a similar (and often better) quality can be obtained when images are *acquired* with a thin collimation and *reconstructed* with a larger section width. In addition, low pitch factors require a higher patient dose

for identical image noise. Using a thin collimation and a large pitch factor has the additional advantage that it is possible to go back to the raw data and reconstruct it again with a thin section width. From such a data set, it will be possible to obtain superior quality multiplanar reformations (see Fig. 2.**8**). Such an approach is especially useful when findings on axial sections are not clear and require further evaluation by another imaging plane. With 8- and 16-slice scanners this difference becomes less apparent because only thin sections are available for data acquisition.

One has to bear in mind, however, that the geometric efficiency in 4-slice scanners (see Fig. 5.**5**) decreases with thinner sections, which will lead to an increase in image noise that may require using higher exposure settings. This limitation is overcome with 8- and 16-slice detector systems because of substantially higher geometric efficiency.

There is a limit to such an approach of using thin collimation, however, on those scanners that do not allow for increasing the reconstructed section width arbitrarily. This is for example the case for current 4-slice GE systems (see Table 1.**8**). A 4×1.25 mm collimation will not allow for reconstructing 5 mm axial sections. In practice, many users will therefore not use such a thin collimation, but instead resort to 4×2.5 mm or 4×3.75 mm collimation. With the GE 8- and 16-slice scanners a section width of 5 mm is available even with the thinnest collimation. For the 4-slice system there is a workaround described below that uses thick MPR from an overlapping thin-section secondary raw data set.

Reconstruction Parameters

The *section width* SW (effective section thickness) has to be larger than or equal to the section collimation SC. Apart from this constraint, SW can be chosen independently from SC for most multislice CT units. The available choices for section width depend on the manufacturer and the type of z-filtering (see Tables 1.**8**–1.**10**). Note that a section width that is identical to the collimation SC will result in a substantially increased image noise, and therefore should be reserved for only those applications with the maximum possible z-axis resolution (e.g., pulmonary or skeletal imaging).

For most routine applications, and for reasons of image noise, a section width of 5–8 mm will be chosen. Only for special indications such as HRCT, skeletal imaging, imaging of the pancreas and adrenals, or preoperative staging of liver tumors will smaller section widths be necessary.

The *reconstruction increment* RI can be chosen in a similar fashion as in spiral CT. For most routine applications, a moderate overlap of some 20% of the section width will suffice. For optimum quality of 3D reconstructions, at least a 50% overlap should be chosen unless the reconstruction increment is already as small as the pixel size. This will depend on the chosen field of view (see Table 4.**4**). For most body applications with an FOV of 30–40 cm, the pixel size is between 0.6 and 0.8 mm. Thus, a reconstruction increment of exactly the same size will yield an isotropic grid of data points. Note, however that this is not necessarily identical with isotropic data sampling (see also pp. 46).

Chapter 4 gives an overview of recommended scan and reconstruction parameters for various clinical requests and various vendors (Tables 4.**4**–4.**6**).

Secondary Raw Data Set

Whenever possible, a thin collimation should be preferred, because this will allow for creating a 3D data set of near isotropic resolution. Such an overlapping thin-section image data set will frequently be too noisy for primary viewing. It therefore forms an intermediate data set (we suggest to call it a "*secondary raw data set*") that is used to create images for clinical interpretation. The most common technique is multiplanar reformatting (MPR) using arbitrary image planes and any desired section thickness.

A secondary raw data set typically consists of 0.5–1.5 mm-thick images reconstructed every 0.4 to 1 mm. The MPR function of the scanner or a workstation can be employed to create axial sections of arbitrary thickness and with arbitrary reconstruction increments. Such an approach can also be used with scanners that have no direct reconstruction of thicker sections from the raw data available. In addition, these sections can be anatomically adapted to compensate for improper positioning of the patient. This is especially helpful for symmetrical structures such as the inner ear or the cervical spine.

Vendor-specific Approaches

In multislice CT, reconstruction algorithms are rather vendor-specific. All vendors use 2D fan-beam z-filtering algorithms for 4-slice scanners that neglect the cone-beam effect. These z-filtering variants largely determine which parameters the user may select and how. In the following paragraphs, the approach of the various vendors to 4-slice scanning is discussed.

The approach to 8- and 16-slice scanning is covered in chapter 4, optimization of scanning technique (p. 122, Table 4.**6**).

General Electric 4-Slice Scanners

General Electric noticed that only at certain pitches the measurements from different detectors are relatively unique and complementary. From this the *preferred helical pitch* concept was developed, which made only two distinct pitch factors and corresponding section widths available. Scanning with P* = 3 is called *HQ (high quality) mode*, while P* = 6 is called *HS (high speed) mode*. The HQ mode provides good contrast resolution, low (cone beam) artifact levels and matches the quality of pitch 1 in single-slice CT. The HS mode is designed for high volume coverage and thin slices, comparable with pitch 2 in single-slice CT. For both pitch levels, image reconstruction is based on a variant of 180° MLI.

On GE scanners, the user chooses the section width SW (reconstruction slice thickness) first, depending on the clinical requirements. This choice is much as in single-slice helical CT. However, only multiples of the width of a single detector row (1.25 mm) are available (Table 1.**8**). The user then has to decide whether to scan with 4 × 1.25 mm or thicker collimation. Images can be reconstructed at arbitrary intervals, just as in conventional spiral CT. If multiplanar reformations are required, the data set can be reconstructed a second time with thinner section width. Consequently, quality of MPR is best if thin sections are chosen for acquisition. There is presently a constraint as to which combinations of section collimation and section width are actually available: for example, the largest section width that allows for using a 4 × 1.25 mm detector configuration is only 2.5 mm (Table 1.**8**). This makes it necessary to use axial multiplanar reformations if section widths shall be reconstructed that are thicker than the maximum section width allowed by the scanner interface. For axial scans (step-and-shoot), raw data from multiple detectors can be averaged (1 i, 2 i and 4 i modes) before image reconstruction to reduce partial volume effects (e.g., in the posterior fossa).

Because of the lower pitch the patient dose ($CTDI_{vol}$, see Chapter 5) is twice as large for the

Table 1.**8** Selectable options in GE Lightspeed systems (HU, 2000)

Detector Configuration	Available table feed TF		Available section width SW (user interface)	Measured section width (FWHM[1])	
	HQ-Mode[2]	HS-Mode[2]		HQ-Mode[2]	HS-Mode[2]
4 × 1.25 mm	3.75 mm	7.5 mm	1.25 mm 2.5 mm	1.3 mm 2.5 mm	*1.6 mm* 2.5 mm
4 × 2.50 mm	7.5 mm	15.0 mm	2.5 mm 3.75 mm 5.0 mm	2.6 mm 3.8 mm 5.0 mm	*3.2 mm* 3.8 mm 5.0 mm
4 × 3.75 mm	11.25 mm	22.5 mm	3.75 mm 5.0 mm 7.5 mm	3.9 mm 5.0 mm 7.5 mm	NA 5.0 mm 7.5 mm
4 × 5.00 mm	15 mm	30.0 mm	5.0 mm 7.5 mm* 10.0 mm*	5.2 mm 7.5 mm 10.0 mm	*6.4 mm* 7.5 mm 10.0 mm

[1] FWHM = full width at half maximum; section width SW is called "reconstruction slice thickness" on user interface; measured SW may be larger than SW displayed on user interface (numbers in italics)
[2] HQ = high quality, HS = high speed
* only available as 2 × 7.5 or 2 × 10 mm; with a special technique 2 × 0.625 mm is also available

HQ mode compared to the HS mode if mA settings are kept unchanged. Even if the scanner is allowed to change the mA to provide equal image quality, HQ requires about 50% more dose than HS. With the SmartHelical protocol, image noise can be reduced for both modes as compared to conventional helical CT. When switching from a GE single-slice scanner to a multislice unit, the patient dose increases dramatically if mAs settings are kept unchanged. The reason for this is the shorter scanner geometry, which yields a higher dose per mAs and problems with focal spot tracking, which were solved shortly after the first release of the LightSpeed scanner. For these reasons, a new user should not apply identical mAs settings but adjust the mAs downwardly to obtain a similar $CTDI_{vol}$ with the two systems.

Siemens 4-Slice Scanners

Siemens makes use of the adaptive array detector system and has developed an optimized fan beam reconstruction algorithm, called Adaptive Array Interpolation (AAI or SureView). This algorithm ensures that the user-selected section width SW remains constant, independently of the chosen pitch factor (Fig. 1.**25 c**). Slice pitches P* between 2 and 8 are available for routine use, and even smaller values for cardiac CT. Available combinations of section collimation and section width are given in Table 1.**9**. In practice, pitch factors P* between 5 and 8 will be used in most situations. Siemens allows the user to prescribe multiple reconstruction protocols from one data set, thus speeding up workflow if both a thick section for image review and thin sections for MPR and 3D imaging are required.

To keep both image noise and patient exposure constant independent of the pitch (Fig. 1.**28 c**), the system raises the mAs settings automatically in proportion to the pitch factor. To make life easier for the user, the user interface on the scanner console does not display the real mAs but values for *effective mAs,* which are defined as

$$mAs_{eff} = mAs / P = mAs \times N / P^*.$$

These effective mAs correspond to the settings that would occur with a conventional step-and-shoot CT technique. The definition of mAs_{eff} can also be applied to other scanners and is valid even for conventional spiral CT. However, it also carries the risk that, should the user switch to a multislice scanner and apply the same mAs settings as on the single-slice unit, the change in definition of "mAs" on the multislice unit may not be accounted for and a substantially higher radiation dose would be applied. For example, a setting of 200 mAs at a pitch of 2 on a single-slice unit would correspond to a setting of 100 $mAs_{(eff)}$ on the multislice scanner. Keeping the 200 mAs setting would double the patient dose.

Philips 4-Slice Scanners

Philips employs the same detectors as Siemens. The image reconstruction algorithm is termed Multislice Interpolation (MSI/MSSI). Exact details for this algorithm, however, are not yet public. User-definable options on the four-slice system are very similar to the Siemens system with collimations of 0.5–5.0 mm, slice widths of 0.5–10.0 mm and pitch factors up to P = 2 (see Table 1.**9**). Philips also employs the concept of effective mAs on their scanners.

Toshiba 4-Slice Scanners

Toshiba has developed a z-filtering fan-beam algorithm called *multislice cone beam tomography reconstruction* (MUSCOT). Toshiba suggests preferred pitch values of P* = 2.5, 3.0, 3.5, 4.5, 5.0,

Table 1.**9** Selectable options in the Siemens Sensation 4; the Philips MX 8000 is comparable

Detector configuration	Available table feed TF	Available section width SW (FWHM)
2 × 0.5 mm	0.5–2 mm	0.5; 0.75; 1.0; 1,25; 1.5; 2.0 mm
4 × 1.0 mm	1.25–8 mm	1.0; 1.25; 1.5; 2.0; 3.0; 4.0; 5.0; 6.0; 7.0; 8.0; 10.0 mm
4 × 2.5 mm	2.5–20 mm	3.0; 4.0; 5.0; 6.0; 7.0; 8.0; 10.0 mm
4 × 5 mm	5–40 mm	6.0; 7.0; 8.0; 10.0 mm
2 × 8 mm	8–32 mm	8.0; 10.0 mm

FWHM = full width at half maximum

Table 1.**10** Selectable options in the Toshiba Aquilion Multi

Detector configuration	Available table feed TF	Available section width SW (FWHM)
4 × 0.5 mm	1.25–3 mm	0.5–2.5 mm in 0.5 mm increments
4 × 1.0 mm	2.5–6 mm	1–5 mm in 0.5 mm increments
4 × 2.0 mm	5–12 mm	2–10 mm in 0.5 mm increments
4 × 3.0 mm	7.5–18 mm	3–15 mm in 0.5 mm increments
4 × 4.0 mm	10–24 mm	4–20 mm in 0.5 mm increments
4 × 5.0 mm	12.5–30 mm	5–20 mm in 0.5 mm increments
4 × 8.0 mm	20–48 mm	8–20 mm in 0.5 mm increments

FWHM = full width at half maximum

5.5 and 6.0. Toshiba prefers non-integer values of P* to optimize sampling density and shift the position of the conjugate data. According to their specifications, however, best image quality is obtained with P* = 3.0 and 5.5. The z-filtering is a multipoint interpolation using different filter widths (FW) that are automatically chosen by the system depending on which section width (SW) is selected by the user. The section width can be increased in 0.5 mm steps from a minimum identical to the collimation SC to a maximum of five times SC (Table 1.**10**). As with all other manufacturer, image noise is increased for SW = SC. As with Siemens scanners, section width is independent of the pitch.

In practice, a pitch factor P* = 5.5 (6.0 for CTA) will be used for most applications since it combines few multislice artifacts with a large coverage per time. For a constant mA setting, patient dose decreases but image noise increases with larger pitch factors. For this reason, mA settings have to be proportionately increased with larger pitch (constant effective mAs or $CTDI_{vol}$). Under such conditions of constant patient dose, noise is relatively independent of pitch.

Workflow, Image Review, Display and Documentation

Multislice CT can be used as a technique for fast spiral scanning or as a true volumetric imaging modality (see also Chapter 4). With *fast spiral scanning*, thicker sections are reconstructed and viewed, very much like spiral CT. With volumetric imaging, a secondary raw data set of thin overlapping axial sections is created first. This data set is then used to reconstruct (anatomically adapted) thick axial sections as well as thick multiplanar reformations or various types of 3D images. The workflow of image processing, display, and documentation may change substantially.

Fast Spiral Scanning

Fast spiral scanning is a technique that is excellently suited for routine imaging tasks. It provides at least equivalent, and often superior results to single-slice spiral CT while retaining the same basic imaging workflow. Display and documentation can remain similar to spiral CT (see above, p. 17). The thicker sections are used for making a diagnosis (preferably using cine displays for viewing) and can be printed on film. They are used to compare findings to older spiral-CT examinations, and are excellent for communicating findings to referring physicians.

If there are remaining diagnostic problems, thin overlapping images can still be reconstructed (if thin-section scanning was performed and raw data are still available) and further processing is done according to the volume imaging procedure described below.

Volumetric Imaging

Volume imaging takes full advantage of the three-dimensional capabilities of multislice CT. Reconstruction of a secondary raw data set of thin overlapping axial images gives the user full control over the available information contained in the data volume. However, such a secondary raw data set consists of several hundred images, depending on the covered scan range and the chosen reconstruction increment. This puts a lot of strain on image reconstruction, image processing, data transfer, image reviewing techniques, archiving, and image demonstration. The imaging workflow has to be completely changed as compared to current scanners. With 4-slice scanners, most of these

processes are not yet optimized because of substantial hardware and software constraints. As a consequence, the volumetric imaging mode will probably not be used as often as it should. Most 6-, 8-, 10- and 16-slice scanners, however, are already optimized for such an approach. Table 1.**11** gives an overview of hardware and software requirements for optimum data handling when using a volumetric imaging technique with multislice CT.

Image reconstruction from the raw data set can take a substantial time, even with sub-second reconstruction, if some 300–400 images are reconstructed for the chest or 400–500 images are reconstructed for one abdominal series. For this reason, very fast reconstruction (multiple images per second) is important to allow for a high patient throughput.

Standard image reviewing is best performed on thick axial or multiplanar reformations that were reconstructed by the CT technician according to a predefined protocol that depends on the clinical imaging task (see Chapter 4, and the various organ chapters). The technicians can also perform various 3D reconstruction tasks according to specific protocols, such as curved planar reformations along the pancreatic duct, volume-rendered or MIP images of the vascular system, or exarticulated 3D views of joint surfaces (see Chapter 2). This allows for substantial time savings in a setting where imaging workstations are not real-time interactive.

Interactive image reviewing is ideal if the imaging workstation is (near) real-time interactive. Most workstations on the market, however, suffer

Table 1.**11** Hardware and software requirements for optimum workflow with multislice CT

	Fast spiral scanning	**Volume imaging**	
		Minimum	**Optimum**
Typical number of images	100–300	200–400	300–1200
Hardware			
CT scanner			
Reconstruction speed	> 1 image/sec	> 2 images/sec	> 6 images/sec
Storage capacity of *raw data*	> 10 patients[1]	> 5 patients	all pts. from one day
Storage capacity for *images*[2]	> 6000	> 10.000	> 40.000
CT workstation			
RAM	512 MB	1 GB	≥ 4 GB
Hard disk[3]	> 40 GB	> 40 GB	> 80 GB
Volume accelerator board	–	–	+
Data transfer rate	100 Mbit/sec	100 Mbit/sec	≥ 1 Gbit/sec
Software			
CT scanner			
Predefined scan protocols	+	+	+
Predefined processing protocols	–	–	+
(Thick) MPR[3]	–	+	+
MIP	–	–	+
VRT	–	–	+
CT workstation			
Real-time thick MPR	–	–	+
Semi-automated segmentation	–	–	+
MIP	–	+	+
Volume rendering	–	–	+

[1] depending on workflow. Raw data should remain available until it is decided whether additional thin sections are necessary
[2] depending on workflow. If further processing is done on the scanner, substantially larger storage capacities are necessary
[3] depending on workflow. Processing (MPR, MIP, VRT) by the technicians can be done on the scanner or on a separate workstation

from substantial constraints because they are usually optimized for only a few specific processing tasks or they are too complex or too slow to be useful in a routine setting. Most important for interactive reviewing is a *thick-section MPR* mode that is truly real-time and allows for fast scrolling through the data set as well as for interactive change of the section thickness. Most software is real-time interactive for one-pixel-thin MPRs and only updates the image to the desired thick MPR as soon as the interaction is stopped. This may be sufficient for data sets obtained with high radiation exposure and thus little image noise. However, it is suboptimum for the vast majority of standard examinations, especially in the abdomen, where noise is very disturbing and can be reduced only by thick MPR. Interactive *volume rendering* is another option that gains increasing importance as a primary tool for image interpretation. Short data loading times, easy handling, proper opacity presets (see Table 2.**4**), and true real-time interaction are important for time-efficient image review and reporting.

Processing workstations need to be equipped with sufficient computing power and memory. For multislice CT with several hundred images, the RAM should be *more* than 1 GB in size. For interactive volume rendering, accelerator boards are available that make real-time interaction possible (several frames per second). They differ with respect to the available matrix size for real-time interaction, and whether they allow for perspective rendering (important for virtual endoscopy).

Data networking may become another bottleneck. Fast networks are mandatory (at least 100 Mbit/s, more for 16-slice units). Shared databases and picture archiving and communication systems (PACS) for data archiving can help substantially to reduce data traffic due to multislice CT data sets. Multislice CT studies at present represent the largest data sets to be transferred over PACS networks. Transferring *all* necessary data (which may be well over 1000 images, if images are transferred to various workstations) from a multislice CT examination must not take longer than the time slot assigned to each patient on such a scanner. Appropriate planning prior to setting up a multislice CT system is essential to avoid clogged networks and suboptimum workflow.

Image documentation will still require printing out of thick axial sections, especially when a patient is transferred to another institution. This is important as long as there are no generally available standards for image reviewing outside of radiology departments in the offices of referring physicians. Most vendors now offer DICOM viewers that can be put on a CD-ROM together with the patient data. There is the additional need to document critically important axial, multiplanar, or three-dimensional images on film or even on paper prints (color, black and white). Paper prints are generally well received by referring physicians because they can be more easily added to the patient record.

Cardiac CT

Electron Beam CT (EBCT) is an established imaging modality for the noninvasive diagnosis of coronary artery disease (see also Chapter 23, Heart). Although cardiac CT is possible to some degree on single-slice or dual detector CT units (calcium scoring), only the introduction of multislice CT opened up cardiac CT for clinical practice. Multislice CT allows for morphologic imaging of the heart, calcium scoring, and coronary CTA. Phase-selective cardiac imaging adds the option of functional heart studies.

A high temporal resolution is needed to freeze cardiac motion and avoid artifacts. To eliminate breathing artifacts the complete heart should be scanned within one breath-hold. ECG synchronization of data is necessary to capture the heart in a (relative) motionless phase. EBCT uses non-mechanic beam rotation with acquisition times between 30 and 100 ms. Multislice CT is based on mechanically rotating CT units that are limited currently to 375–500 ms rotation time, but in the future may provide faster rotation of the order of 300 ms. With current four-detector-row systems with 0.5 s rotation time, a temporal resolution of 100–250 ms can be accomplished, depending on the heart rate, the pitch, the rotation time and the segmental reconstruction capabilities. Even these systems are at their limit in terms of spatial and temporal resolution. These problems, however, probably will be solved

with 16-slice cardiac scanners with faster rotation times and narrower section collimation which may reach a temporal resolution of 50–65 ms, comparable to current EBCT.

Prospective ECG Triggering

Prospective ECG-triggering is used for sequential acquisition of four simultaneous sections. Temporal resolution is achieved by a partial scan technique.

A prospective trigger is derived from the ECG to initiate scanning at a user-selectable time after the preceding R-wave or before the next R-peak. This delay is defined to coincide with the end-diastolic phase of the heart cycle. It is usually chosen between 40% and 80% of the RR interval. Due to limitations in scan cycle times (table movement), every other heart beat is used for data acquisition (Fig. 1.**29**). In order to capture the heart within one breath hold, in 4-slice scanners a 4 × 2–3 mm collimation is employed, depending on the available detector configuration and the scan length. The table feed should be identical to the total collimation width (10–12 mm) or slightly less (6–10 mm) for overlapping sections. With 16-slice units collimation comes down to 1–2 mm with table feeds in the 12–32 mm range.

Standard partial scan techniques require acquisition of data from half a rotation plus the fan angle of the x-ray beam. This will result in a temporal resolution of some 320–360 ms for a 0.5 s rotation time. Some manufacturers offer optimized reconstruction that is achieved by rebinning the fan beam data to parallel beam geometry and using a reduced field of view of 240 mm or less. This results in an effective scan time of 50–55% of the tube rotation time, yielding a temporal resolution only slightly above 250 ms. The exposure time should be less than 40% of the RR interval, i.e., the heart rate should be below 96 beats per minute (bpm) for 250 ms exposure time, and below 75 bpm for 320 ms exposure time. Administration of a beta blocker is advisable only if the heart rate is too high, and the diastole needs to be prolonged. Almost motion-free images of the heart are obtained up to a heart rate of 70 bpm.

Since all data are used for image reconstruction, no increase in radiation dose to the patient is necessary as compared to a conventional CT. At identical noise levels, dose is similar to or smaller than that of EBCT.

In 16-slice scanners, the decreased rotation times of 0.40–0.42 s results in routine temporal resolutions in the order of 80–200 ms. Also, the critical value of the heart rate for optimal temporal resolution has shifted to higher values (80–85 bpm), which is important in clinical scanning.

Retrospective ECG Gating

In retrospective cardiac gating, a continuous spiral scan is acquired with simultaneous ECG-recording. In order to obtain enough projectional raw data during each part of the cardiac cycle, oversampling with a low pitch factor

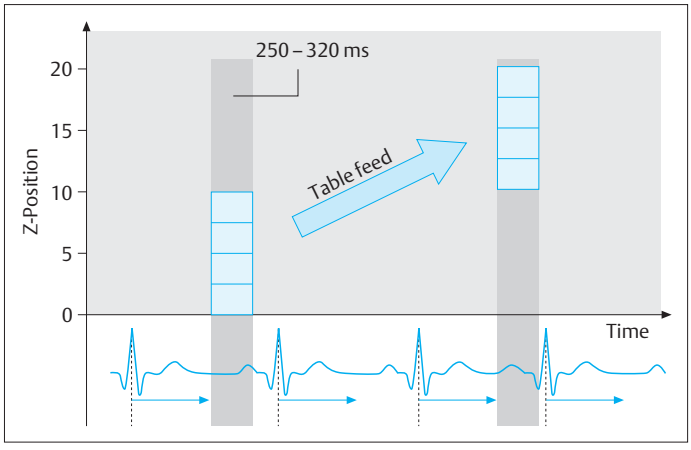

Fig. 1.**29** Prospective ECG gating. A partial scan is triggered by the R-wave of the ECG. Alternate heart beats are used for scanning and table incrementation, respectively.

(P = 0.2–0.4) is required. The pitch is adapted to the heart rate, with higher pitch for higher heart rates. The oversampling will necessarily increase radiation exposure to the patient.

The user can prospectively or retrospectively select a gate during the RR interval of the ECG for which data for image reconstruction are to be accessed. Gating can be performed with a relative approach (time delay as a fraction of the heart cycle) or with absolute approaches (either a fixed delay after the preceding R-peak or before the next R-peak). More sophisticated approaches take the relative duration of systole and diastole into account.

Overlapping reconstruction further improves image quality on MPR and 3D images. Retrospective gating reduces the sensitivity to cardiac arrhythmia. Multiphase reconstructions during various time points within the RR-interval allow for phase-selective or functional cardiac imaging.

Single Sector Reconstruction

With single sector reconstruction, only data from the prescribed time range during one cardiac cycle are used for partial scan reconstruction of images. This yields a temporal resolution of about 250–320 ms for 0.5 s rotation time and 200–270 ms for 0.4 s rotation time.

Images can be reconstructed using no interpolation at all ("nearest neighbor") by including only those data from the various detector rows that are closest to the desired plane of reconstruction. This works best for very low slice pitch factors P $<$ 0.25 but, depending on the heart rate, pitch can be increased up to P = 0.4 without major artifacts.

Multislice Cardiac Volume Reconstruction (MSCV, Siemens) is an algorithm that combines partial scan reconstruction with multislice spiral weighting. For each projection angle in the multislice data set a two-point linear interpolation is performed between data acquired during the desired heart phase (Fig. 1.**30**). This algorithm produces a constant relation of the average slice width to the chosen slice collimation: SW $\approx$ 1.3 ($\pm$ 0.2) SC. Also, retrospective generation of thicker slices from the same dataset with SW = 1.5, 2 or 3 times the chosen collimation SC is possible, resulting in slices with lower noise and better low-contrast resolution at the expense of reduced z-resolution.

Multisector Reconstruction

Multisector reconstruction (e.g. Snapshot Burst, GE; ACV, Siemens; Adaptive Multisector Interpolation, Toshiba) can increase the temporal resolution of the above algorithm by using scan data from more than one heart cycle for image reconstruction (segmented reconstruction, Fig. 1.**31 a**). Each heart cycle provides a part ("sector") of the data required for partial scan reconstruction. For m sectors (and thus, m heart cycles), the maximum temporal resolution is RT/2 m. A 0.5 s scanner will provide a maximum temporal resolution of 125 ms with two sectors, and less than 65 ms with four sectors.

At particularly unfavorable heart rates, however, the tube position relative to the heart is identical for each consecutive heartbeat. Mul-

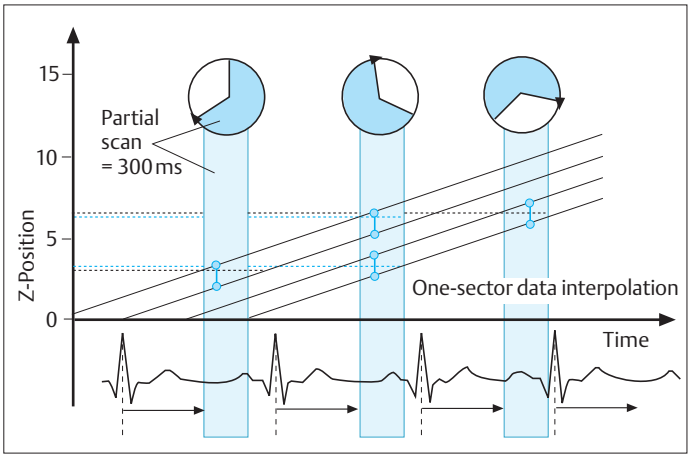

Fig. 1.**30** Retrospective ECG-gating by multislice cardiac spiral interpolation. For image interpolation, only a short acquisition window (here: 300 ms, corresponding to a partial scan of 220°) is chosen. Oversampling with low pitch factors is a prerequisite. Note that there is a range of z-positions reconstructed from the same heart beat (compare the two blue z-positions). The sharp transition to the next heart beat (black z-positions) may cause band-like artifacts on 3D images.

tisector reconstruction can only lead to improved temporal resolution if the patient's heart rate and the tube rotation are appropriately desynchronized so that the projection angles of the start and end-points of each sector fit together and form a complete partial scan data segment. For m sectors, the temporal resolution will vary between RT/2 and RT/2 m depending on the heart rate (Fig. 1.**31**). On a 0.5 s scanner, a high temporal resolution with 2-sector reconstruction is achieved at 65–70 bpm and 90–100 bpm, while 80 bpm leads to synchronization and therefore reduced temporal resolution. Choosing a different rotation time can shift these phases of maximum and minimum temporal resolution (Fig. 1.**31 c**). The relation between SW and SC remains fairly independent of heart rate: SW ≈ 1.3 (± 0.2) SC.

The heart rate usually varies during the course of the scan. This led to the development of adaptive algorithms that not only vary the number of sectors with heart rate (Fig. 1.**31 b**) but also optimize the size of each sector depending on each individual RR interval (Fig. 1.**31 c**). For optimum temporal resolution, however, the rotation time has to be adapted to the expected range of heart rates. Because rotation time remains fixed during the scan, temporal resolution deteriorates if the heart rate changes too much. In addition, spatial resolution will suffer if the position of the heart is not identical for all sectors.

With 10- and 16-slice scanners, thinner collimation (SC = 0.5–0.75 mm) improves spatial resolution and reduces geometric artifact in coronary stents. Reconstruction techniques that neglect cone-beam geometry can be applied since the heart is sufficiently centered and does not contain very high contrast structures. Cone beam corrections, however, are able to further improve image quality and allow for higher pitch factors.

Pitch

Continuous volume coverage with retrospective ECG-gating and *single sector* reconstruction requires limiting the pitch dependent on the heart rate. For optimum spiral weighting with two interpolation partners for every projection the following restriction applies:

$$\text{Pitch } P \leq (N-1)/N \times RT / (T_{RR} + RT_Q) \quad (1)$$

(RT = full rotation time, e.g., 500 ms, and RT_Q = partial scan rotation time, 250–360 ms).

If faster volume coverage is needed and 50% of projections are generated with nearest-neighbor interpolation, this restriction is reduced to $P \leq RT/T_{RR}$. Heart rates of 45–100 bpm correspond to pitch factors of P = 0.375–0.825 (P^* = 1.5–3.3 for 4-slice scanners) for 0.5 s rotation time. Temporal resolution is in the order of 250 ms.

For *multisector* reconstruction, the pitch should be adapted as follows to the heart rate:

$$P \leq k \times RT / (T_{RR} \times m) \quad (2)$$

T_{RR} is the maximum RR interval that is expected during the scan, and k is a constant (close to 1) that depends on the implementation, the number of active detector rows N, and the number of sectors m.

At higher heart rates, pitch can be increased but there has to be a stepwise increase in sectors m as well to retain temporal resolution. As a consequence, the available range of pitch factors remains limited and usually varies between P = 0.2 and 0.5. For high temporal resolution (acquisition window around 15% of the RR interval), pitch factors have to remain around 0.2 to 0.25. For faster rotation times RT, the pitch has to be decreased. Reformulating equation (2) shows that the maximum table speed TS is independent of RT:

$$TS \leq k \times (SC \times N)/(T_{RR} \times m) \quad (3)$$

The required scan range determines how low a table speed is possible. In practice, covering a 12 cm scan range with 4 × 1 mm collimation within 40 s on a 0.5 s scanner requires a table speed of 1.5 mm/s (P^* = 1.5; P = 0.375). Scanning speed increases with 16-slice scanners but varies substantially (4–12 mm) depending on the implemented multisector interpolation and cone-beam corrections.

ECG-gated Reconstruction with Extended Coverage

Some clinical applications do not require complete suppression of motion artifacts but profit from reduced pulsation effects. Such applications include imaging of coronary artery bypass grafts, cardiac morphology, or imaging of the central vessels. For such applications, ECG-gating can be modified to allow faster scan speeds and reduced radiation exposure. This is done by excluding only those phases of the heart cycle from reconstruction that contain most motion artifacts (systole or phase of systolic pulse wave). The excluded time window ΔT_S can be varied but usually some 250 ms are used for this propose. The resulting temporal

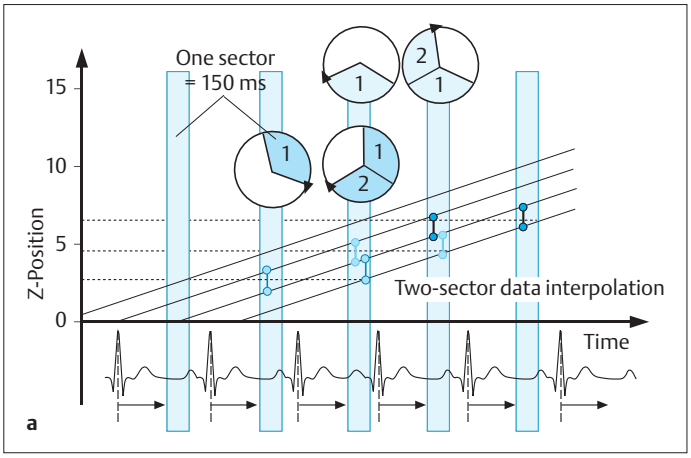

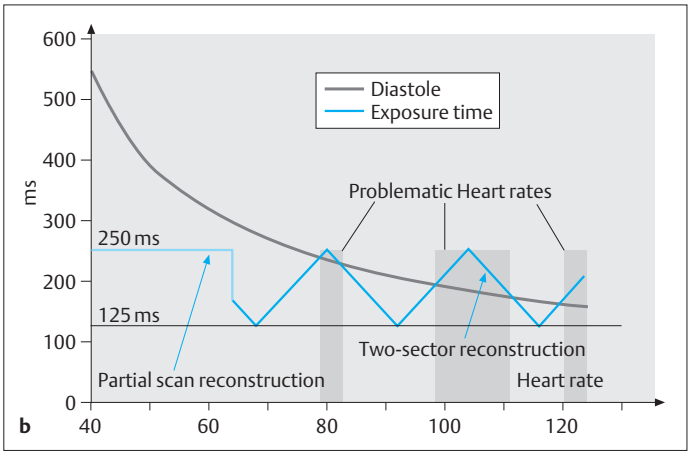

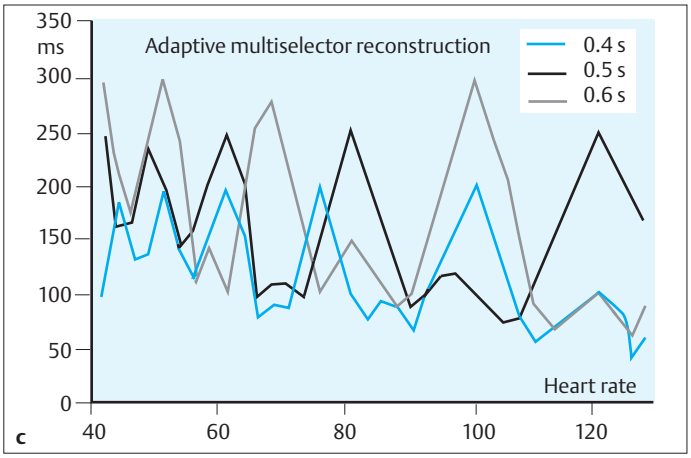

Fig. 1.**31** Retrospective ECG gating with multisector interpolation. The same phase of more than one heart cycle is used to collect data for interpolation, thus effectively improving the temporal resolution. The 220° of data required in this example are filled by two sectors of 110°, each of which corresponds to data from an acquisition window of some 150 ms (**a**). This is only possible if sectors do not overlap completely, i.e., if data from each heart cycle provide different projection angles. In practice, this happens only at particularly favorable heart rates, which causes temporal resolution to vary with heart rate (**b**). The most recent adaptive multisector interpolations automatically choose the smallest sectors available for each consecutive RR-interval and thus can further improve temporal resolution. For best results, however, the rotation speed of the scanner has to be adjusted as well in order to avoid synchronization between rotation speed and heart rate (**c**).

resolution is RT/2. The approach is phase-inconsistent but yields images of substantially better quality than a non-gated approach. The reconstructed image stacks should overlap in the z-direction giving a pitch limitation of:

$$P \leq (N-1)/N \times RT / (RT/2 + \Delta T_S) \quad (4)$$

In the chest for $\Delta T_S = 250$ ms, the resulting pitch $P = 0.75$ ($P^* = 3.0$) allows for covering 220 mm in 36 s with 4×1 mm collimation. Different values of ΔT_S used for other applications will lead to different preferred pitch values. With 16-slice scanners, the whole chest and abdomen can be covered with such a technique in 16×1.5 mm collimation.

Radiation Exposure

Retrospective gating uses only a small portion of the acquired raw data for image reconstruction. As a result, the patient exposure required to obtain a given image quality increases substantially. The dose increases as the time window used for reconstruction (e.g., 150 ms) gets shorter relative to the duration of the RR interval (e.g., 750 ms for a heart rate of 80 bpm). This increase is larger for smaller pitch factors. The dose is usually increased by a factor of 3–7 as compared to ECG triggered techniques or non-triggered multislice scanning.

Various dose reduction techniques are presently being developed by the manufacturers. By positioning the heart close to the center of the scan field (patient slightly shifted to the right of the examination table), the scan angle may be reduced, thus excluding the more peripheral portions of the chest. Such a technique will cause artifacts close to the periphery of the exposed scan field (see Fig. 7.**45 c**) but these artifacts only involve the very periphery of this region and can be excluded from the display field of view. By choosing a smaller field of view (< 24 cm) centered on the heart such artifacts are no longer visible but the radiation dose to the skin and breasts is substantially reduced. Similar effects as with a reduced scan field of view can be generated by special bow-tie filters placed behind the x-ray tube that reduce the radiation dose to the periphery of the body outside the region of the heart.

ECG-controlled modulation of the tube output (ECG-pulsing) holds substantial potential for further dose reduction. With this technique, the mA is substantially (80%) decreased during the (systolic) phases of the heart cycle that are usually not used for image reconstruction (see Fig. 23.**15**). Functional imaging, however, still remains possible because image quality generally suffices for volumetric assessment of the ventricles.

Other new dose-reduction developments include edge-preserving image filtering and low-kVp scanning. In edge-preserving image filtering special postprocessing filters can reduce image noise while anatomical edges are preserved. The technique may be used to lower radiation exposure or to improve low-contrast resolution, alone or in combination with ECG-pulsing. Scanning at 80 to 100 kVp can increase contrast-enhancement in coronary CTA and coronary calcium density at the expense of a little increase in noise. The resulting dose reduction can be as high as 30%, while contrast-to-noise ratios will be preserved.

CT Fluoroscopy

CT fluoroscopy is a technique that produces constant updates of the scanned data and therefore provides fluoroscopic cross-sectional images.

Principle and Image Reconstruction

To gain a high temporal resolution despite a much longer rotation time of the x-ray tube, images are generated in a temporarily overlapping fashion. For this purpose, partial scanning is employed. Data from only slightly more than half a tube rotation are reconstructed (180° + fan angle). In addition, the 360° rotation is subdivided into sectors, and after the tube has scanned a new sector, the old one is dropped from the image and the new one is incorporated into the image. To speed up reconstruction, each sector may be reconstructed separately by filtered backprojection, and the final image is assembled simply by superimposing each sector. High refresh rates, up to 8 or more images per second, are possible with this technique (Fig. 1.**32**).

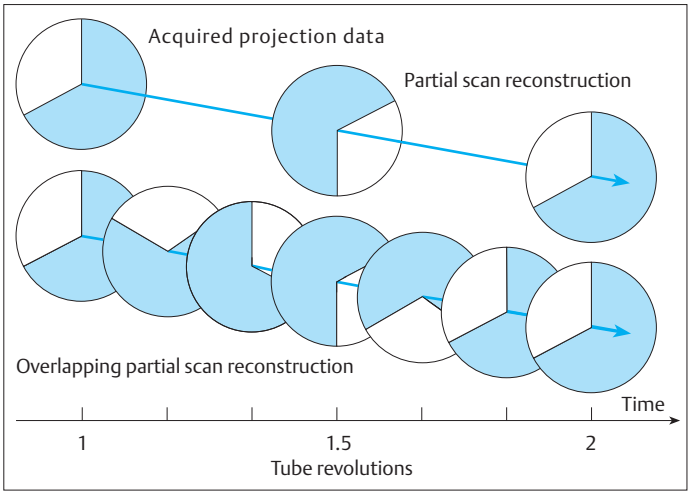

Fig. 1.**32** Principle of CT fluoroscopy. Partial scan reconstruction improves temporal resolution. Temporal overlap of images provides a fluoroscopic effect.

Technique

Fluoroscopy is employed for real-time monitoring of interventional procedures. A foot switch or table switch together with a monitor close to the gantry are necessary in order to follow the procedure. A moving table helps to find the region of interest or the needle tip interactively. However, it can sometimes be quite cumbersome to reposition the table if the needle leaves the scan plane because it is not always evident in which direction it does so.

CT fluoroscopy using a multislice scanner can be used to acquire multiple sections simultaneously and to see more easily in which direction a needle is deviating from the prescribed path. Some vendors offer the option to fuse the inner two sections (target plane), and simultaneously display and update the sections above and below this target plane (see Fig. 6.**3**). This way it is much easier to determine in which direction the needle or table have to be repositioned.

Radiation Safety

When identical mAs settings are used as for diagnostic scanning, radiation dose to the scanned section increases substantially. As compared to a 1 s conventional section, a 10 s fluoroscopy will cause 10 times the radiation exposure. For this reason, fluoroscopy always employs low mA settings, and—if possible—also low kVp settings. Too low an exposure, however, will substantially decrease image quality and may hamper the detection of the target lesion or a safe path towards the lesion. For this reason, the dose has to be adapted to the patient size (higher kVp settings in obese patients) and the organ region (higher mAs for the abdomen than for the lungs). Still, radiation dose in fluoroscopy is usually substantially higher than in a conventional CT-guided biopsy.

Usually conventional step-and-shoot techniques may be almost as fast as fluoroscopy-guided procedures, provided that there is a foot switch and display monitor in the examination room. Fluoroscopy should be reserved for difficult cases, in which conventional techniques are less safe or substantially slower (e.g., pulmonary nodules close to the diaphragm, difficult approaches in the abdomen).

Protective gloves and special instrumentation (e.g., needle holders) should be used that protect the hands of the examiner from the radiation beam.

2 Image Processing and Display Techniques

M. Prokop

Computed tomography is primarily a cross-sectional imaging technique. Even with conventional scanning, a three-dimensional body region is mapped by CT but information along the patient axis (z-axis) is only available in discrete steps. With the advent of spiral and multislice scanning, CT has moved from a transaxial to a truly volumetric imaging tool.

All techniques of two-dimensional (2D) and three-dimensional (3D) image processing rely on a set of individual axial sections acquired by CT scanning. These sections are stacked together in the computer to form a data volume that can be further processed and manipulated.

Spiral and multislice CT have revolutionized data acquisition. With proper selection of the scan parameters, 2D and 3D images of exceptional quality can be generated. This contrasts with the relatively poor quality of many 2D and 3D reformatted images in conventional CT. With multislice CT data sets, near isotropic resolution becomes standard but images suffer from increased image noise. For this reason, new noise-suppression techniques have to be developed to take full advantage of the improved spatial resolution.

There is a multitude of 2D and 3D processing techniques which are summarized in Table 2.**1**. Multiplanar reformations (MPR) are the most important 2D tools to create images in arbitrary, even curved planes through the volume. Maximum intensity projections (MIP) are popular for display of CT angiographic data sets. Shaded surface displays (SSD) have been used to visualize complex vascular anatomy and skeletal structures. Volume rendering techniques (VRT) are the most versatile rendering methods that allow for transparency as well as 3D effects. Interactive manipulation of data sets becomes more and more important the larger the data volumes become and the more complex and subtle the diagnostic questions to be answered.

Table 2.**1** Overview of selected 2D and 3D processing tools

2D Display Tools	
Cine displays	
Multiplanar reformation	MPR
Thick MPR	
Curved planar reformation	CPR
Vessel tracking	
3D Display Tools	
Maximum intensity projection	MIP
Minimum intensity projection	MinIP/mIP
Shaded surface display	SSD
Volume rendering technique	VRT
Tissue transition projection	TTP
Ray sum projection	
Segmentation Tools	
Cutting functions	
Region growing	
Dilation/erosion	
Closing functions (removal of holes)	
Removal of flying pixels (floaters)	
Watershed algorithms	
Automated bone removal	
Automated volume analysis	

Data Volume

Voxel-based vs. Grid-based Models

In conventional CT the data volume is subdivided into volume elements (voxels) in which the voxel cross-section (in the axial x–y-plane) equals the pixel cross-section, while the voxel height (along the z-axis) is defined by the section collimation (Fig. 2.**1 a**). With spiral CT, and with some conventional CT protocols as well, overlap of sections becomes possible. In addition, the section sensitivity profile is bell-shaped, and a voxel may actually contain information from adjacent voxels. This makes a *voxel-based model* of 3D image data sets hard to handle: voxels no longer have sharply defined upper and lower boundaries (due to the section profile), and voxels overlap substantially along the z-axis. Thus, a *grid-based model* is more helpful: here the center of each former voxel is used to define a 3D grid. The spacing along the z-axis then corresponds to the reconstruction increment, and the spacing in the x–y-plane corresponds to the pixel size (Fig. 2.**1 b**). Each grid intersection is assigned the CT number of the corresponding pixel in an axial CT image.

3D Sampling Function

The CT number samples information from the surrounding volume according to a sampling

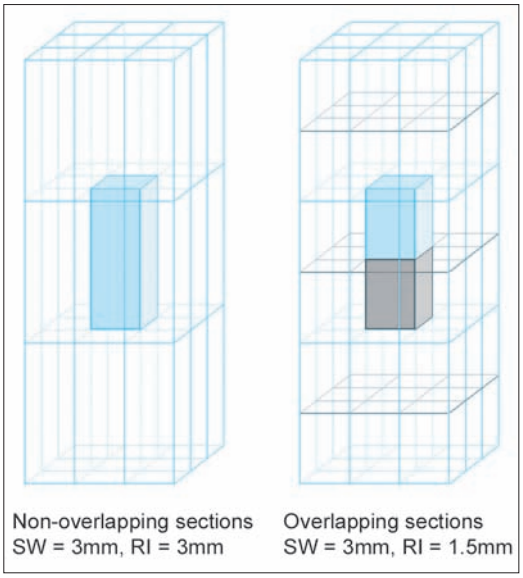

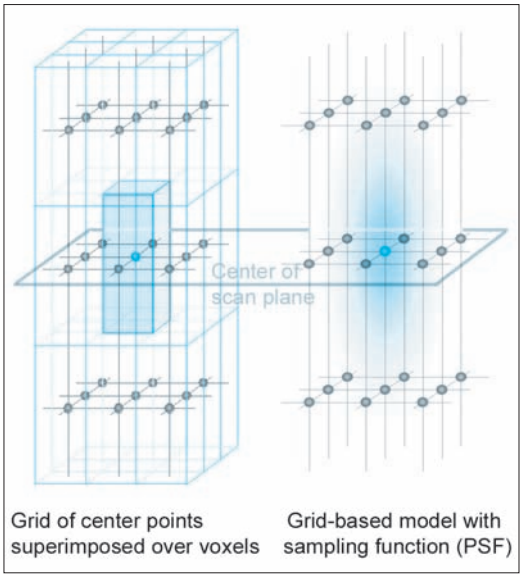

Fig. 2.**1** Representations of a 3D data volume. The voxel-based model relies on box-shaped voxels (**a**) but has a problem dealing with overlapping image reconstruction and non-rectangular section profiles. A grid-based model (**b**) assigns a node to the center of each voxel. Each node samples information along the z-axis (according to the section sensitivity profile) and within the scan plane (according to the point spread function).

function defined by the section profile in the z-direction and by the point spread function in the x–y-plane. This sampling function can be directly visualized by scanning a tiny lead bead and looking at the resulting image in the x–y-plane and the x–z- or y–z-plane (Fig. 2.**2**). As can be seen, the sampling function is not a voxel-shaped box but instead an ellipsoid with a short axis that is determined by the spatial resolution in the x–y-plane (i.e., by the convolution kernel) and a long axis that is determined by the section profile. Fig. 2.**2b** demonstrates that the sampling function is spherical for 1 mm collimation, i.e., there is no distortion along the z-axis with

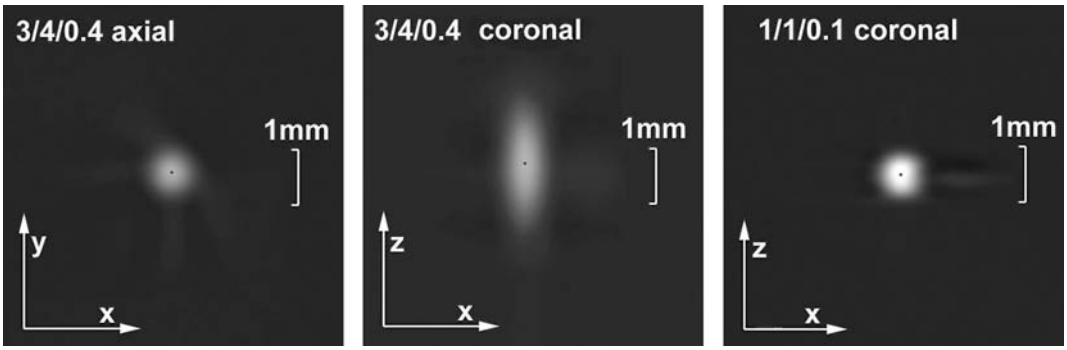

a **b** **c**

Fig. 2.**2** Sampling function (point spread function). The information sampled by each grid point in the data volume can be visualized by scanning a tiny lead bead (represented as a red dot in these images). Note that there is already blurring within the scan plane (x–y-plane) (**a**). Longitudinal distortion occurs along the z-axis for SC/TF = 3/4 (**b**). Resolution is isotropic with SC/TF = 1/1. The distortion effects along the z-axis are identical to those in the x–y-plane (**c**).

the results that there is isotropic resolution with such a scanning protocol. Note, however, that results change if a different convolution kernel (e.g., a high resolution algorithm) is used.

Secondary Raw Data Set

The more *isotropic* the data set, the better the resulting image quality of 2D and 3D reconstructions. For multislice CT, reconstruction of a secondary raw data set consisting of thin overlapping axial sections forms the basis of near-isotropic imaging. Image *noise*, however, may pose a problem with very thin sections. Increased noise may introduce artifacts in various rendering protocols and therefore should be kept low by using a sufficient radiation dose, a smoothing convolution kernel, or by applying noise-reducing prefiltering techniques.

Cine Viewing

Cine viewing is an excellent tool for evaluating large numbers of sections, be they axial or multiplanar. It is important that the user has full control of the direction and speed of such cine displays. Such mouse- or trackball-controlled scrolling can be further improved if the system allows for fast scrolling through large ranges as well as finely controlled scrolling though just a few sections of interest.

It has been demonstrated that interactive cine viewing speeds up the evaluation of large data sets, allows for more accurate assessment of complex structures that cross the sectional plane multiple times (e.g., vessels or bowel loops), improves lesion detection (e.g., in the lungs or the liver), and increases productivity in picture archiving and communication systems (PACS) environments. Cine viewing becomes the primary mode of evaluation with multislice CT because of the large number of images to be viewed.

Pitfalls

In the initial phase, when moving from film reading to interactive cine viewing, there may be an increased risk of missing findings. The reason is that film reading is more pattern-based than interactive viewing: any finding that lies outside the normal will be detected by an experienced viewer, even if it is located in unusual sites (e.g., cutaneous metastases). With cine viewing, the radiologist has to evaluate each organ system at a time, which means that many radiologists will have to change their normal search pattern.

Multiplanar Reformations

Principle

Multiplanar reformations (MPRs) are two-dimensional reformatted images that are reconstructed secondarily in arbitrary planes from the stack of axial image data (Fig. 2.**3**). Coronal or sagittal reformations are generated by extracting and displaying only those voxels from the data volume that are positioned one above the other within the coronal or sagittal plane. Oblique or curved reformations are constructed in an analogous fashion, but the image data must be interpolated between adjacent voxels.

Defining the Plane of Image Reformation

The image plane for a MPR is defined interactively on a workstation using a suitable reference image, which may consist of an axial image, another MPR, or a 3D image such as a maximum intensity projection (MIP) or a shaded surface display (SSD). By drawing a "cut line" on the reference image, the radiologist defines a section that is perpendicular to the reference image. The cut line may be drawn in any direction (orthogonal, oblique, or curved).

Curved-planar reformations (CPR) are generally needed to depict structures that pass through multiple axial planes of section (e.g., a bronchus or blood vessel). In these cases it is necessary to have a workstation that allows the user to define the reformation plane on multiple reference images because the structure of interest usually leaves and enters the reference images repeatedly. For depicting tubular struc-

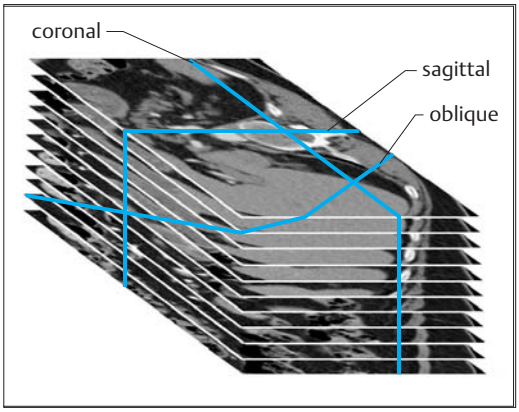

Fig. 2.**3** Principle of multiplanar reformation (MPR). The images are reconstructed from a "stack" of axial slices.

tures, software is currently available that provides semiautomatic positioning of the cut line and keeps the line centered on the structure of interest (Fig. 2.**4**). Ideally only a few reference points have to be dropped on the structure of interest (usually a vessel), and the software should automatically generate a centered path through these regions (*vessel tracking*).

Thick MPR

As a rule, MPRs have a width equal to one voxel. Averaging a series of adjacent data points perpendicular to the reformatted plane can produce reformations with a greater section thickness (thick MPR). This is advantageous because it leads to reduced image noise and improved image quality (Fig. 2.**5**). This is an efficient technique to keep image noise low without losing in-plane spatial resolution, especially with thin-section multislice CT data sets. As with MRI, high-quality sections of arbitrary angulation can be obtained with a section width of 1–7 mm, depending on the clinical indication.

The effect of noise-reduction by creating thicker sections is direction-dependent. Along the z-axis, image noise is highly correlated: even with highly overlapping reconstruction, the CT numbers on adjacent sections will not change much if a large section collimation was used. This will result in a suboptimal noise suppression along the z-axis when thick axial MPR are reconstructed (Fig. 2.**6**). In the axial (x–y) plane, image noise is hardly correlated between adjacent pixels unless very small fields-of-view have been used for image reconstruction. Thus, CT numbers in adjacent pixels change due to variations in noise. On MPRs perpendicular to the axial plane, noise therefore cancels out rapidly if multiple pixels are averaged and thicker MPRs are created (Fig. 2.**6c**). With thin collimation, however, the difference between axial and coronal or sagittal reformations becomes smaller because correlation of noise along the z-axis decreases substantially.

In summary, the image quality in coronal or sagittal reformations (perpendicular to the axial scan plane) can be greatly improved by increasing the section thickness to several millimeters. Thick axial reformations (parallel to the scan plane) can only be recommended when the CT data has been acquired with thin sections. Thick axial reformations are therefore mainly used in multislice CT. Note that excessive section thickness in the MPR leads to troublesome partial volume effects.

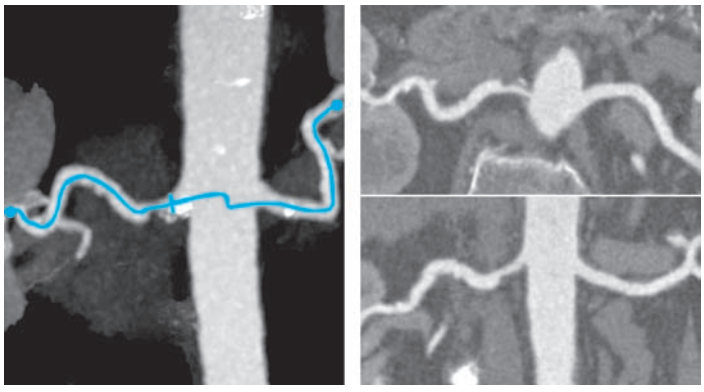

Fig. 2.**4** Vessel tracking uses seed points that are dropped on a vessel (e.g., using MPR or MIP) to find the center of the vascular structure that connects these points (**a**). The resulting image can then be rotated around this centerline, allowing for detailed analysis of the vessel wall (**b**).

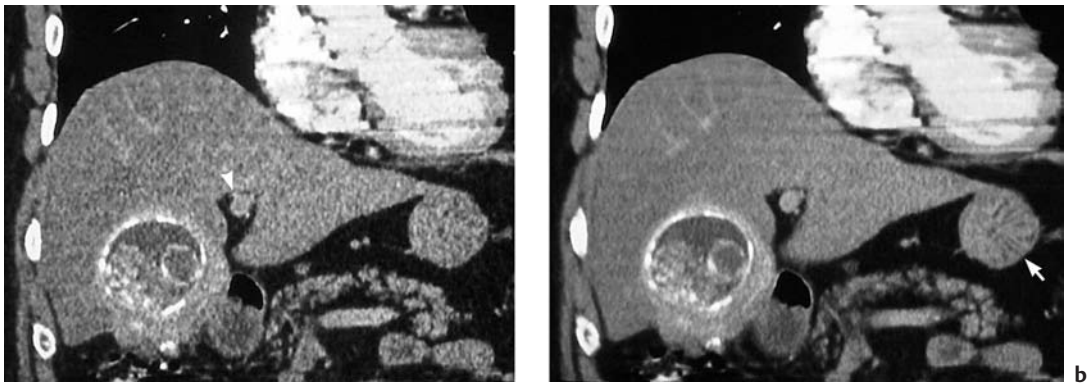

a b

Fig. 2.5 If image noise is high (especially for thin-section imaging), the quality of MPR can be improved by increasing the width of the section: (**a**) 1 pixel wide (0.6 mm), (**b**) 5 pixels wide (3 mm) coronal sections from a 4 × 1 mm multislice CT data set. Note that low-contrast resolution improves and the gastric folds can be better delineated (arrow) while the partial volume effects through the imaging plane also increase and small detail may vanish (arrow head).

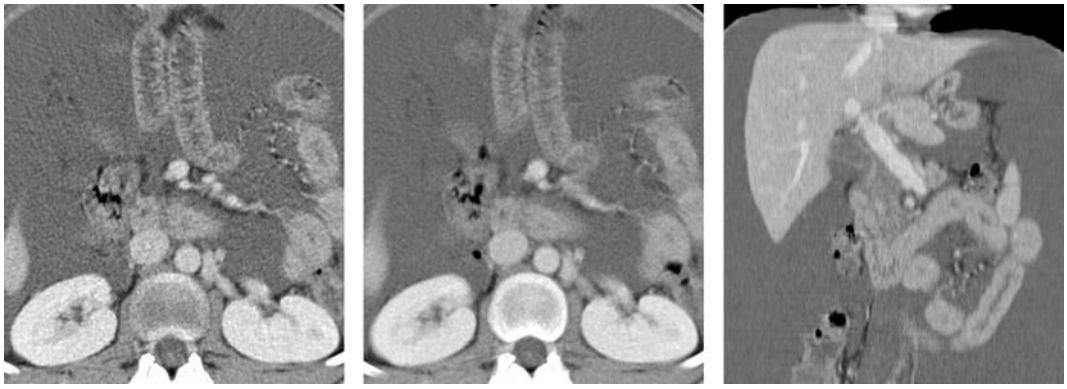

a b c

Fig. 2.6 Thick axial MPR. Because section width (z-axis) is usually larger then the pixel size (x–y-plane), axial sections have to be thicker than coronal sections to efficiently reduce image noise unless very thin collimation has been used. Primary 3 mm thick axial section from a 4 × 2.5 mm multislice CT data set (**a**). Image noise on a 7.5 mm thick axial MPR (**b**) is identical to noise on a 3 mm thick coronal MPR (**c**).

Ray-Sum Projection

For a ray-sum projection, the CT numbers encountered in the viewing direction are averaged or added together. Thus, a simple ray-sum projection is identical to a (very) thick MPR. The result simulates a conventional radiograph of the selected imaging volume (Fig. 2.7). If a threshold range is preassigned, only voxels with CT numbers within that range are averaged.

Summed projections from an imaging volume in which the bony structures were removed result in DSA-like images. This effect can be enhanced if a threshold value above the soft-tissue range (e.g., > 80–100 HU) is used as well.

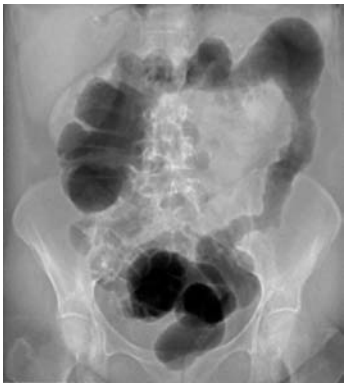

Fig. 2.7 Ray-sum projection (80 mm thick MPR) of the CO_2-filled colon (CT colonography) in a patient with Crohn's disease.

Artifacts

The quality of MPR images is best in imaging planes that deviate little from the scan plane. At the same time, the resolution along the z-axis affects all sections that are perpendicular to the scan plane. The smaller the section width and the smaller the reconstruction interval, the better the image quality (Fig. 2.**8**).

Section-by-section scanning and large section thickness in conventional CT generally lead to stair-step artifacts in reconstructions that are perpendicular to the axial plane. Spiral or multislice CT are much less vulnerable to such step artifacts because of overlapping image reconstruction. Good-quality MPRs require an overlap of some 30–50% of the section width. Thin collimation (for scanning) and thin section width (for data reconstruction) yield reformatted images of outstanding quality in any plane of section desired. Thicker collimation leads to loss of sharpness along the z-axis (Fig. 2.**8**).

For objects outside the center of the gantry or interfaces that are oriented obliquely but almost parallel to the scan plane (such as the calvaria, tibia plateau or wrist bones) step artifacts and serrations of contours may also occur with spiral or multislice CT data sets if larger pitch factors are used (Fig. 2.**9**). These artifacts can be caused by the data interpolation process and by undersampling of data in z-direction.

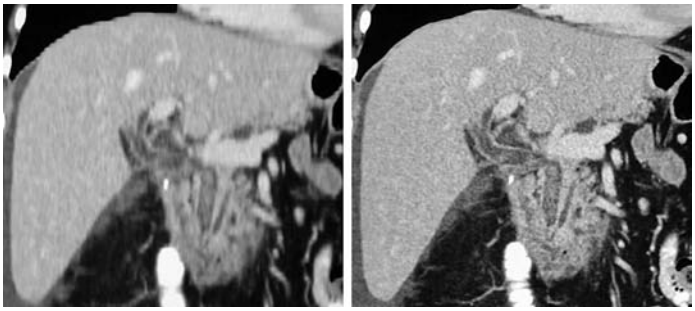

a b

Fig. 2.8 Using thinner collimation (e.g., 4 × 1 mm instead of 4 × 2.5 mm) improves the quality of reformatted images. (**a**) SW/RI = 3/2.5, (**b**) SW/RI = 1.25/0.7. Note the improved delineation of the choledochal wall.

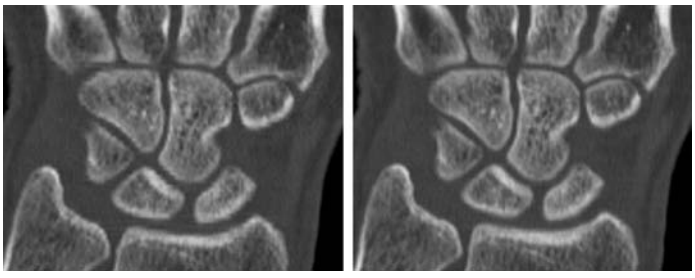

a b

Fig. 2.9 Step artifacts and serration artifacts occur in multislice CT data sets at high-contrast interfaces oblique to the scan plane if higher pitch factors are used. MPR of the wrist bones scanned with 2 × 0.5 mm collimation at a pitch P = 1.5 (**a**) and at a pitch of 0.8 (**b**).

Applications

Multiplanar reformations are seldom worthwhile in conventional CT, because generally the image quality is too poor to yield substantial additional information. Spiral and multislice CT, however, open up many new potential applications for multiplanar imaging. The fact that MPRs have been underutilized in the past was due primarily to a lack of user-friendly software.

Anatomically Corrected Data Sets

MPRs can compensate for faulty *positioning* and can provide symmetrical images for improved side-to-side comparisons (of the inner ear, neck, pelvis or shoulders, for example).

Especially for coronal reformations, the MPR should be positioned parallel to the most important anatomic structures (e.g., the posterior ribs or the pelvis) to improve anatomical orientation. Tilted MPR may be helpful for the chest (parallel to the trachea or parallel to the sternum) or for the abdomen (parallel to the abdominal aorta). Appropriate tilting will ensure that important anatomic detail are sectioned longitudinally. In general, similar cut planes can be used as in MRI.

Problem-solving

MPRs can be used as a problem-solving tool in cases where it is necessary to trace pathologic structures through multiple planes and in cases that require imaging in a second plane. In spiral CT this applies consistently to skeletal investigations, frequently to CT angiography, and occasionally to investigations of tumors involving the liver, kidneys, or lower abdominal organs (Fig. 2.**10 a**). With thin-section multislice CT the role of MPR is vastly increased. MPRs are important for defining the relation of focal lung lesions to the pulmonary fissures, chest wall and mediastinal structures, for assessing lymph nodes in all three planes, for defining tumor infiltration into adjacent structures, and for evaluating the bowel and structures of the small pelvis. Curved planar reformations are essential for delineation of soft plaques in CTA (see Fig. 2.**4 b**), evaluation of the pancreatic duct in one image (Fig. 2.**10 b**), or for the display and differentiation of ureteral stones from paraureteral calcifications.

Noise Reduction in Standard Displays

Thick MPRs can be employed as the most important technique for *noise reduction* when thin collimation has been used to acquire a data set (see Fig. 2.**5**). The technique can be applied to spiral CT as well as to multislice CT data. Thick axial MPR can substitute for reconstructing thick axial sections directly from the raw data set. Thick MPR are a way to increase image quality substantially in *low-dose applications* of multislice CT (see Figs. 5.**16**–5.**18**).

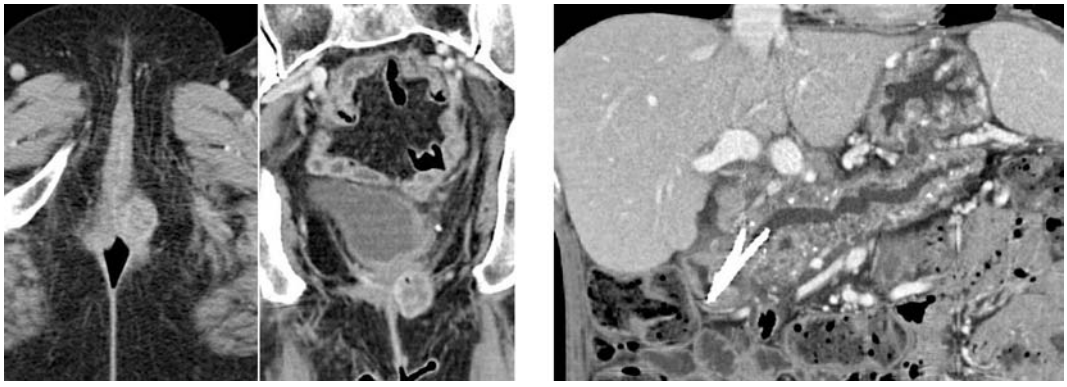

a **b**

Fig. 2.**10** Examples of applications of MPR:
(**a**) The relation of this tumor recurrence to the muscles of pelvic floor is better appreciated on the coronal MPR. (**b**) Excellent overview of the pancreatic duct in a patient with chronic pancreatitis and stents in the pancreatic and common bile ducts.

Image Analysis and Documentation

When MPR is used selectively to answer a question that cannot be resolved in the axial plane, it is usually best to perform the reformation interactively on a workstation. Software should be used that provides a "soft" transition between the reformatted sections when the imaging plane is changed. Abrupt transitions may cause lesions to be missed.

Most modern CT workstations are now able to do that. They process the secondary raw data sets with hundreds of images in real time, which requires updating the displayed image 5–15 times per second. Under such conditions, image analysis can be performed truly interactively on the whole data volume using thick MPR or volume rendering. With multislice data, this will become the evaluation technique of choice.

In situations where it is important to document one or more additional planes, such as sagittal and coronal reformatted images of the calcaneus, a standard protocol can be established that allows the CT technicians to compute and document the sections. To ensure the best image quality, the width of the MPR should be appropriate for the region under study (Table 2.**2**).

Table 2.**2** Recommended section width (SW) of axial, coronal, and sagittal reformations

Region	Suggested width (SW) of MPR (mm)		
	axial	coronal	sagittal
Neck			
Routine	3	2	3
Larynx	2	1.5	2
Chest			
Routine	5–7	–	–
Bronchial system	1.5	1.5/10	–
Peripheral tumors	1.5	1.5	1.5
Chest wall	3–5	3	5
Mediastinum	3–5	3	5
Abdomen			
Routine	5–7	–	–
Liver (tumors)[a]	3–5	3–4	3–5
Pancreas (tumors)[a]	3–4	3	3–5
Kidneys (tumors)[a]	3–5	3–4	3–5
Bowel[a]	3–5	3–4	3–5
Small pelvis[a]	3–5	3–4	3–5
Musculoskeletal system			
Cervical spine	1	1	1
Thoracolumbar spine[a]	2–3	2	3
Pelvis[a]	2–3	2	3
Foot	1	0.75	1
Hand	≤ 1	0.75	0.75

[a] depending on patient size

Maximum Intensity Projection (MIP)/Minimum Intensity Projection (MinIP)

Principle

Maximum intensity projection (MIP) and minimum intensity projection (MinIP or mIP) are volume-rendering techniques in which suitable editing methods are used to define the volume of interest (VOI). All of the CT image data set may be used, or the volume may be confined to a region of interest. In the most difficult case, only selected organ systems are included or excluded from the VOI.

The actual images are generated by projecting the volume of interest into a viewing plane and displaying the maximum CT numbers (for MIP) or the minimum CT numbers (for MinIP) that are encountered along the direction of the projection, called the viewing angle (Fig. 2.**11**). Both techniques ensure that optimum contrast is produced between small, high-contrast structures and surrounding tissues.

MIP views are used for CT angiography and for specialized pulmonary studies, while MinIP views are used mainly for visualizing the central tracheobronchial system. The following discussion of the use of MIP in CT angiography also applies to other MIP applications and to MinIP views.

Attenuation Information

MIP preserves the attenuation information of structures with maximum CT numbers, so an anteroposterior viewing angle in most body regions would display skeletal structures rather than contrast-enhanced vessels. Thus, unlike MR angiography, some view angles in CTA make

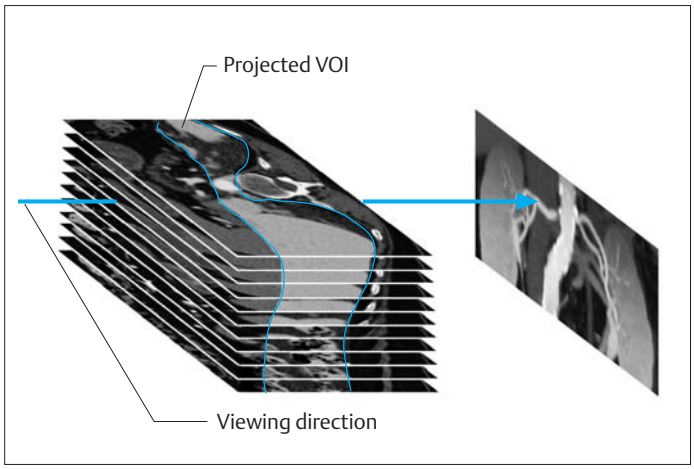

Fig. 2.**11** Principle of the maximum intensity projection (MIP). This technique displays the maximum CT numbers that are encountered along the view angle of the projection. Vascular imaging requires editing of the data volume to eliminate bony structures.

it necessary to edit bony structures out of the CT image. This editing process may be done manually, semiautomatically, or automatically, depending on available workstation software (see Segmentation, p. **73**).

A major advantage of the MIP view is that contrast-enhanced vessels can be distinguished from wall calcifications by their different attenuations (Fig. 2.**12 a**). Even small vessels (1 mm or less in diameter) will be visualized as

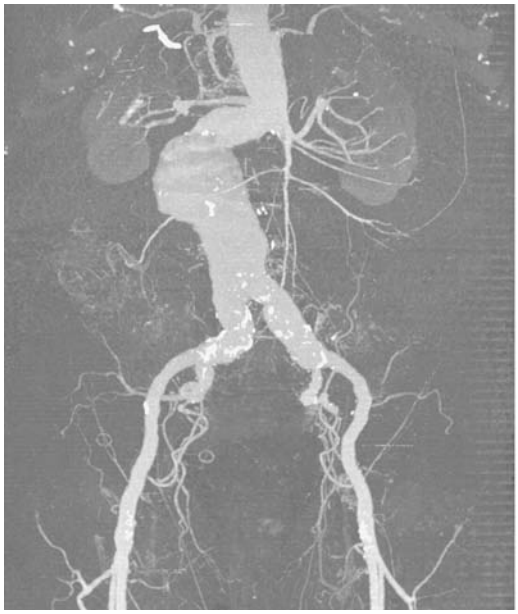

a

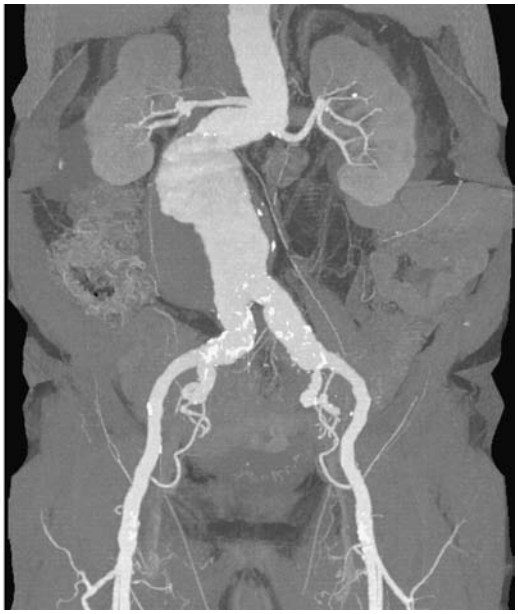

b

Fig. 2.**12** MIP of the abdominal aorta. (**a**) When the projected volume encompasses the whole body, all vessels are superimposed over each other. Calcifications are well displayed, but thrombi are not directly visualized. There are linear artifacts in the periphery of the image (due to variations in image noise related to spiral interpolation). (**b**) Reducing the width of the VOI (curved thin slab MIP) improves the contrast between small vessels and the background. Superimposing mesenteric vessels are removed and the thrombus becomes visible. Note that there are small bilateral renal artery aneurysms.

long as they have a higher CT number than their surroundings within the VOI.

Image Background

The image background depends on the voxels with the highest CT numbers in the structures surrounding the vessels.

If the surroundings are homogeneous, the MIP will display voxels that have the highest CT numbers based on statistical fluctuations (i.e., image noise). Because of this, an increase in image noise in the original data set is associated with an increase in background attenuation in MIP images.

Arterial vessels generally have heterogeneous surroundings consisting of fat, unenhanced soft tissues, contrast-enhanced organs, and venous vessels. As the CT number of the surrounding structures increases, so does the background attenuation. It is therefore important to exclude as much contrast-enhancing surrounding structures from the VOI as possible in order to optimize vessel-to-background contrast (Fig. 2.**12**).

Image Contrast

Image contrast in MIP images is determined both by the CT numbers of the vessels of interest and by the difference between these CT numbers and the background attenuation. Accordingly, MIP image contrast increases with the level of intravascular contrast, and it decreases as a result of partial volume effects (which reduce the attenuation of small in-plane vessels) and as a result of higher background attenuation.

For the evaluation of small blood vessels such as the renal arteries, the scans should be performed with a thin collimation, optimum intravascular contrast should be achieved, and background attenuation should be kept as low as possible. Background attenuation can be minimized by selecting a thin VOI in the direction of the projection and by eliminating all higher-attenuating superimposed structures such as contrast-enhanced organs or venous vessels by proper segmentation techniques.

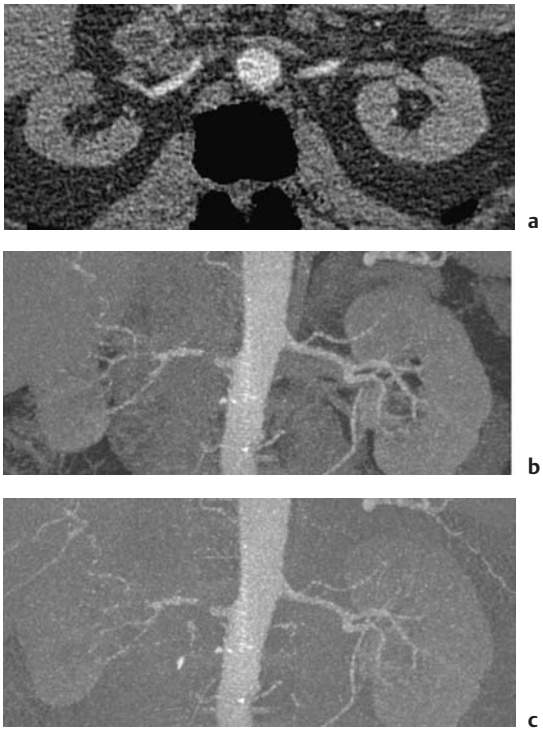

Fig. 2.**13** Image noise on MIP. (**a**) Axial section after bone removal in a very obese patient. (**b**) Noise in small vessels remains unchanged but noise in the aorta and the background is reduced on MIP images (here, 1 cm slab width). (**c**) Background attenuation on MIP images increases and the background noise decreases as the projected VOI becomes wider (here, 5 cm slab width)

For optimum image quality in the MIP (or MinIP) view, the volume of interest (VOI) should be as thin as possible (Figs. 2.**12** and 2.**13**).

Viewing Angle

Given the different degrees of spatial resolution within the scan plane and along the z-axis, better image quality is obtained with axial viewing angles (i.e., nearly parallel to the z-axis) than with perpendicular view angles (e.g., anteroposterior or lateral).

Where feasible, it is advantageous to render the MIP in a craniocaudal or slightly oblique direction. For evaluation of the renal arteries, the projection can be limited to the few sections that actually contain the vessels. An oblique projection can separate the aorta from the vertebral column, thereby eliminating superimposed structures and avoiding the need for a more complex segmentation process (see Fig. 24.**75 a**).

Cine Loop

A single MIP conveys only two-dimensional information; it does not encode depth relationships. Consequently the foreground and background are not differentiated (Fig. 2.**12 a**), and a superimposed structure can obscure a less attenuating (usually smaller) vessel.

Generating multiple images at constant angular intervals and viewing the images from various perspectives in a cine loop can improve 3D orientation.

Image Noise

Image noise in the axial data set will propagate to MIP images in a more complex fashion than noise in thick MPR. In a homogenous region, noise leads to random deviation of CT numbers from the "real" CT attenuation is this region. MIPs display the pixels with maximum CT numbers, i.e., those pixels with maximum deviation from the real CT numbers. Because of noise, the CT numbers on MIP images of a homogenous region grow, the wider this region is (and thus, the more pixels are traversed). The bell-shaped histogram of CT numbers in a homogenous region indicates that the probability of encountering a higher CT number decreases the more this number deviates from the real attenuation. Thus, the wider the homogenous region that is projected, the smaller the resulting image noise on a MIP. If only a small homogenous region (such as a small vessel) is projected, image noise is largely unaffected by MIP.

- Noise in small vessels remains unchanged but background noise is reduced on MIP images (Fig. 2.**13 b**).
- Background attenuation on MIP images increases and the background noise decreases as the projected VOI becomes wider (Fig. 2.**13 c**).
- Contrast between small vessels and the background is improved if a thin slab is used (Fig. 2.**12**).

Only if noise on the original image is excessive, such as for low dose applications of multislice CT, image noise on MIP images remains high

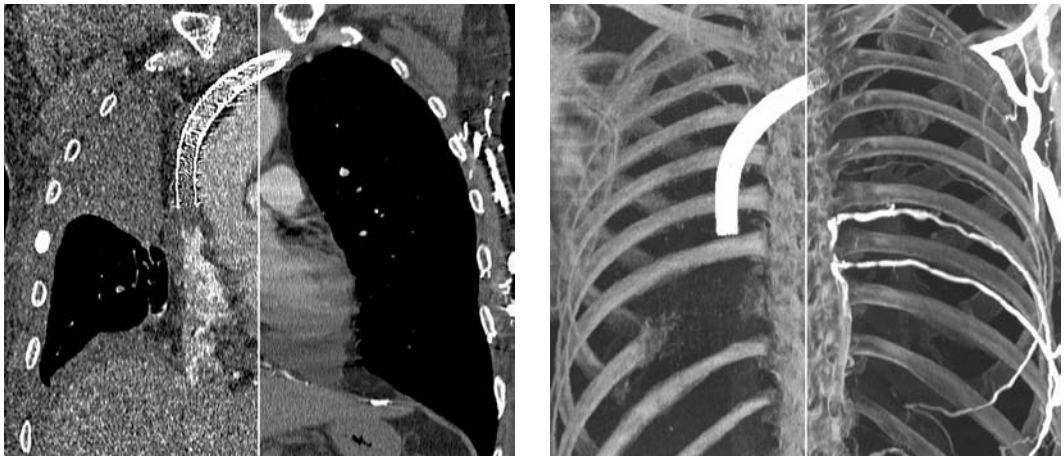

a **b** **c** **d**

Fig. 2.**14** Noise-reduced MIP. High image noise (due to an high resolution filter kernel) on the MPR (**a**) leads to MIP of suboptimum quality with losss of bony detail (**c**). Reconstructing 3 mm thick coronal sections (**b**) and using those for MIP substantially improves image quality (**d**).

and may obscure diagnostically relevant information. In such a situation, we suggest improving image quality by creating an overlapping set of thick MPR first (in the same orientation as the final MIP; e.g., coronal MPR for anterior-posterior MIP), and then reconstructing an MIP from this noise-reduced data set. Such a technique (noise-reduced MIP, nr-MIP) is excellently suited for large vessels but may reduce the contrast of small structures (Fig. 2.**14**).

Thin-Slab MIP

As noted above, a thin VOI can improve the quality of the MIP image. In a technique called *thin-slab MIP*, this is accomplished by dividing the imaging volume into multiple thinner subvolumes, called "slabs," that have a specified thickness ranging from a few millimeters to several centimeters. A maximum intensity projection is then performed on each slab. An axial view angle is preferred with spiral CT because of better spatial resolution. In multislice CT, thin-slab MIPs in arbitrary planes become feasible.

By generating overlapping thin-slab MIPs and surveying the images interactively (*sliding thin-slab MIP*) one can improve spatial orientation and can cover the whole scan range.

Comparing a thin-slab MIP view of designated thickness with an axial section or MPR of the same thickness, we note that the spatial resolution is identical. Small structures of high contrast (e.g., pulmonary vessels) decrease in contrast with increasing width of the axial section or MPR as a result of partial volume effects, but the contrast on MIP images remains fairly constant regardless of the width of the slab used for the MIP (Fig. 2.**15**).

Minimum Intensity Projections (MinIP)

The imaging characteristics and artifact behavior of minimum intensity projections (MinIPs) are analogous to those of MIPs. They will be discussed for imaging of the tracheobronchial system. As a rule, only the central portions of the tracheobronchial system can be evaluated with this technique.

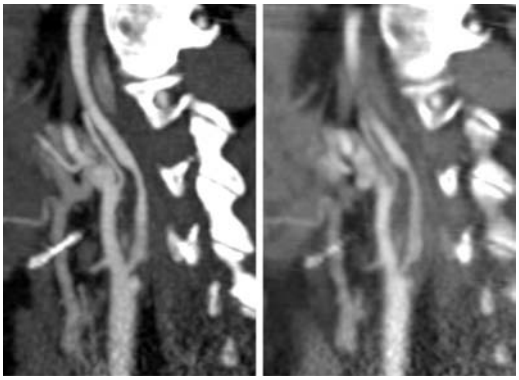

a **b**

Fig. 2.**15** Comparison of a thin slab MIP (**a**) and a thick CPR (**b**) each of 10 mm width. Note the better contrast with MIP and the lower noise with MPR.

Image Contrast, Noise and VOI

The greater the attenuation difference between air-filled bronchi and surrounding tissues, the more clearly the bronchi will be visualized. While MinIPs will clearly define bronchi that are surrounded by structures of soft-tissue density (mediastinum or consolidated lung), they will rarely delineate bronchi that are surrounded by aerated lung parenchyma or emphysematous lung (Figs. 2.**16** and 2.**17**).

MinIP created from high resolution data sets will suffer from the increased noise, which will cause a reduction in background density (similar to the increase in background density with MIP) and will obscure bronchi. This effect increases with wider VOI (Fig. 2.**16**)

As a rule, intrapulmonary bronchi or bronchi obscured by superimposed lung parenchyma are depicted only if they have an attenuation value of approximately –1000 HU. The attenuation values of smaller bronchi are increased due to partial volume effects. Especially when oriented roughly parallel to the scan plane, small and even medium-size bronchi will not be visualized in sections that are more than 3 mm thick. The thinner the sections, the better the image quality.

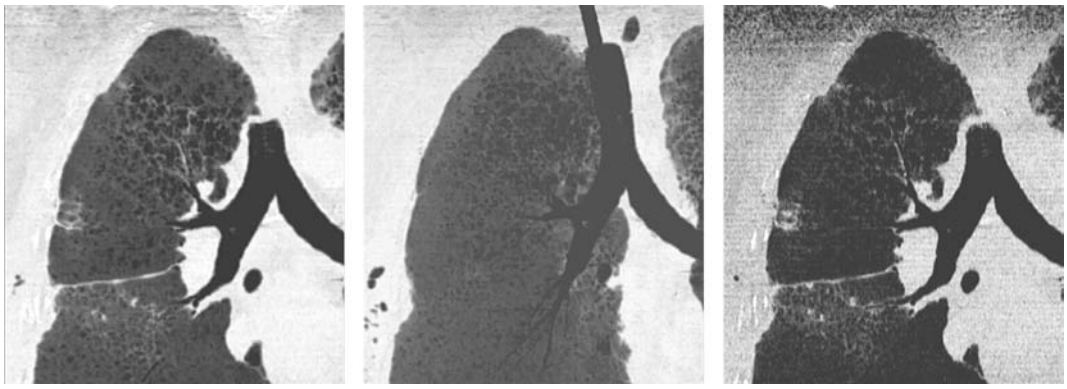

a b c

Fig. 2.**16** Minimum intensity projection (MinIP). (**a**) A narrow VOI (1 cm) in this patient with pulmonary fibrosis and centrilobular emphysema displays the central bronchi and the distribution of the small bullae to good advantage. Note that the fibrotic changes cannot be securely detected. (**b**) Increasing the width to 3 cm substantially decreases the distinction of bullae and the display of the upper lobe bronchi. (**c**) Using a noisy high-resolution data set for MinIP decreases background density and makes evaluation of the lung parenchyma virtually impossible.

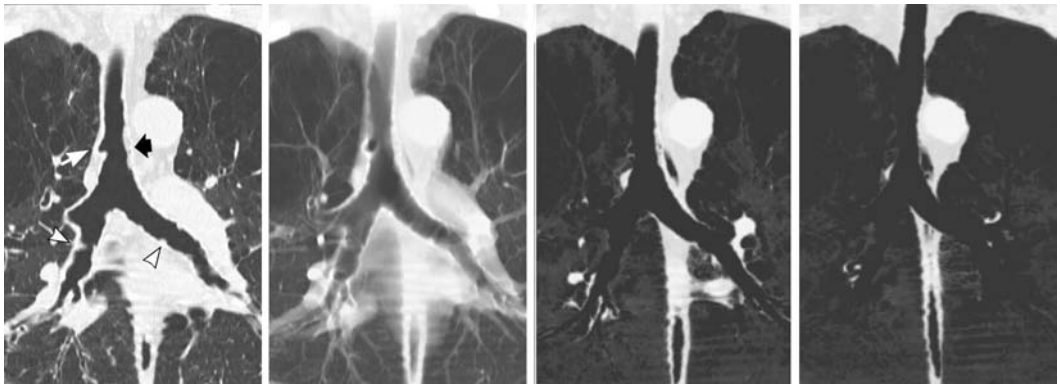

a b c d

Fig. 2.**17** Comparison of MPR and MinIP in a patient with a tracheal diverticulum (arrow), multiple tracheobronchial polyps (arrowheads), mucus in the trachea (wide arrow) and marked emphysema. (**a**) 1 pixel thick MPR, (**b**) 10 mm thick MPR, (**c**) 10 mm thick MinIP, (**d**) 3 cm thick MinIP. Note that the polyps and the mucus are easily missed on MinIP, and that the emphysema makes evaluation of more peripheral bronchi impossible.

Imaging Volume and Viewing Angle

A basic concern in the segmentation of MinIPs is to eliminate superimposing air from the imaging volume. This air may be extracorporeal or be any air present in soft tissues or in a pneumothorax. Otherwise the extremely low attenuation value of the air will obscure the bronchi.

When an anteroposterior viewing angle is used, the imaging volume should be selected so that the central portions of the tracheobronchial system are displayed while the VOI is kept as thin as possible (Figs. 2.**16** and 2.**17**). An attempt should be made to include a minimal amount of paramediastinal lung tissue in the VOI, as this would cause an unacceptable reduction in bronchial contrast.

When a craniocaudal (axial) viewing angle is used, a somewhat broader imaging volume (2–5 cm) can be selected. Any greater thickness of the VOI would generally lead to excessive superimposition of bronchial structures. A lateral viewing angle is rarely feasible.

Artifacts and Pitfalls

CT Angiography

If the selected VOI is too wide or if surrounding structures of higher attenuation are present, smaller vessels with CT numbers less than or equal to the *background attenuation* may be missed. This is often a result of partial volume effects or insufficient arterial contrast.

Intravascular lesions such as mural thrombi or soft plaques often cannot be directly visualized with MIP. However, partial volume effects between a soft plaque and the opacified vessel lumen can cause an apparent decrease in luminal attenuation in the affected region.

Intimal flaps due to dissection can be detected only if they are precisely parallel to the MIP viewing angle (Fig. 2.**18 a, b**). If the true lumen and false lumen show different degrees of contrast enhancement, the width of the higher attenuating lumen will generally be overestimated unless the projection is parallel to the intimal flap.

Calcifications have a higher attenuation and therefore superimpose on vascular structures. They are optimally detected on MIP images. At the same time it may become impossible to estimate the degree of a stenosis caused by a hard plaque (Figs. 2.**18 c, d**). For optimum evaluation of stenoses caused by hard plaques, curved planar reformations are necessary.

Pulmonary MinIP and MIP

Contour irregularities can be appreciated only when they are defined in a profile view. Thus, minimum intensity projections tend to underestimate the extent of *endobronchial lesions*, or miss them entirely if they are small, due to the obscuring effect of superimposed endobronchial air (Fig. 2.**17**). Consequently, MinIPs are not useful for the detection of intraluminal tumors.

Vascular pulsations transmitted to the lung tissue and respiratory artifacts can cause areas of low attenuation to appear at the point of vascular branching. This creates multiple focal hypoattenuating lesions on *MinIP* images, especially in the retrocardiac space, that may simulate emphysema.

Pulsation of the retrocardiac vessels can lead to artifactual beading of the vessels on pulmonary *MIP*, even when individual sections are reconstructed in an overlapping fashion.

When relatively *thick slabs* are used for pulmonary MIP, there may be rare cases in which small structures (e.g., pulmonary nodules) are obscured by larger ones (e.g., pulmonary vessels).

If the selected imaging volume is too broad, MinIP can only visualize the central potions of the bronchial system (Fig. 2.**17 d**). Failure to eliminate extracorporeal air from the imaging volume results in “black images”.

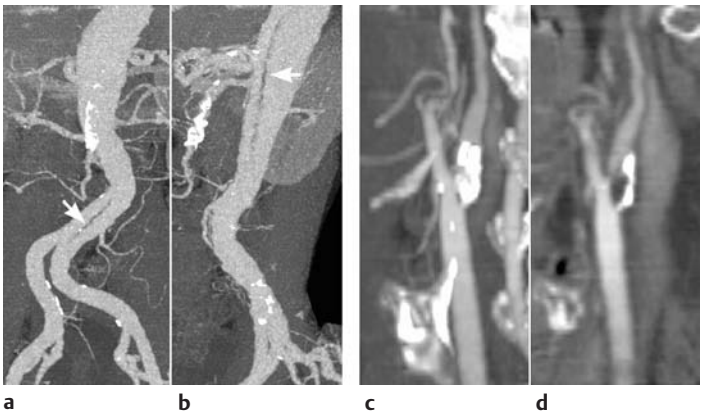

Fig. 2.**18** Artifacts in CT angiography. (**a**, **b**) Intimal flaps in aortic dissection are only displayed when the flap is parallel to the projecting direction. (**c**, **d**) Calcifications may superimpose on vascular structures and can make the evaluation of stenoses impossible. Compare MIP (**c**) to CPR (**d**).

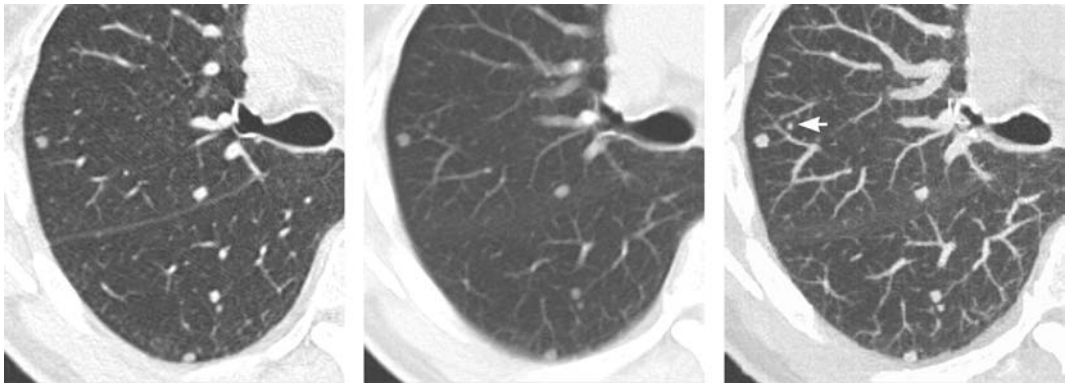

a b c

Fig. 2.**19** Sliding thin-slab MIP for nodule detection. Compare (**a**) 1.25 mm thick axial section, (**b**) 5 mm thick axial section, and (**c**) 5 mm thick MIP. Note that the high contrast of the 1.25 mm thick section is retained in the MIP while differentiation between vessels and nodules is improved.

Applications of MIP and MinIP

MIPs are mainly used to present findings of *CT angiography*. They are best suited for visualizing abdominal arteries (see Fig. 2.**12**) and the pelvic and lower limb vessels. MIPs are useful for thoracic studies only if the anatomic relationships in the imaging volume are relatively simple. MIPs are not recommended for the evaluation of complex vascular malformations, aortic dissections, central pulmonary emboli, or free-floating clots.

Thin-slab MIPs are useful for imaging small *pulmonary lesions* in cases where thin collimation has been used for data acquisition. They improve the detection of small pulmonary nodules (Fig. 2.**19**). Diffuse lung diseases can be detected more accurately and at an earlier stage than with other methods. The images combine the high contrast of a thin section with the superior anatomic orientation of a thicker section.

Minimum intensity projections are used in evaluations of the *central tracheobronchial system*. They may be useful for the localization of extrabronchial air collections or bronchial abnormalities (Fig. 2.**17**) and for demonstrating strictures, concentric stenoses, and dilatations, but MinIPs have very limited applications in the detection of tumor-associated changes. Minimum intensity projections are a sensitive tool to display *parenchymal density*, in particular obstructive pulmonary disease and emphysema (Fig. 2.**16**).

Thin-slab MinIP can be applied for evaluation of the *intrahepatic bile ducts* and the *pancreatic duct*.

3D Surface Rendering (Shaded Surface Display)

Principle

A shaded surface display (SSD) is a surface-rendered image that provides a realistically looking three-dimensional view of the surface of a structure of interest within the acquired volume data set.

When creating a SSD, it is first necessary to define the “3D object” of interest, such as the bony pelvis or abdominal aorta. This process of separating the object from the background, called *segmentation*, may be quite simple or extremely difficult depending on the object contrast. The simplest segmentation process is to define a 3D object by selecting a suitable range of CT numbers (e.g., all voxels whose attenuation exceeds a threshold value of 150 HU).

A three-dimensional display of the object surface is created by illuminating the object with one or more virtual light sources and then computing and displaying the intensity of the light that is scattered back into the plane of observation (Fig. 2.**20**). At each point in this plane, the data points of the object that are encountered first in the viewing direction are used to generate a 3D surface image. The distance of the surface from the light source and the surface gradient of the CT densities are used to create shadowing effects and heighten realism of the 3D display.

Most programs allow only one virtual light source to be used. By varying the position of the light source details of the object surface can be high-lighted differently. With some programs, multiple objects can be displayed simultaneously and encoded in various colors.

The projection of the object into the viewing plane can be done either by casting parallel rays (*orthographic rendering*) or by casting rays from a virtual eye on to the object (*perspective rendering*). While orthographic rendering is excellent for gaining an overview of the spatial relationship of structures, perspective rendering with various viewing angles (usually 15°–90°) allows for maneuvering through the data volume and is the prerequisite for techniques such as virtual endoscopy.

The quality of the SSD depends on the scan parameters, as in a 2D reformatted image, but generally the effect is less obvious because of the considerable amount of information that is lost in the thresholding process. A more important determinant of SSD image quality is object segmentation, especially the selection of the segmentation threshold.

Threshold Selection and Size Representation

The optimum threshold value for segmentation is the value that depicts a structure in its true, complete size. In theory, this value is midway between the CT number of the object (e.g., the aorta) and that of its surroundings (i.e., surrounding fat or other soft tissues). We know from practical experience that the theoretical value should be reduced by about 10%, depending on various imaging parameters. However, only structures that are larger than the section width SW will be portrayed at their true size.

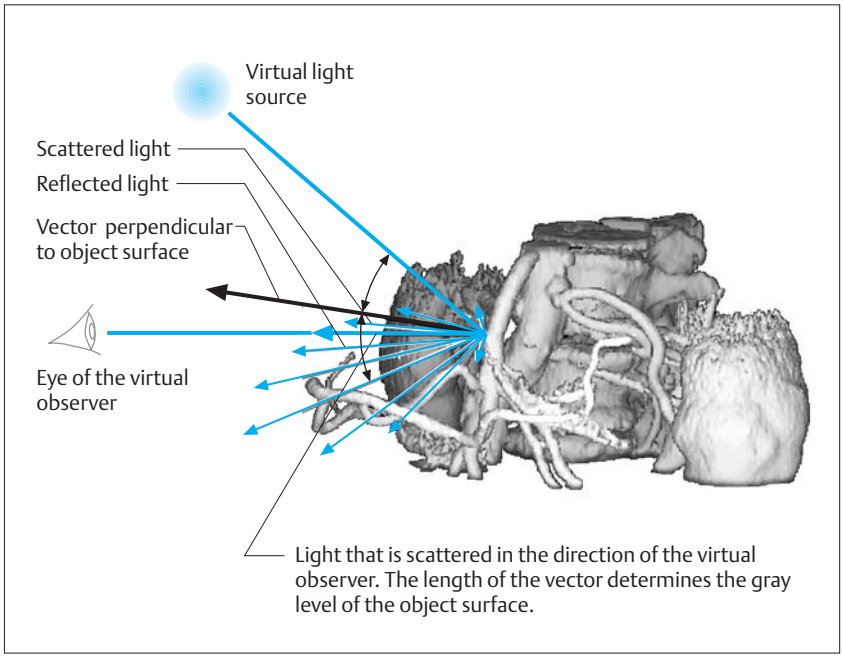

Fig. 2.**20** Shaded surface display (SSD). A virtual light source illuminates the 3D object, and software calculates the light intensities that are scattered and reflected toward the observer.

The larger the section width, the more object elements will be falsely represented in the display. Relatively small or thin details that are oriented parallel to the scan plane will lose contrast due to partial volume effects, with smaller objects appearing progressively diminished, and finally vanishing completely, as their diameter decreases. The choice of threshold, therefore, is always a compromise (Table 2.**3**).

When SSD is used in skeletal examinations, this diminishing effect can lead to bony pseudodefects or the non-visualization of thin bony plates (e.g., the orbital floor). In CTA, small vessels that course horizontally may appear narrowed, may show pseudo-stenoses or pseudo-occlusions, or may not be visualized (Fig. 2.**21**).

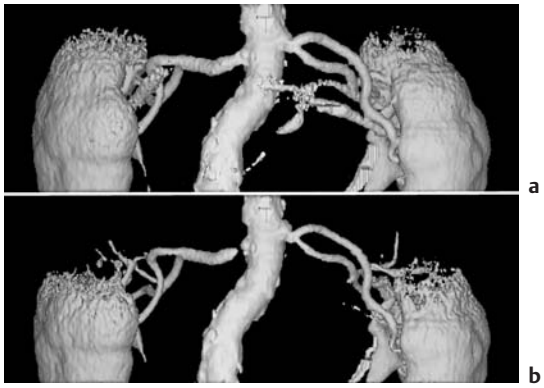

Fig. 2.**21** The selected threshold value profoundly affects the appearance of the SSD. In this patient with a high-grade renal artery stenosis, no apparent pathology is seen with a threshold of 120 HU (**a**), while a threshold of 200 HU simulates a vascular occlusion (**b**).

Lowering the Threshold

When the threshold is lowered, more voxels contribute to the displayed object, and the apparent diameter and volume of the object increase. This can partially compensate for partial volume effects, enabling smaller structures to be portrayed more realistically. Lowering the threshold also leads to longitudinal distortion of larger structures of higher contrast. If the threshold value is lowered even further, the CT number of single pixels will exceed the threshold due to image noise. This will cause *flying pixels* to appear in the 3D display (see Fig. 7.**32**), and useful image details will be obscured. Noise can also cause "stalactite" artifacts to appear on the upper and lower surfaces of low-contrast structures. Soft tissues whose CT numbers lie above the threshold value (e.g., after intravenous contrast administration) may also obscure structures of interest. The remedy is either to raise the threshold value or use more sophisticated segmentation techniques to separate the object of interest from other structures that also lie above the selected threshold value (see Fig. 2.**40**).

Raising the Threshold

When the threshold is raised, fewer voxels contribute to the object display, and the apparent diameter and volume of the object decrease. This can eliminate flying pixels and superimposed structures of lower attenuation, but it

Table 2.**3** Threshold values for segmentation in 3 D surface rendering

Tissue	Threshold	Application	Comments
Bone	> 150	Skeletal studies	Lower values are used in osteoporosis
Vessels	> 150	CTA	Lower values can be used after smoothing
Soft tissues	–	–	Feasible only in exceptional cases
Fluid	–	–	Feasible only in exceptional cases
Fat	–	–	Not feasible
Lung	> –600 < –200	Bronchogenic carcinoma Lung surface	Relation of tumor to vessels and pleura (Sub)pleural abnormalities, lung volume
Air	> –500 < –500 < –500 < –900	Skin Colon, larynx Central bronchi Peripheral bronchi	Skin surface "Luminal cast" "Luminal cast" "Luminal cast"

also increases artifacts such as the pseudo-stenoses noted above. Frequently the optimum threshold value in skeletal applications is quite low, especially in patients with osteoporosis, but higher values must be selected to eliminate superimposed structures despite the fact that more *"holes"* appear in the bone.

Applications

Shaded surface displays yield impressive images that can define surface structures and clarify *complex three-dimensional relationships*, for example among bone fragments or vascular structures (e.g., see Fig. 24.**42** or Fig. 25.**15**). Objects rendered by SSD can be rotated and viewed from any desired angle, and SSDs can be used preoperatively to give the surgeon a three-dimensional impression of the operative situs.

SSDs are primarily a tool for the *presentation of findings* and are only occasionally used as an aid to diagnosis in complex anatomic or pathologic situations (e.g., acetabular fractures, complex vascular relationships). As a result, SSDs are used predominantly in *skeletal studies* (see Chapter 25) and *CTA* (see Chapter 24) and they have occasional applications in bronchial examinations (e.g., see Fig. 9.**14**). The rendering of other types of soft-tissue structures is a laborious process that cannot be recommended for routine clinical investigations.

SSD have a role in *virtual endoscopy* (see p. 70) because the rendering process is much faster than with volume rendering techniques. SSD is therefore well suited for interactive navigation though a virtual endoscopic data set (see Fig. 2.**50**).

Volume Rendering Techniques

Principle

Maximum and minimum intensity projections are simple examples of volume rendering techniques. The image is generated by casting rays through the volume of interest (ray tracing), and projecting a numeric value that is derived from the data encountered along each ray according to prescribed rules (e.g., the maximum CT number in MIP).

Generally, however, volume rendering technique (VRT) is the term applied to a complex procedure that is very versatile and can combine characteristics of surface rendering and MIP. VRT assigns a range of opacity values to CT numbers and thus yields better definition of object contours or semitransparent display of structures (Fig. 2.**22**). VRT is quickly becoming an established standard technique for rendering of spiral CT or multislice CT data sets. Image quality is high and the user has a whole range of rendering effects at his disposal.

VRT can best be understood when comparing it to shaded surface displays (SSD). Such surface rendering is a "binary" process in which all CT numbers belonging to the 3D object (within the chosen threshold range) have maximum opacity, while all CT numbers outside the range have zero opacity and do not contribute to the image. Since all the voxels within the CT range have maximum opacity, only the surface of the object is depicted in the SSD.

In volume rendering, opacity values are continuous and can vary between 0% and 100%. The behavior of VRT is determined by the opacity curve. This curve may be drawn manually, a procedure that is tedious and not very reproducible. A very comfortable way of creating the curve is to use preset curve forms and to control its precise location on the CT number scale by window and level operations (Figs. 2.**22a** and 2.**23**, Table 2.**4**). Alternatively, opacity curves may be produced by a number of (partially overlapping) trapezoids that can be altered in form, height and position on the CT scale (Fig. 2.**22b**). These trapezoids can be chosen to represent the attenuation range of various tissues, e.g., fat, other soft tissues, contrast-enhanced blood vessels, and bone. A different color can then be attributed to each of these trapezoids to be able to differentiate between these tissues on the final image.

VRT can either create a transmission display (similar to a ray-sum projection or MIP) or

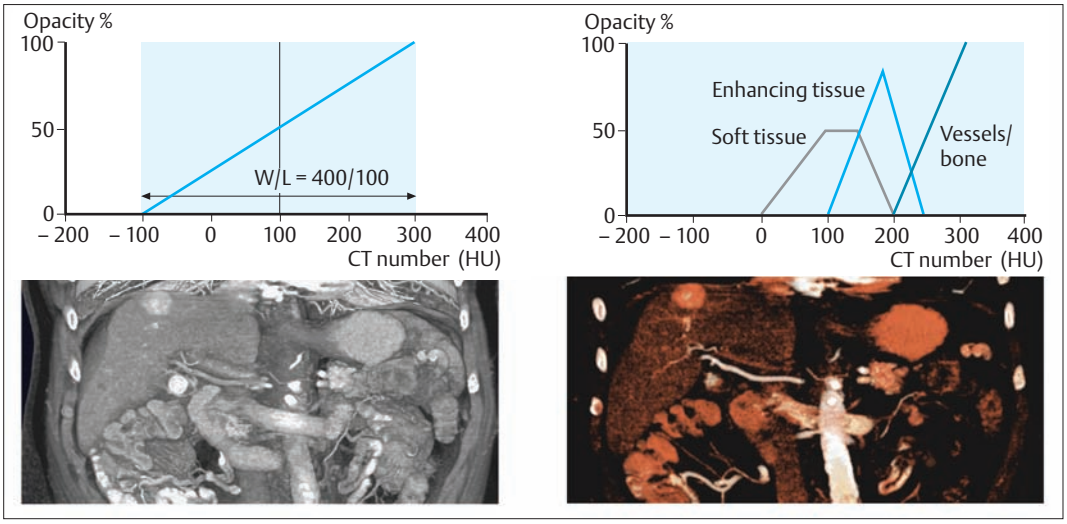

a b

Fig. 2.**22** Principle of volume rendering (VRT). During the creation of a volume rendered image, an opacity curve determines the opacity of various tissues depending on the CT numbers of each voxel. For most instances, a simple technique based on a single opacity ramp from full transparency to full opacity yields good results (**a**). This ramp can be determined similar to the window/level operation of normal CT images. Alternatively, multiple trapezoids with various colors that are assigned to tissues of different CT numbers can be used as an opacity function (**b**). Note that structures with low opacities (e.g. fat) will appear semitransparent with both techniques. No gradient shading (reflectivity = 0) was used in these examples.

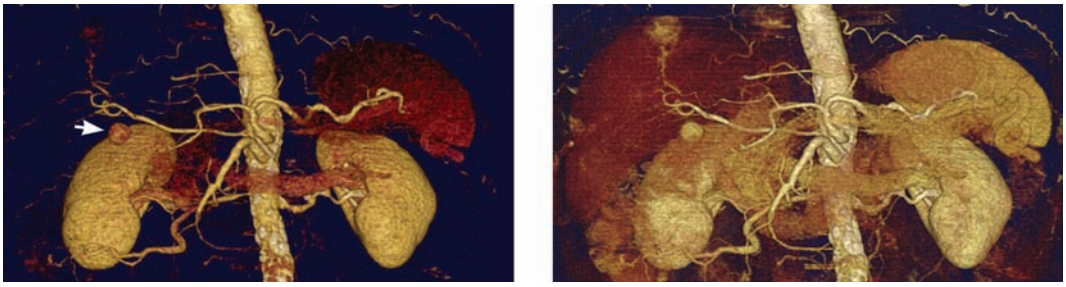

a b

Fig. 2.**23** The opacity curve and the reflectivity determine the resulting volume rendered image. A narrow opacity ramp (W/L = 400/400) yields an excellent surface display of the abdominal vasculature (**a**). Note the calcified gallstone (arrow). Shifting the opacity curve towards lower values yields semitransparent displays of soft tissues (**b**, W/L = 400/200). Additional gradient shading was used on these images.

a surface display (similar to the SSD) depending on the amount of gradient shading that is used to simulate reflectivity. This "reflectivity constant" may be determined either by using presets or by adjusting its numeric value.

Color Coding

Color coding may be performed on a per-trapezoid basis as described above. Ideally, various tissues are colored in a different way, thus allowing for visual differentiation. In practice, however, there is substantial overlap between

Table 2.4 Opacity settings for volume rendering

Application	Opacity settings			Comments
	W/L	Range	Curve	
Skeletal studies	300/200	100…400	Ramp	Lower values are used in osteoporosis
CT angiography	400/300	100…500	Ramp	Values depend on vessel opacification
Diagnostic viewing				
Soft tissue	400/100	100…300	Ramp	MRP-like rendering
Lungs	1500/–300	–1050…450	Ramp	
Colon	1200/–300	–900…300	Ramp	
Tissue-transition projection	500/–500	–750…–250	Spike	Air/soft tissue interfaces
Luminal casts	500/–500	–750…–250	Inv. ramp	Air/soft tissue interfaces
Virtual endoscopy				
Bronchoscopy	1200/–300	–900…–300	Ramp	
Laryngoscopy	1200/–300	–900…–300	Ramp	
Colonoscopy	1200/–300	–900…–300	Ramp	
Angioscopy	200/150	100…–300	Inv. ramp	Double spike for calcifications

Opacity settings may vary depending on contrast enhancement and implementation of volume rendering
In this table, a single step is used for most applications (which is sufficient for most imaging tasks)
Inv. ramp: inverse ramp with full opacity for lower CT numbers and zero opacity for high CT numbers
Spike: deltoid opacity function, maximum opacity for center of range
Color coding: best achieved by fixed color schemes, but may require use of multiple trapezoids on some workstations

various tissue types, e.g., between contrast-enhanced organs and blood vessels, and between vessels and bone, and no secure discrimination is possible (Fig. 2.**22b**).

Alternatively, a color scale can be assigned to the CT number scale. This color scale may be fixed relative to the CT numbers thus providing an absolute reference color depending on the attenuation or tissue type (Fig. 2.**24a**). This technique is ideal for displaying non-contrast-enhanced structures. Because contrast enhancement may vary substantially between patients, a flexible assignment of colors and CT numbers is advisable, depending on the actual setting of the opacity curve. This can be done by assigning the color scale to the slope of the opacity curve (Fig. 2.**24b**).

Spatial Resolution and Matrix Size

Fast response is usually obtained by reducing the spatial resolution of the VRT image during user interaction. A 128-matrix will only give a rough orientation but a 256-matrix already provides enough detail to find the optimum viewing angle for demonstrating a structure of interest. A 512-matrix, however, further improves spatial resolution and has a positive effect on the display of small vessels or bony surface detail (Fig. 2.**25**). A 1024- or 2048-matrix is also used in some systems, at least as an intermediate step during the rendering process. Such large matrices are especially helpful if structures have to be greatly enlarged from the original data set (such as the environs of a cerebral aneurysm), or if very long ranges have to be displayed (e.g., chest and abdomen or abdomen and legs).

Interactive Rendering—Movies

Presets make it easy to choose a proper display setting, and in most of the recent software, selection of parameters can be performed interactively close to real time. With specific volume rendering boards that can be installed in standard PCs, *real-time* interaction with >8 frames per second becomes feasible.

Movie sequences can be generated that allow for an off-line viewing of VRT data without having real-time interactive VRT software available. If standard digital movie formats (e.g. AVI, MPEG) are used, these sequences may be displayed on any PC. Alternatively, images can be transferred to videotapes and be displayed on any videocassette recorder. Such

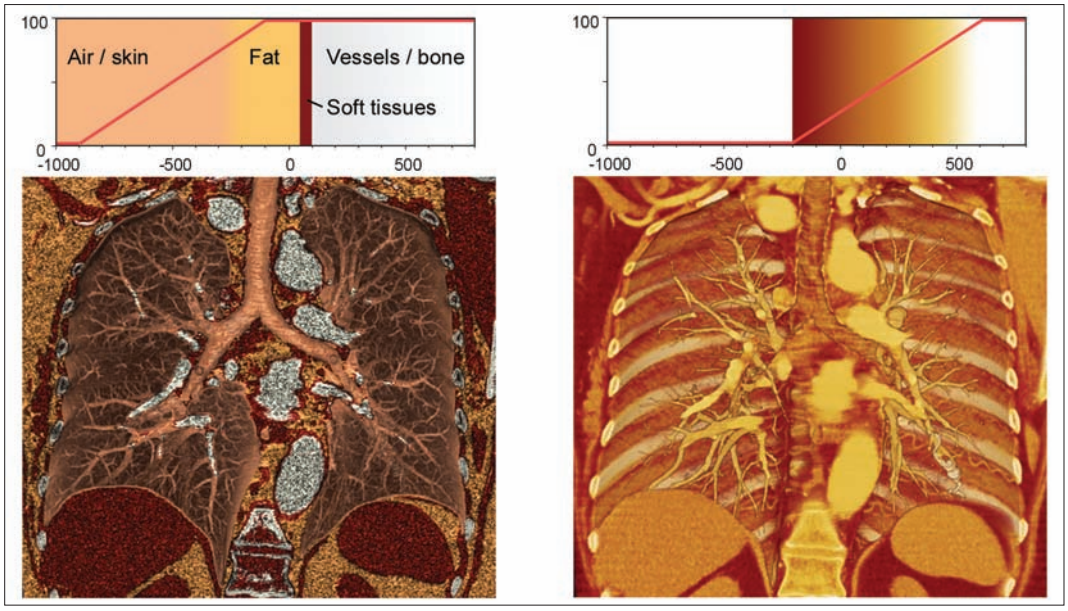

a b

Fig. 2.**24** Color coding. An absolute color scale assigns colors to various soft tissues, depending on their CT numbers but independent of the opacity setting (**a**). A relative color scale assigns colors to the opacity window but not to the CT number scale (**b**). Additional gradient shading was only used in (**a**).

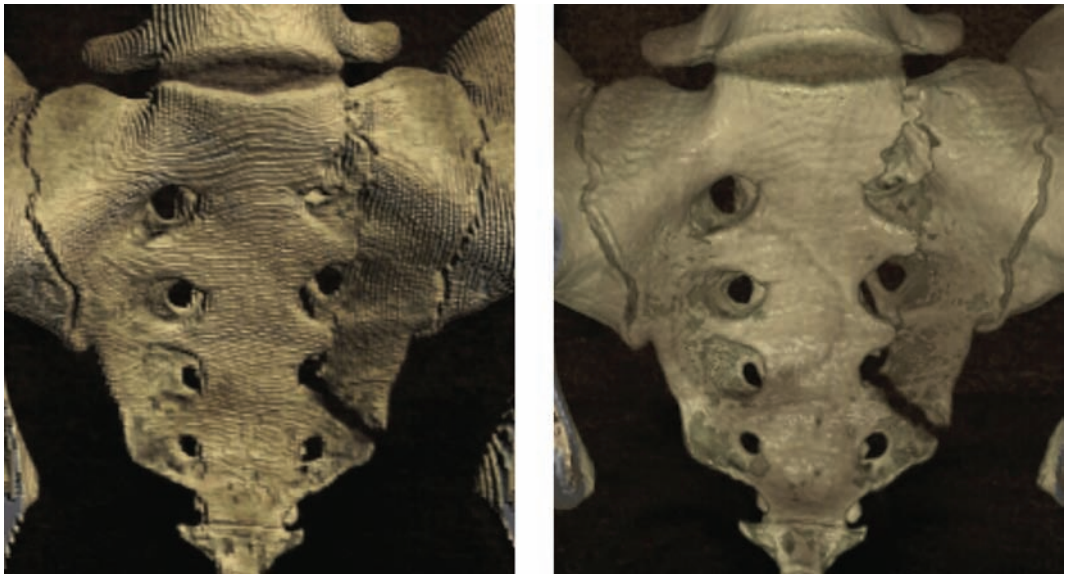

a b

Fig. 2.**25** Matrix size and image quality. (**a**) VRT with 256^2 resolution. (**b**) VRT with 512^2 resolution.

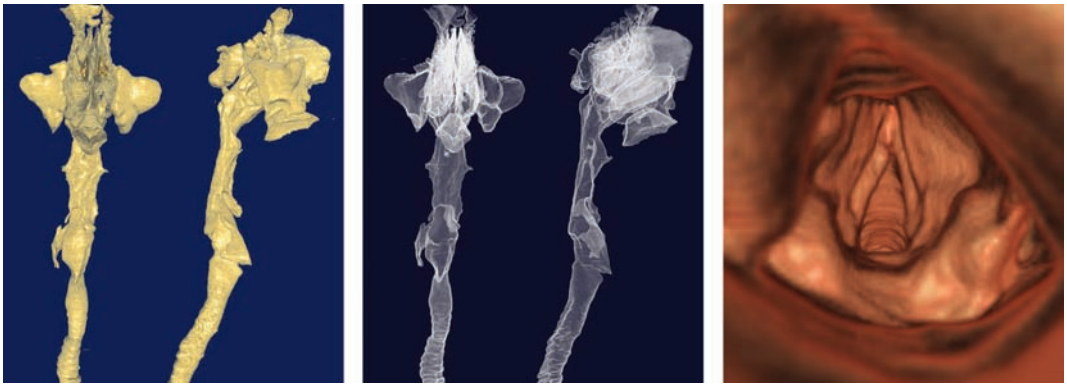

a b c

Fig. 2.**26** VRT of air-containing structures in the paranasal sinuses, pharynx and larynx. (**a**) Display of surface (cast). (**b**) Tissue transition projection of the airway wall. (**c**) Virtual endoscopy of the larynx.

movies are especially helpful for displaying complex anatomy to referring physicians. They already are being used for the display of renal cell carcinomas prior to nephron-sparing surgery, for the display of the anatomy in the evaluation of living renal donors, and for surgical planning of cerebral aneurysms.

Special Techniques

Air Casts

Inverted opacity curves that provide a high opacity for low-attenuation regions and low opacity for high-attenuation regions can be used to selectively display a *"cast"* of the tracheobronchial system, the larynx, or the colon (Fig. 2.**26 a**, see also Figs. 2.**36 a** and 2.**50 a**).

Tissue Transition Projections

Tissue transition projections selectively render the walls of the structure of interest. With VRT this can be reached by using an opacity curve that has the shape of a *"spike"* that is centered on the CT number between the two structures of interest (e.g., -500 HU for imaging of soft tissue—air interfaces such as in the colon or the trachea). This display technique, for example, produces images that simulate a double-contrast examination (Fig. 2.**26 b**, see also Figs. 2.**36** and 2.**50**).

MPR-like Rendering

MPR-like rendering is a technique that can substitute for traditional MPR. With VRT such images can be obtained by using a linear opacity curve with a slope that covers a range similar to conventional window settings. No reflectivity should be employed, to allow for optimum evaluation of cut surfaces. By using interactive cut planes, the radiologist can section through the data volume in a fashion similar to interactive MPR but has the additional advantage of depth information provided by these images (Fig. 2.**27**, see also see Fig. 2.**22 a**).

Table 2.**4** provides suggestions for proper opacity settings, depending on the clinical imaging task.

Artifacts and Pitfalls

VRT is less susceptible to *pseudo-stenoses* or pseudo-occlusions compared to SSD, although suboptimum opacity settings also lead to image artifacts (Fig. 2.**28**).

Venetian blind artifacts depend on the viewing angle and may be found incertain implementations of volume rendering (Figs. 2.**29 a**, **b**).

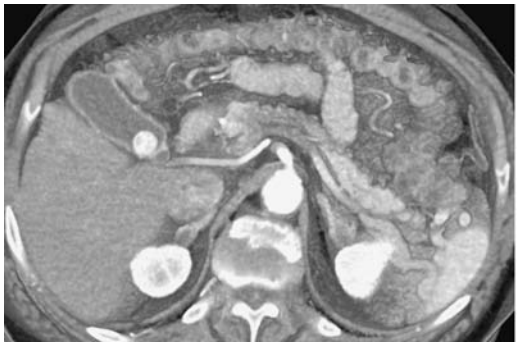

a

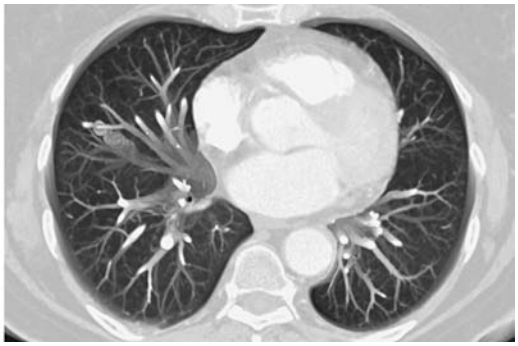

b

Fig. 2.**27** MPR-like VRT. Cutting into a volume rendered image (with reflectivity set to 0) creates MPR-like views that add the advantages of volume rendering (depth information) to that of MPR (evaluation of cut planes). (**a**) Soft tissue setting (W/L = 400/100), (**b**) lung setting (W/L = 1500/-300).

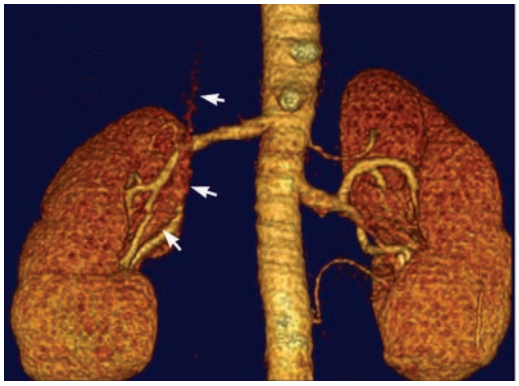

a

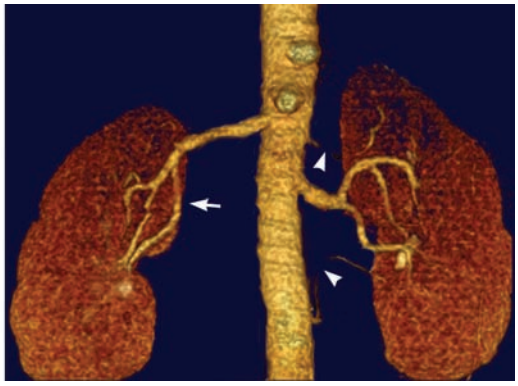

b

Fig. 2.**28** Volume rendering uses the whole 3D data set for image creation. However, only parts of the 3D data are displayed, depending on the opacity function. With an opacity window of W/L = 400/250 (**a**) there is superimposition of the right renal vein (arrows). With an opacity window of 400/300 (**b**) portions of the accessory renal arteries on the left are lost (arrow heads) but the lower pole artery on the right is visualized (arrow).

Image noise may cause irregularities of the object surfaces (Fig. 2.**29 c**) or may even obscure underlying pathology. Depending on the opacity function, noise may also cause a veil-like shadowing of structures that are deeper inside the displayed volume.

It has been stated that VRT does not lose information because the whole data volume is projected. However, VRT does *not* display all the information in the data volume but, like all 3D rendering techniques, selectively displays portions of the scanned object, depending on its CT attenuation and position relative to the viewer (Fig. 2.**28**).

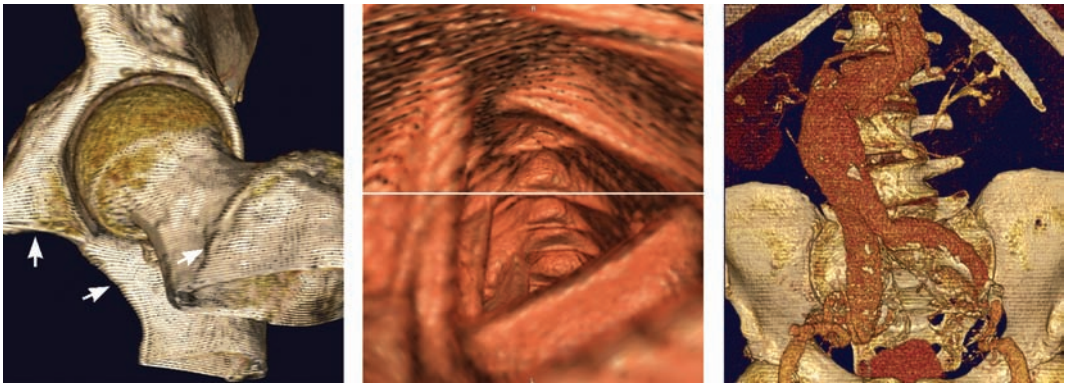

a b c

Fig. 2.**29** Artifacts. (**a**) Venetian blind artifacts are typical for some software implementations of volume rendering. (**b**) They are especially disturbing on virtual endoscopic views (upper portion of image). (**c**) Image noise is especially disturbing in VRT with gradient shading (reflectivity) and a 512^2 resolution.

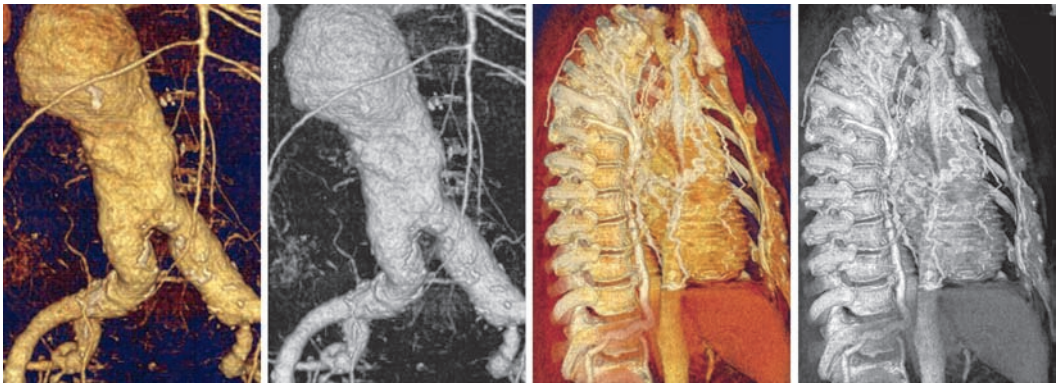

a b c d

Fig. 2.**30** Differentiation between calcified plaques and vessel lumen is simplified on color displays (**a**) compared to black-and-white rendering (**b**). In this patient with a superior vena cava occlusion, color display (**c**) improves the visualization of the collaterals in the mediastinum relative to black-and-white displays (**d**).

Applications

Volume rendering can be used for CTA, skeletal imaging, tracheobronchial imaging, display of the lungs, the colon, abdominal organ and even as a primary tool for image analysis.

CT Angiography

In CTA, volume rendering is becoming the new standard for the display of the pulmonary vessels, the aorta, and the abdominal vessels. Color-coded VRT provides display of vessel lumen and calcifications in separate colors, thus making it easy to localize calcified plaques (Fig. 2.**30**). Color coding also may allow differentiation between arterial and venous vessels, as well as between organs with different contrast enhancement (Fig. 2.**31**). When the aorta is eliminated by editing procedures, excellent displays of the celiac and mesenteric vessels become available (Fig. 2.**32**). Segmentation can be used to eliminate superimposing soft tissues and make it possible not only to display the vessel lumen but

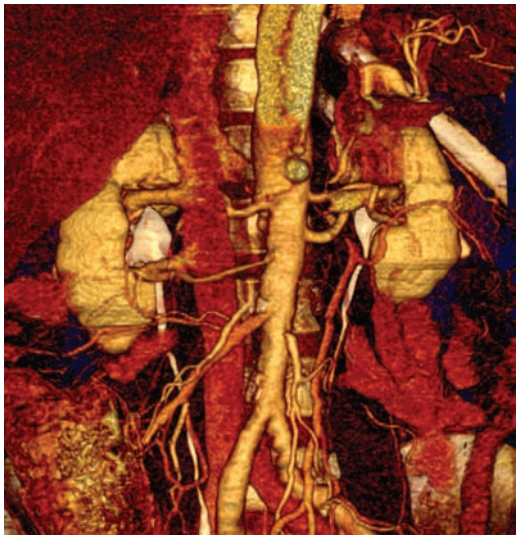

Fig. 2.**31** Differentiation between arteries, veins, and contrast-enhanced organs is possible with VRT if there is differential enhancement.

also thrombosed portions of the vessel (e.g., of an abdominal aneurysm) as well (Fig. 2.**33**).

Skeletal Imaging

For skeletal imaging, VRT is an excellent tool for classifying complex fractures (e.g., of the acetabulum), for demonstrating the spatial position of fracture fragments, and for planning of complex or minimally invasive surgery. In orthopedic applications, VRT is superior to SSD because it is less susceptible to partial volume effects with pseudo-defects in thin bony laminae or osteoporotic patients. In addition, VRT allows for simultaneous display of bones as well as tendons or muscles, and even allows for assessment of the skin contours (Fig. 2.**34**), e.g., in patients prior to corrective surgery. In the spine, the vertebrae as well as the intervertebral disks can be displayed, making it an ideal tool for assessing and demonstrating pathology of the spinal column (Fig. 2.**35**).

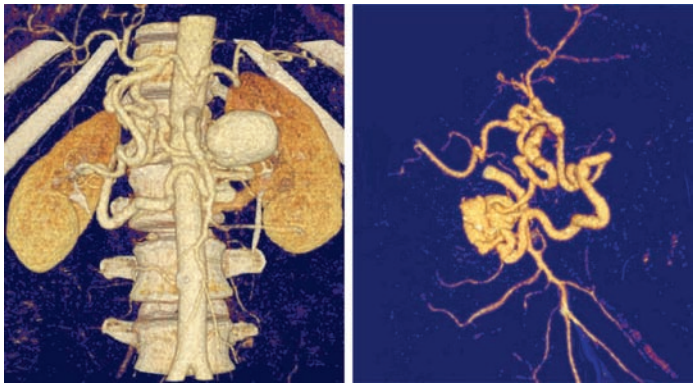

a b

Fig. 2.**32** Removal of the aorta allows for excellent display of the celiac and mesenteric vessels. In this patient the relationship of the aneurysm to the mesenteric side branches can best be demonstrated on a PA view (**b**).

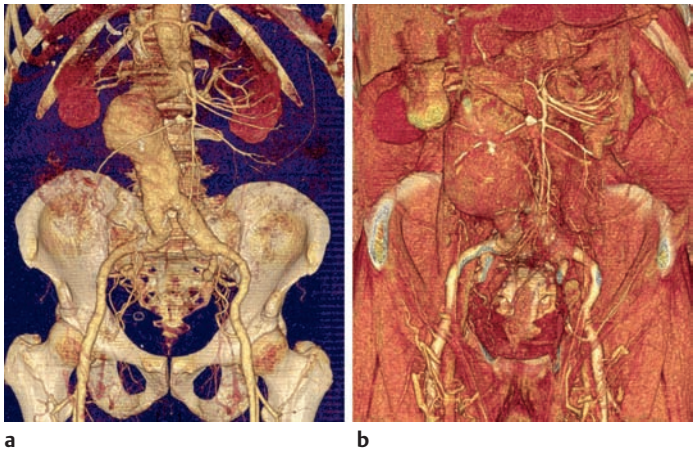

a b

Fig. 2.**33** With a soft tissue setting for VRT, and elimination of superimposing soft tissue by image segmentation, direct display of thrombi is possible.

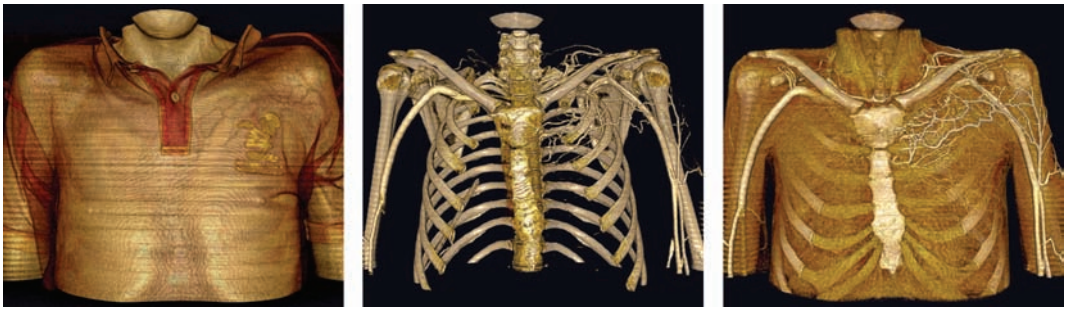

a b c

Fig. 2.**34** VRT not only allows for a selective reconstruction of the skin (**a**) or bone (**b**), but also semitransparent display of skin that make the underlying bone visible (**c**). Note the bilateral obstruction of the brachiocephalic veins.

Tracheobronchial Imaging

For imaging of the tracheobronchial system, VRT provides either casts or semitransparent walls of the tracheobronchial tree (Fig. 2.**36**). VRT is especially helpful when it comes to virtual bronchoscopy (see p. 81) because even segmental bronchi may be evaluated if a thin-section multislice CT data acquisition was used.

Lungs

For the lungs, volume (or surface) rendering can be employed to create images of the lung surface (see Fig. 2.**47**) and to assess the spatial relationship of focal lung lesions to the chest wall or mediastinum (Fig. 2.**37**). It can be used to create color-coded density maps that help detect and

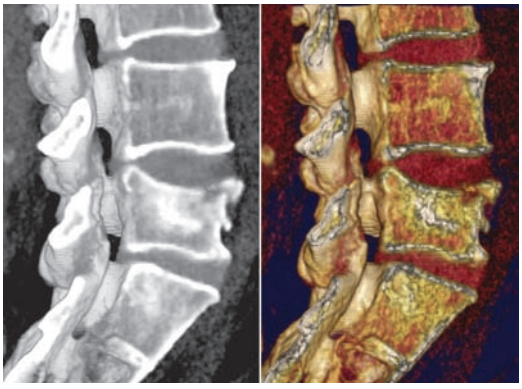

Fig. 2.**35** Volume rendering of the spinal column allows for demonstration of the vertebrae as well as the intervertebral disks.

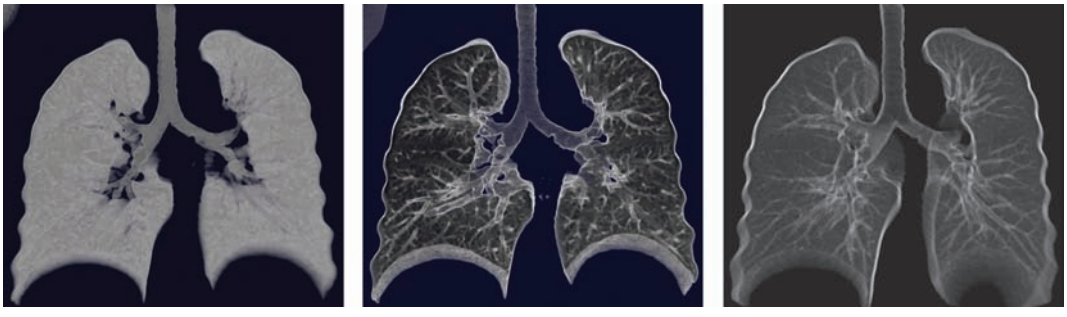

a b c

Fig. 2.**36** The tracheobronchial system can be visualized as an "intraluminal cast" using SSD or VRT (**a**) or using a tissue transition projection (**b**). Similar effects are possible using a 20 mm thick MPR after removal of the mediastinal tissues by region growing (**c**).

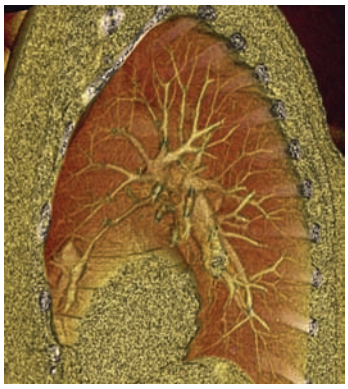

Fig. 2.**37** Volume rendering allows for excellent displays of the location of focal lesions relative to the chest wall and the pulmonary vessels. Note that this metastasis is due to a tumor thrombus spreading within a peripheral pulmonary artery.

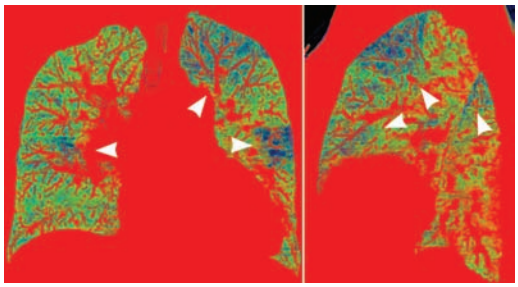

Fig. 2.**38** Color-coded density maps can be created when using a rainbow spectrum and a lung-centered opacity curve (W/L = 500/–750). Note the wedge-shaped perfusion defects (arrowheads) in this multislice CTA of chronic pulmonary embolism.

quantify regions with focal air trapping or perfusion abnormalities (Fig. 2.**38**).

Colon

In the colon, VRT is an excellent technique for virtual colonoscopy but also for surveying the data with the help of sliding thin slabs (see below) that combine the advantages of axial, coronal, or sagittal MPR with the depth information provided by VRT. Again, casts or semitransparent displays of the colon become available, some very similar to conventional barium enema studies (see Fig. 2.**50**).

Routine Reporting

In the chest and abdomen, VRT with proper opacity settings provides semitransparent or color-coded displays of soft tissues (see Fig. 2.**27**). In the abdomen, in particular, VRT allows for excellent display of the liver, portal vessels, bowel structures, the pancreas, and even the suprarenal glands.

VRT with opacity settings that mirror those of conventional CT imaging have been suggested as a *primary viewing mode* for making the diagnosis. By analogy with a soft-tissue window, the opacity settings should be chosen in a way that makes normal fatty tissue transparent but is able to demonstrate increased density in the fat on the rendered images (see Fig. 2.**27**). For the purpose of using VRT as the primary diagnostic tool, however, cut planes have to be available that expose cross-sections of organs that would otherwise be rendered opaque. In addition, interaction has to be real-time to allow for fast maneuvering through the data volume. There is still no hard data, however, that such a procedure is safe and does not miss important findings.

Segmentation

Principle

Both 3D volume rendering (e.g., MIP, VRT) and 3D surface rendering (SSD) require a segmentation process that defines the volume of interest and separates it from structures that should not be represented in the 3D image. The process of manipulating the data set to control what structures are included or excluded in the rendering is termed "editing". *Positive editing* is based on marking the structures of interest that will be retained in the 3D image. *Negative editing* involves marking the unwanted structures that will be removed. A distinction is drawn between 2D editing functions, which are applied section by section, and 3D editing functions, which are applied to the 3D data set as a whole.

Cutting Functions

Cutting functions may be used on the original data volume before 3D rendering or on the 3D-rendered object itself.

Cutting can be performed in the original data volume on a section-by-section basis, a technique that is very time consuming and can only be recommended in exceptional and complex cases in which a small set of sections are edited. It is more sensible to perform cutting functions on 3D-slabs, i.e., stacks of images that are a few mm to several cm wide. This can substantially reduce the effort of editing but is still comparatively time consuming if larger ranges, such the whole chest or abdomen, have to be processed.

The most efficient technique is based on cut lines that are drawn on a number of unevenly spaced reference sections. The program then performs a three-dimensional interpolation between these cut lines and thus defines the volume to be included or excluded from the volume of interest that is chosen for further processing (Fig. 2.**39**). This technique allows the lungs or the abdominal vessels to be edited in a few minutes, and even allows for complex procedures in which portions of organs are removed for better visualization of neighboring structures (see Figs. 2.**31**–2.**33**).

Cutting in a 3D-object first requires a view in which the cut plane can be drawn. This plane will be perpendicular to this view, so the user has to make sure that the structures to be separated do not overlap. The cutting functions are best used to exclude unwanted objects but they can also be employed to focus on certain regions and include the structures of interest.

Threshold Techniques

Threshold techniques are simple processes that use a threshold value or range of CT numbers to define the volume that will undergo segmentation (see Table 2.**3**). Threshold techniques are generally used in the rendering of SSDs.

When threshold techniques are used alone, it is common for an image to include different anatomic structures that need to be displayed separately. This would apply, for example, to opacified vessels and the vertebral column, or to the femoral head and acetabulum. For this reason, threshold techniques are often combined with other methods that can separate objects within the same threshold range.

Connectivity

Connectivity algorithms are used to identify contiguous image regions that have a certain property in common. Such a **"***region-growing*" algorithm starts at a seed point and detects all voxels that satisfy the specified condition and are interconnected to the seed point. The usual condition is that the voxels lie within a prescribed range of CT numbers.

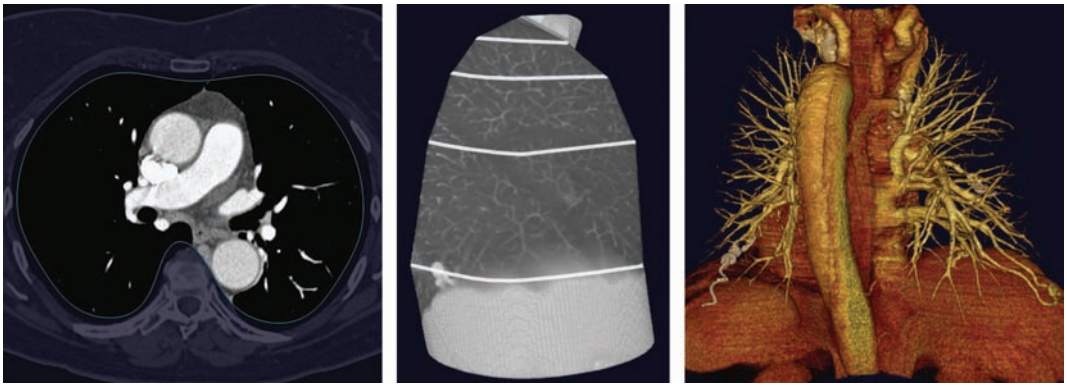

a **b** **c**

Fig. 2.**39** Cutting functions using a "rubber sheet" algorithm are highly efficient for complex editing tasks. A number of arbitrary regions of interest (ROI) are drawn at a few levels throughout the chest (**a**). Display of remaining volume with indicated ROI levels (**b**). A volume-rendered vascular display (W/L = 600/200) demonstrates multiple AV-shunts in either lung.

Connectivity algorithms can be applied to single axial sections, to slabs consisting of multiple sections, or to the 3D volume as a whole. The larger the volume, the faster the theoretical rate of segmentation, but there is a greater risk that artifactual "bridges" will form between image regions that are actually separate. Various methods can be used to eliminate these bridges (Fig. 2.**40**). Frequently, object separation can be achieved simply by changing the threshold range. Other methods involve the use of manually drawn separating lines or "morphologic operators" to erase the unwanted connections.

Watershed algorithms are very helpful for separating two structures that are connected by a bridge. They determine the plane with the lowest CT number within that bridge and cut at that level. In practice this means that the operator only has to place a seed point on the structure to be included and others on the structures to be excluded and let the watershed algorithm do the separation. In many cases such a procedure will be sufficient; in some more complex cases, a repeat of this procedure at another level of the data volume will become necessary.

Morphologic Operators

Morphologic operators depend on the morphology of a structure rather than its attenuation values. The most simple but useful operators are those that remove rows of voxels from the surface of an object (*erosion*) and those that attach rows of voxels to the surface of an object (*dilation*). Erosion operators can be used to remove bridges between adjacent objects. Dilation can then be performed to restore the object to its approximate original size, although surface details will be lost (Fig. 2.**40**). The sequence of erosion followed by dilation is called *"opening"* because it opens up connections between structures, while the combination of dilation followed by erosion is called *"closing"* because it removes holes within an object.

After successful detection of objects (e.g., the skeletal structures) to be excluded by region growing, it is advisable to perform a dilation procedure on these objects to include and eliminate also voxels at the object boundary that contain higher CT numbers than the surrounding structures. If these voxels are not excluded (Fig. 2.**41**), ghosting artifacts will result in 3D rendered images.

Other morphologic operators can recognize small groups of voxels and can therefore be used to erase "flying pixels" from an image (Fig. 2.**42**).

Automated Techniques, Computer-assisted Diagnosis

There is an increasing amount of fully or semiautomated techniques being developed that require no or only minimal input (such as positioning of various seed points) for complex editing tasks. Such tools allow for automated *extraction of the lungs*, or *bone removal* in CTA (Fig. 2.**43**), or *automated vessel analysis* (Fig. 2.**44**). Computer-aided diagnosis tools are able to automatically detect, extract, and measure the *volume of pulmonary nodules* for lung cancer screening. Similar tools are being developed for colon cancer screening.

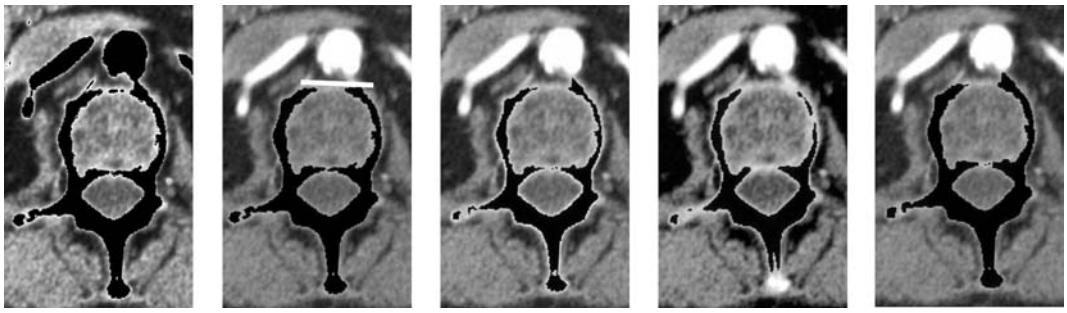

a **b** **c** **d** **e**

Fig. 2.**40** Segmentation. Connectivity algorithms can be used to mark contiguous regions that have common characteristics. "Bridges" that persist between structures to be separated (**a**) can be eliminated by the use of cutting functions (**b**), erosion operators (**c**), or by increasing the threshold (**d**). Subsequent dilatation can be performed to remove the higher-attenuating areas that remain around bony structures (**e**).

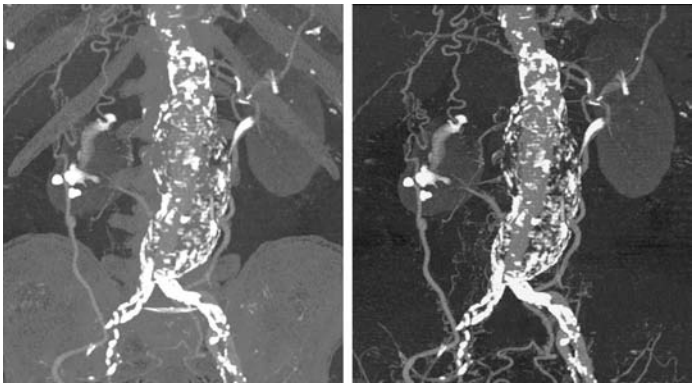

a b

Fig. 2.**41** Bone removal by region growing. Region growing with a threshold above 200 HU allows separation of bones from vessels but leaves high-attenuation areas around bony structures that lead to ghosting artifacts on MIP (**a**). This ghosting may completely obscure smaller vessels. Dilatation of the bone and removal of holes in the vertebral body using "closing operators", yields high quality MIP (**b**).

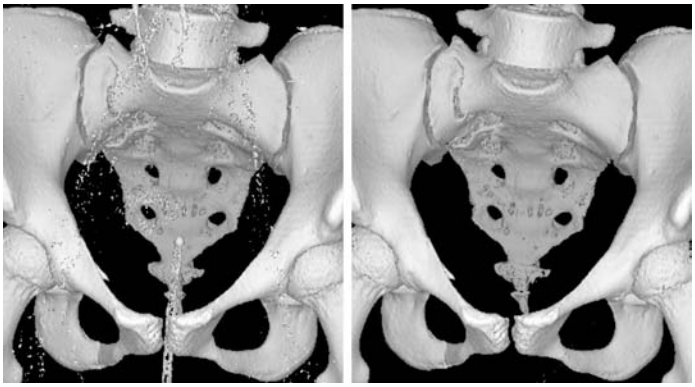

a b

Fig. 2.**42** Flying pixels ("floaters") due to image noise are especially disturbing on low dose data sets (**a**) but can be removed by size-dependent filter functions or region-growing of the structures of interest (**b**).

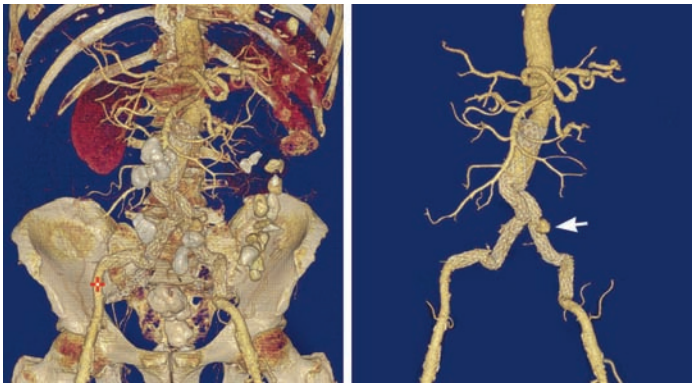

a b

Fig. 2.**43** Automated bone removal is now feasible on some workstations. By clicking on the structures to be removed or, in this case, retained (**a**), automatic removal is quite effective (**b**). Note the type II endoleak after aortic stent grafting (arrow).

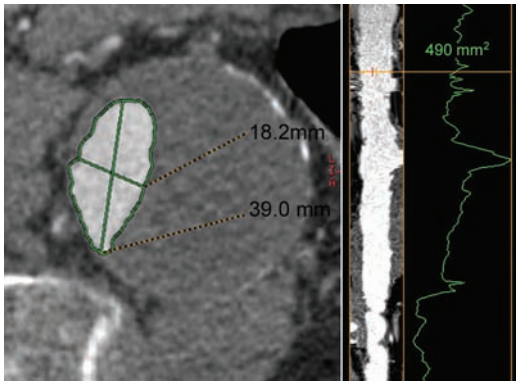

Fig. 2.**44** Automated vessel analysis is based on automatic vessel tracking but adds measurements perpendicular to the vascular course. Depending on the software, local cross-sectional area, and the minimum and maximum diameter of the vessel of interest are calculated and a rubber-band image of the vessel is displayed.

There are programs that include some form of artificial intelligence to account for anatomic variations. Many of these tools have just entered the market or are about to be introduced soon, pending FDA approval.

Applications

Segmentation is a prerequisite for *CTA* with MIP images in an anteroposterior direction. Positive editing is generally sufficient if there is a focused question. For the presence of a renal artery stenosis, for example, best results are obtained if a thin curved slab is included that just encompasses the renal arteries from the origin to the intrarenal branches and excludes the renal veins as well as portions of the anterior and posterior renal cortex (see Fig. 2.**13b**). Negative editing with exclusion of the skeletal structures can be recommended if a survey of the thoracic, abdominal, or peripheral vasculature is required (Table 2.**5**).

Segmentation can improve visualization of *complex vascular anatomy* or pathology (posterior-anterior views) if SSD or VRT are used (see Fig. 2.**31**). In addition, it can provide *selective views* of certain vascular territories (e.g., mesenteric vessels) by eliminating the aorta or other superimposing structures (see Fig. 2.**32**). For visualization of the *pulmonary vasculature* with MIP, SSD, or VRT, prior removal of the chest wall is necessary (see Fig. 2.**39**).

Segmentation of *soft tissues* is only useful for VRT. Using such a technique, visualization of complex anatomic relationships becomes possible (see Fig. 2.**33**). For the *lungs*, segmentation can be employed to selectively display the lung tissue in order to obtain density maps or to depict the pulmonary surface (see Fig. 2.**47**). Removal of all soft tissue structures in the chest that are connected to the mediastinum (connectivity with a threshold $>$ –200 HU followed by a 2–3 pixel dilatation) will yield an overview of the aerated lung. Thick MPR from such a data set will create images that are similar to tissue-transition projections ("tissue transition MPR", Fig. 2.**45**).

In the skeleton, segmentation can be used for *bone exarticulation* and provide selective views of the joint surface, e.g., of the acetabulum, but also of the glenoid or the calcaneus (Fig. 2.**46**, see also Fig. 25.**41**).

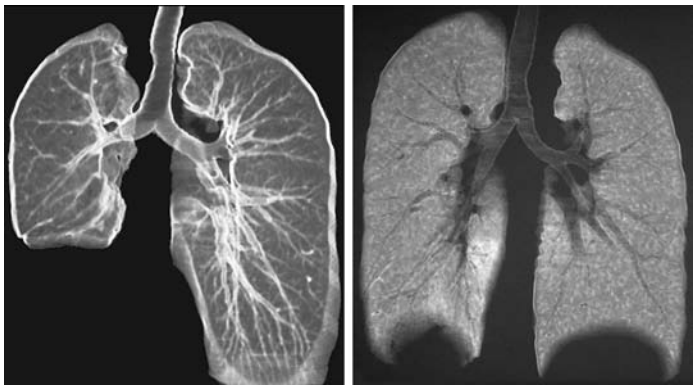

a **b**

Fig. 2.**45** Tissue-transition MPR can be obtained by removing all extracorporeal air as well as all soft tissues ($>$ –200 HU), followed by a 2-pixel dilation, and then using a thick MPR to visualize interfaces of air-filled structures. Note that also the pulmonary vessels appear translucent (**a**). If no dilation is performed, the resulting image will selectively display the aerated lung (**b**).

Table 2.5 Segmentation procedures for various clinical tasks

Application	Display goal	Technique
Bone removal	CTA	Automated bone removal *or*
Chest wall	Pulmonary vessels	Cutting (rubber sheet): include all except chest wall
Abdomen	Abdominal vessels	Mark bone (RG/WS > 180 HU), dilate bone (2–3 pixels), remove bone Cutting (rubber sheet): include all except abdominal wall
Neck	Carotid arteries	Mark carotids (RG/WS = 150–400 HU) using lower + upper threshold, create two VOI roughly including skull and neck/cervical spine, mark bone (RG/WS > 500 HU – skull, RG/WS > 180 HU spine), dilate bone (2–4 pixels) remove bone Draw center line through carotids (manual/semiautomated), produce 3 – 5 mm thick slab curved MPR/MIP/VRT
Bone exarticulation	Joint surface	Mark bone of interest (RG/WS > 180 HU), dilate 2–3 pixels, mark bone to be removed (RG/WS), dilate 2–3 pixels, remove bone
Lung extraction	Volume measurements Surface display	Mark trachea + large bronchi (RG <–900 HU), dilate 2–4 pixels, extract each lung (RG <–200 HU)
Colon extraction	Selective display	Block ileocecal valve if necessary (0 HU line), mark colon (RG <–500 HU) use multiple seeds if necessary, dilate 3 pixels for SSD or VRT
Tracheobronchial extraction	Selective display	Mark tracheobronchial tree (RG/WS <–900 HU), increase threshold until overflow into lung parenchyma just does not yet occur, dilate 2–3 pixels for VRT/SSD
Tissue-transition MPR	Transparent wall of air-filled organ (larynx, trachea, bowel)	Mark air-filled organ (RG <–200 HU), dilate 2–3 pixels, remove rest

RG = region growing; WS = watershed algorithm; suggested thresholds in brackets have to be individually adapted. After dilation of bony structures, filling of holes may be necessary

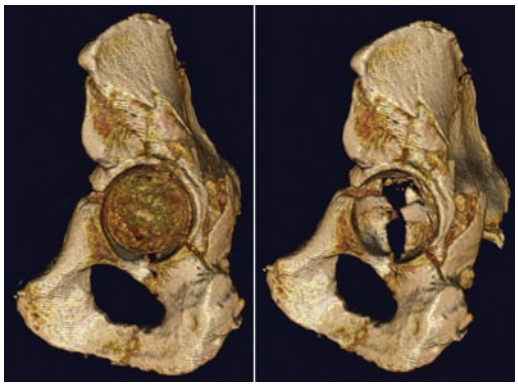

Fig. 2.46 Bone exarticulation can be used to create an ▶ unobscured view of articular surfaces (here: complex fracture of the acetabulum).

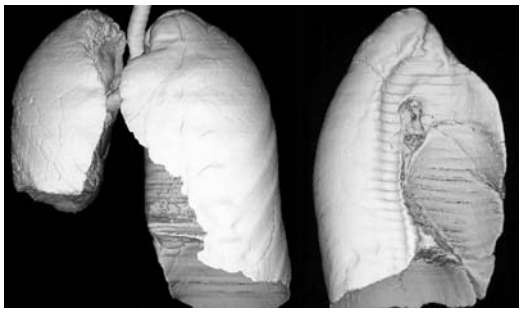

Fig. 2.**47** Quantification of the lung volume may be helpful prior to lung transplantation (especially for living donors) or for follow-up after surgery. The total volume of the aerated lung including the tracheobronchial tree or an isolated lung are easily determined using region growing techniques.

For *volume quantification* of organs or lesions, the structure has to be isolated first by proper editing procedures. The techniques may be fully automated (pulmonary nodule detection and quantification, see Fig. 9.**18**) or will require substantial user input (e.g., quantification of hepatic or splenic volume). Often, a combination of connectivity (seeding) and manual cutting functions will provide the quickest results (Fig. 2.**47**).

Virtual Endoscopy

Principle

Virtual endoscopy is a 3D-rendering technique that simulates endoscopic views. The first step is to select suitable threshold ranges (SSD) or opacity settings (VRT) that define the internal surfaces of interest, such as the bronchi, paranasal sinuses, blood vessels, or the gastrointestinal tract (Table 2.**6**). The endoscopic effect is produced by perspective rendering along a path within the data set. This provides an "endoscopic" view of internal objects (Fig. 2.**48** and 2.**49**).

Maneuvering through the Data Volume

The viewer can interactively change his or her location, viewing direction, and the visual field of the virtual endoscope. Good *viewing angles* that come close to those of real endoscopes vary between 60° and 90°.

Orientation can be established from multiplanar reconstructions and from the virtual endoscopic image itself. In some systems the operator can preprogram a *"flight path"* through the organ system or define the path interactively. A good first approximation of the flight path through tubular organs can be gained by calculating a centerline using so-called skeletonization algorithms. Techniques to view the walls are helpful, and back-mirror techniques that inverse the viewing direction are essential for some applications such as virtual colonoscopy.

Still, at present, maneuvering through the data sets is a tedious and time-consuming effort. For this reason, virtual endoscopy is mainly used as a problem-solving tool, for example to

Table 2.**6** Threshold values for virtual endoscopy

Application	Interface	Threshold[a]	Opacity settings[b]		
			W/L	Range	Curve
Bronchoscopy	Mediastinum/air	>–500	1200/300	–900…300	Ramp
	Bronchial wall/air	>–900	300/700	–950…–550	Ramp
Laryngoscopy	Soft tissue/air	>–500	1200/300	–900…300	Ramp
Colonoscopy	Soft tissue/air	>–500	1200/300	–900…300	Ramp
Angioscopy	Soft tissue/contrast material	< 150	200/150	50…250	Inv. Ramp

[a] surface rendering (SSD), [b] volume rendering (VRT)

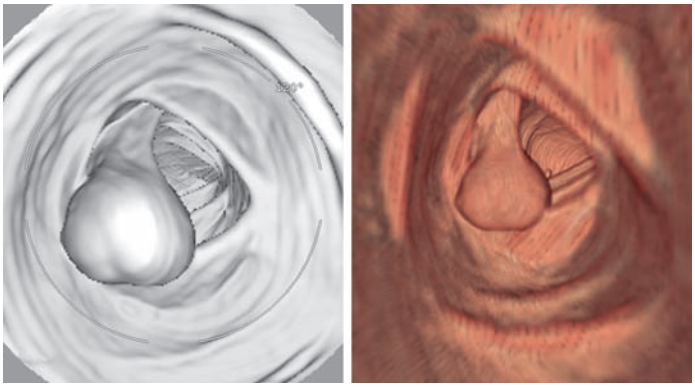

a b

Fig. 2.**48** Virtual endoscopy yields perspective views by using a central projection instead of the parallel projection used in other techniques. Internal surfaces can be displayed using SSD (**a**) or volume rendering (**b**).

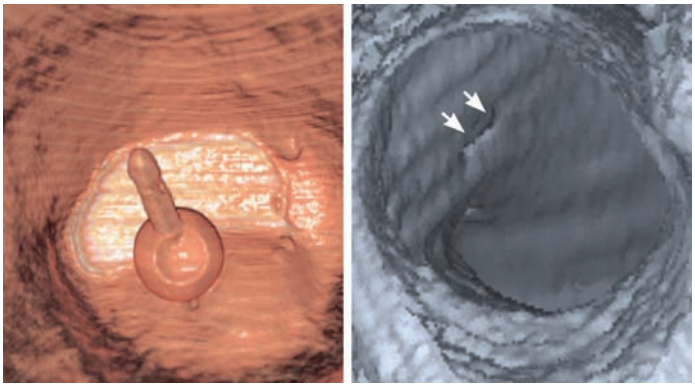

a b

Fig. 2.**49** Virtual endoscopy relies on a high contrast between lumen and surrounding tissues. Most applications such as virtual cystoscopy (**a**) rely on air as a negative contrast material. For virtual angioscopy (**b**) or cholangioscopy, the positive contrast in the structure of interest requires an inverted opacity curve. Note the small entry tear in this type B.

differentiate a colonic fold from a real polyp in CT colonography.

Alternative Visualization Techniques

Casts of a luminal organ are known from CTA and there represent the standard display technique with SSD or VRT. Similar techniques are possible with the tracheobronchial system, and yield a tree-like structure. Distal branches are displayed best if the data was acquired with thin-section multislice CT. For the colon, these casts resemble a monocontrast barium enema, but they are superior because they provide a three-dimensional display of the colonic surface (Fig. 2.**50 a**). Casts, however, have an intrinsic drawback: they are less sensitive for displaying small endoluminal protrusions such as polyps or wall-adherent tumors. These lesions appear as small indentations on the surface of the cast and may easily be overlooked.

Tissue transition projections render the walls of the structure of interest in an opaque or translucent fashion. They can be created either by using SSD or VRT with a narrow range of CT numbers that correspond to the transition zone between luminal contents (air or contrast medium) and the surrounding tissues. This display technique, for example, produces images that simulate a double-contrast barium enema (Fig. 2.**50 b**). Alternatively, a tissue transition MPR (see also Fig. 2.**36**) can be chosen that provides similar results (Fig. 2.**50 c**).

Thick MPR is useful for displaying small vessels (thickness 3–5 mm) or the central tracheobronchial system (thickness 7–20 mm). They provide an overview of anatomy and pathology (see Fig. 2.**36**) and make it easier to detect focal lesions because these will alter the attenuation of the vessel or bronchus.

Sliding thin-slab VRT is a method similar to sliding thin-slab MIP but uses volume rendering

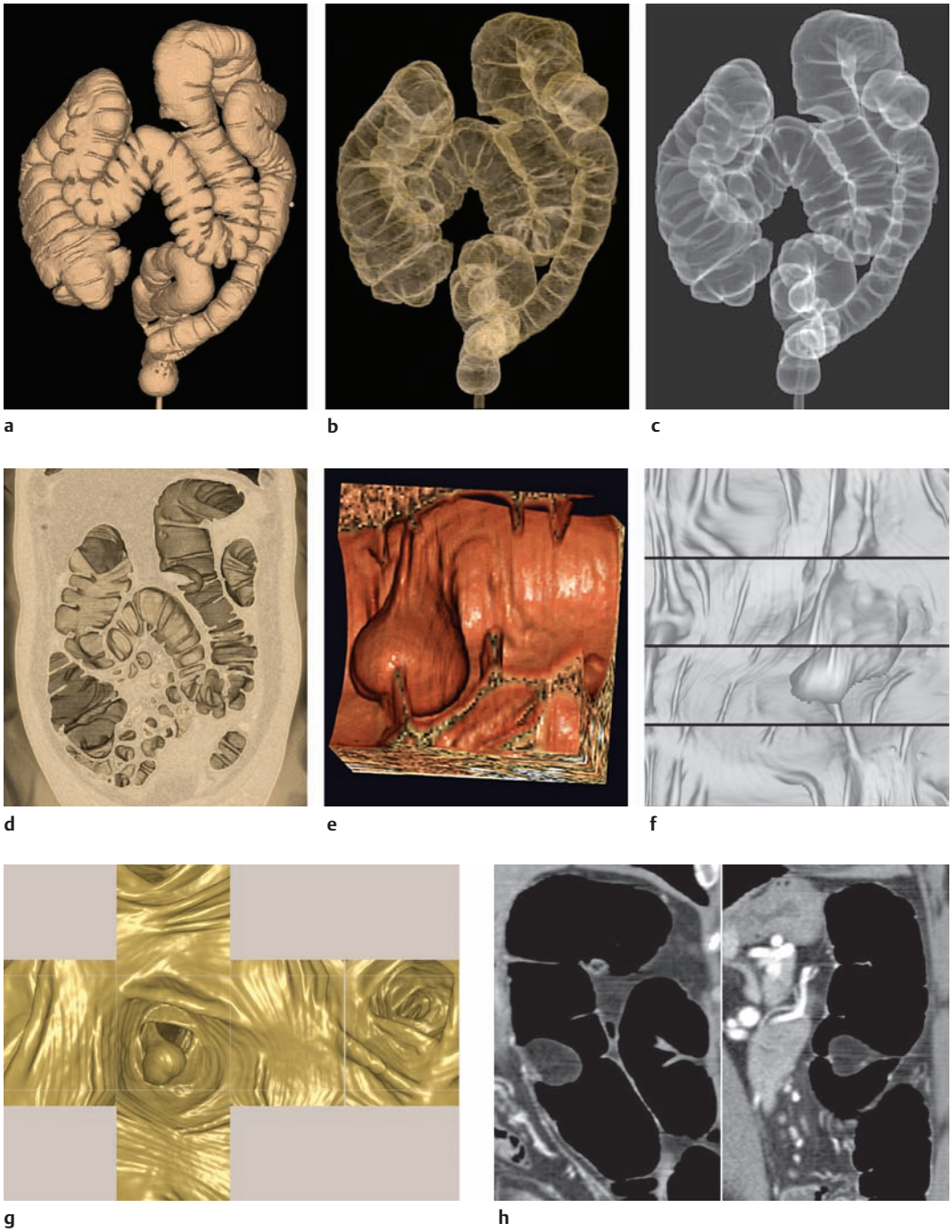

Fig. 2.**50** Alternative visualization techniques may provide a helpful adjunct to virtual endoscopy, as demonstrated in this patient with a colonic lipoma and small polyps in the proximal transverse colon. (**a**) Intraluminal cast. (**b**) Tissue transition projection using VRT. (**c**) Tissue transition MPR. (**d**) Thin-slab VRT. (**e**) Coned-down VRT. (**f**) Virtual colonic dissection ("virtual gross pathology"). (**g**) Virtual colonoscopy using a panoramic view ("unfolded cube"). (**h**) MPR demonstrating fat attenuation in the lesion, proving it to be a colonic lipoma.

instead of maximum intensity projections. This technique can be employed in CTA, tracheobronchial imaging as well as CT colonography (Fig. 2.**50 d**). It provides a good overview of the anatomy even in complex and spatially contorted cases.

Coned-down VRT allows for in-detail analysis of a subvolume of interest and is helpful for vascular structures as well as CT colongraphy (Fig. 2.**50 e**).

Virtual dissection (virtual gross pathology) is a new technique for CT colonography that finds the centerline of the colon, stretches it out and performs a virtual longitudinal cut in order to obtain a flattened view of the inner colonic surface (Fig. 2.**50 f**). In order to avoid spatial distortion, only slim stripes of the colon wall are displayed.

A *panoramic view* (Fig. 2.**50 g**) yields endoscopic projections in and against the direction of movement as well as views of the sides of the colon. This allows for almost complete endoscopic evaluation of the colonic surface and improves detection of polyps hidden behind larger folds. Other techniques have been tried as an alternative to virtual colonoscopy and include Mercator's projection, bull's eye views and others, but they have not yet gained clinical acceptance.

Finally, *multiplanar reformations* (Fig. 2.**50 h**) must not be neglected because they are able to yield information about CT attenuation, contrast enhancement as well as transmural extent of a lesion.

Artifacts and Pitfalls

Threshold-based techniques (SSD) are inherently more susceptible to artifacts than volume rendering techniques.

Even with optimum thresholding, SSDs are degraded by pseudo-occlusions and pseudo-stenoses in small vessels (virtual angioscopy) and by pseudo-defects in the bronchial or colonic wall (virtual bronchoscopy and colonoscopy, respectively). These effects are less pronounced in volume rendering when suitable parameters are selected. With VRT even smaller vessels and airways can be evaluated.

In virtual colonoscopy, it is often difficult to distinguish between intraluminal contaminants and polyps. In virtual colonoscopy and gastroscopy, residual intraluminal fluid can obscure the surface of the stomach or bowel and prevent their evaluation. Optimum preparation is critically important. Thin bowel walls, especially when two bowel loops are adjacent to each other, or haustra may appear translucent and require readjustment of threshold or opacity values.

In virtual bronchoscopy, breathing and pulsation may lead to ring-like distortion of the bronchial walls. Mucous can mimic polypoid lesions, although it often appears elongated and is therefore easily distinguished from real pathology.

Measurements of luminal diameters and degrees of stenosis are strongly dependent on the viewer's perspective and, especially, on the selected threshold value.

Applications

Virtual colonoscopy is the most widely used virtual endoscopic technique (see also Figs. 15.**16**–**18**). It is part of a CT colonography study and has been proposed for colon cancer screening as well as for detection of concomitant lesions in stenosing colon cancers. However, very few people use it to examine the whole colon. Instead it is used mainly as a tool to differentiate colonic folds that mimic polyps from real polypoid lesions. With further refinement of the technique, however, virtual colonoscopy may also become a method for screening the whole colon because it should have a higher sensitivity for detecting small polyps that are easily missed on cross-sectional images alone.

Virtual bronchoscopy at present has very few clinical indications because most diagnostic decisions can also be made based on alternative display techniques such as thick MPR. Because of the strong enlargement of structures, however, it might gain a role with multislice scanning of the tracheobronchial system. Virtual bronchoscopy can more readily detect small polypoid protrusions into the bronchial lumen and is able to depict lymph nodes that bulge the bronchial wall at the level of a bronchial bifurcation, a sign considered indicative of malignant disease by bronchoscopists. What remains is a guiding tool for fiberoptic bronchoscopy that

helps in biopsies of more peripheral lesions, or for determining the safest point for transbronchial biopsies in a central location close to a main vessel.

Virtual cystoscopy has the potential to detect very small polypoid bladder lesions, even in regions that may be hard to inspect by real cystoscopy. For best results, the technique requires filling of the bladder with contrast material or air.

Virtual angioscopy has provided almost no additional information over other visualization techniques. The only indication may be the display of the relative location of the struts of aortic stent grafts relative to the ostium of branching vessels. A major disadvantage of this techniques is the overestimation of stenoses due to calcified plaques (blooming effect).

Virtual cholangioscopy, *virtual gastroscopy*, *virtual enteroscopy*, or endoscopy of other organ systems have been suggested as well, but most techniques fail to provide helpful information over other, less complex visualization tools.

3 Patient Preparation and Contrast Media Application

M. Prokop, A. J. van der Molen

The strategies applied in CT examinations are determined by the technical characteristics of the CT scanner and by the nature of the clinical question. Examinations without contrast medium are suitable only for intrinsically high-contrast structures (bone, stone detection, and lung parenchyma) and for the detection of hematomas. Almost all other types of soft-tissue examination will profit from the parenteral administration of contrast medium. Newer techniques rely on the analysis of multiple perfusion phases in contrast-enhanced scans. Bowel opacification is necessary for most abdominal CT examinations.

Preparation for CT Examinations

When a *patient is scheduled* for CT examination, it must be decided whether special patient preparation is required (Table 3.**1**). In patients who have significant renal function impairment or other relative contraindications to contrast-enhanced CT, other imaging modalities (ultrasound, MRI) should be considered as an alternative.

Table 3.**1** Patient preparation

When the examination is schedulded, determine the following:
• Renal function status (serum creatinine > 130 μmol/l) • Allergy to contrast materials? • Metformin therapy for diabetes? • Hyperthyroidism? Papillary or follicular thyroid carcinoma? • Bowel preparation (e. g., for CT enteroclysis, virtual colonoscopy)? • Fasting (for CT of stomach or pancreas)? • Coordinate with anesthesiologist or pediatrician: Intensive care patient on ventilatory support? Small child requiring sedation?
When patient arrives for examination:
Review the points listed above. • Determine scan protocol (if not already done). • Informed consent: Contrast administration Hypotensive agent (Buscopan or glucagon) Interventional procedure • Bowel opacification • Hydration necessary? • Place needle for CM
Positioning
• Radiation protection of the gonads (apron, other shielding) • Comfortable supine, prone, or lateral decubitus position • Padding beneath head, knees, or lower legs • If necessary, gastrointestinal contrast administration is repeated • Buscopan or glucagon administration?

The patient should come in advance if oral contrast will be administered. For CT examination of the upper abdomen, patients should be scheduled some 30 minutes before the planned scan, and 60–90 minutes before the scan if the whole abdomen is to be examined with good bowel opacification.

When the *patient arrives* on the day of the examination, the radiologist should review the contraindications to the procedure and inform the patient of potential side effects from the examination (contrast administration, use of antispasmodics or H_1/H_2 blockers) or from any CT-guided intervention. Gastrointestinal contrast material is administered orally if required. If the definitive protocol for the examination has not already been prescribed, it is done at this time.

Patients with Impaired Renal Function

Iodinated contrast media (CM) can induce renal injury through a combination of changes in renal hemodynamics (initial vasodilatation followed by prolonged vasoconstriction) and direct tubular toxicity. Contrast nephropathy (CMN) can occur in patients with risk factors and is generally defined as an *increase in serum creatinine >25% or >0.5 mg/dl (44 μmol/l) within 48–72 hours* compared to baseline. Established risk factors are pre-existing renal insufficiency, diabetic nephropathy, large contrast volumes, and dehydration. Possible risk factors include congestive heart failure, recurrent contrast procedures, and multiple myeloma patients with dehydration.

For patients with normal renal function (≤ 1.5 mg/dl or ≤ 130 μmol/l) there are no renal contraindications for contrast-enhanced CT. In

patients with risk factors, the serum creatinine levels provide an indicator of renal function. The creatinine clearance (CCr) as a better indicator of the glomerular filtration rate (GFR) can be estimated using the *Cockroft-Gault formula*:

CCr (ml/min) = (140 – age) × body weight (kg) / (serum creatinine (μmol/l) × 0.81)

For females an additional correction factor of 0.85 is usually used. Based on this formula, patients can be adequately stratified in risk categories (Table 3.**2**). As large volumes of CM are considered an independent risk factor, it is advisable to keep the contrast volume as low as reasonably possible. A useful rule was described by Cigarroa (1 mg/dl = 88 μmol/l):

5 ml CM per kg body weight (max. 300 ml) / serum creatinine (mg/dl)

Hydration is an important part of prevention of CMN (Table 3.**3**). The inpatient can be prepared by infusing 100–150 ml/h of 0.9% saline starting 4–12 hours before the examination. In outpatients, 1000 ml can be infused starting approximately 30–60 minutes prior to contrast administration. Intravenous or oral hydration should be continued for 12 to 24 hours after the examination. Urine output should be monitored if possible. There is no associated benefit from using mannitol or diuretics. Nonionic low-osmolar contrast media, often already used routinely for all intravascular injections, are always indicated in patients at risk for CMN. The use of iso-osmolar contrast media may also provide some protection.

It is important to reduce other exogenous risks by withholding nephrotoxic medications such as non-steroidal anti-inflammatory drugs, ACE inhibitors, diuretics, or the antiplatelet

Table 3.**2** Stratification of contrast material-induced risk in patients with impaired renal function (Waybill, 2001)

High risk patients
• Patients with stable creatinine clearance < 25 ml/min • Patients with stable creatinine clearance 25–50 ml/min and risk factors*
Moderate risk patients
• Patients with stable creatinine clearance 25–50 ml/min • Patients with stable creatinine clearance 50–75 ml/min and risk factors*
***Risk factors**
• Diabetic nephropathy • Congestive heart failure • Recent administration of CM • High volume of CM required

Table 3.**3** Suggestions for prevention of contrast nephropathy (modified from Waybill, 2001)

Identification of patients with increased risk
• Measure serum creatinine in patients with (suspected) decrease in renal function, diabetes mellitus, or other risk factors scheduled for any intravenous administration. • Estimate creatinine clearance and identify patients who are at moderate or high risk (c.f. Table 3.**2**).
Preparation of patients at moderate or high risk
• Choose alternative imaging modality if possible. • Discontinue *non-steroid anti-inflammatory drugs* and *Dipyridamole* 48–72 hours before the procedure. • Withhold diuretics or *ACE inhibitors* for 24 hours before the procedure. • *Hydration* in moderate risk patients: 0.9% saline @ 1.0–1.5 ml/kg/hr (based on volume status) beginning 4 hours before procedure, and continuing 8–12 hours after the procedure. • *Hydration* in high risk patients: 0.9% saline @ 1.0–1.5 ml/kg/h (based on volume status) beginning 12 hours before procedure, and continuing 12–24 hours after the procedure.
Examination of patients at moderate or high risk
• Use low osmolar contrast material. • Minimize volume of contrast material.
Follow-up of patients at moderate or high risk
• Discontinue *Metformin* 48 hours *following* the procedure, and restart only if creatinine levels are normalized. • Closely monitor urine output; and increase intravenous fluid rate to maintain input greater than output. The goal is to maintain positive fluid balance with high urine flow rate. • If patient develops decreased urine output or progressive increase in creatinine, consult a nephrologist. • Check blood urea nitrogen and creatinine 24 hours after the procedure. If there is any increase, admit the patient, continue hydration and observation, and recheck daily until serum creatinine levels have returned to baseline (this may also be done on an outpatient-basis in selected cases).

agent dipyramidole for 48 hours prior to the examination if clinically possible.

Metformin (e.g., Glucophage), an oral antihyperglycemic agent, has attracted interest recently because of the risk of causing lactic acidosis (pH <7.25, lactate >5 mmol) in diabetic patients with impaired renal function. Current guidelines (e.g., European Society of Urogenital Radiology, ESUR) advise the following: if the study is elective and renal function is normal, metformin should be discontinued for 48 hours *following* the examination. It can be reinitiated if renal function (serum creatinine) remains normal. If renal function is impaired (>130 μmol/l), alternative diagnostic modalities should be considered first. If CT is still required, metformin should be stopped and the exam should be postponed for 48 hours. Metformin can be reinitiated 48 hours after the study if renal function has not deteriorated. If the study is urgent and imperative, metformin should be stopped, patients should be hydrated as described above and renal function should be closely monitored. Patients with preterminal renal disease may need an individualized regime for preventive hydration because of an increased risk of developing renal failure.

A recent publication suggests that a two-day regimen of hydration combined with acetylcysteine 600 mg twice daily—one day before and on the day of the examination—can protect the kidneys from CMN, even in patients with already decreased renal function. The role of other agents, like theophylline, prostaglandin E1, dopamine, fenoldopam, and the newer endothelin antagonists, in the prevention of CMN is still unclear. Patients on chronic dialysis can receive a normal contrast dose. No special scheduling with respect to dialysis sessions is needed.

Patients with Allergy to Contrast Media

The necessity to prepare patients depends whether or not nonionic low-osmolar contrast media (LOCM) are routinely used. There is controversy as to whether this risk can be reduced pharmacologically in the case of nonionic contrast media, but this has been proven for ionic media. Two basic precautionary measures are available:

- prophylactic short-term infusion of H_1 (and H_2) antihistamine agents
- prophylactic treatment with corticosteroids.

When LOCM are used routinely for CT, only those patients with a history of a proven moderate to severe adverse reaction to contrast media should be premedicated if there are no alternative options (MRI, US). When corticosteroids are used in elective studies, it is important that the first dose is given at least 12 hours prior to the CT examination. The chemotoxic effects are probably not improved by these agents. In most strategies the steroids are combined with H_1-antihistamines. There is conflicting evidence about the proved benefit of adding H_2-antihistamines, but at least a theoretical benefit is suggested.

When LOCM are only used selectively, they should be used in all patients with known risk factors for adverse reactions: proven history of multiple allergies, bronchial asthma, severe congestive heart failure or recent heart attack, diminished renal function, and proven history of any adverse contrast reaction. For patients with a moderate or severe reaction in the past, proceed as above. A practical protocol is outlined in Table 3.**4**.

Table 3.**4** Preparation of high risk patients (dose has to adapted in children, slim or obese patients)

Medication	Time of administration	Category
40–50 mg (methyl)prednisolone[1] p. o. or i. v.	12 h and 2 h before the examination	Glucocorticoidsteroid
300 mg cimetidine[2] in 20–50 ml saline[3] i. v.	2 h before the examination	H_2-antihistamine
50 mg diphenhydramine[4] i. v.	directly prior to the examination	H_1-antihistamine
18 G i. v. line	during examination	

Always use nonionic low-osmolar contrast media
[1] A dose of 50 mg prednisolone is equivalent to 250 mg hydrocortisone or 10 mg dexamethasone
[2] Alternative: 50 mg ranitidine (e.g. Zantac)
[3] Dilution at the discretion of the radiologist, either as a slow injection or short infusion
[4] Alternative: 2 mg clemastine (e.g. Tavegil)

Patients with Thyroid Disease

Iodinated contrast media solutions may contain maximum free iodide levels of 35–90 μg/ml, depending on shelf-life. Additionally, some 0.05% of the bound iodine is liberated from the contrast molecule in the body during the first 24 hours after injection (more for biliary-excreted contrast media). A routine CT examination delivers approximately 25–40 times the minimum required daily intake of iodine (3.5–5.3 mg). *Overt hyperthyroidism* is therefore an absolute contra-indication to iodinated contrast media

Iodine-induced thyrotoxicosis (IIT) is not clinically relevant in unselected patient groups or in normal individuals. An increased risk is seen in patients with Graves disease and in patients with thyroid autonomy. In iodine-deficient areas, there is a higher incidence of multinodular goiter with autonomous thyroid tissue, especially in the elderly. When high-risk patients are subjected to an excessive iodine load, this may result in thyrotoxicosis, which is often difficult to treat. The risk of developing IIT is estimated to be 0.03% in iodine-sufficient areas, and 0.25–0.35% in iodine-deficient areas.

Prophylaxis is controversial, because the protective effect differs between areas of iodine sufficiency and deficiency. In unselected patient groups, side effects from these medications may be as high as the risk of IIT. Premedication (Table 3.**5**) is therefore not generally recommended in areas of iodine sufficiency but can be useful in areas of iodine deficiency. Additionally, patients with papillary or follicular thyroid cancer may also benefit.

Patients who are scheduled to receive *radioactive iodine* should not undergo contrast-enhanced CT studies without physician consultation. Diagnostic scintigraphy may be rendered nondiagnostic for 2–6 weeks following iodinated contrast medium administration. Injecting iodinated contrast material in nonpremedicated patients with papillary or follicular thyroid cancer will make radioactive iodine treatment ineffective for 2–3 months and thus may seriously influence the overall prognosis of the disease.

Bowel Preparation

The contents of the gastrointestinal tract can hamper or prevent evaluation of the stomach, duodenum, and colon on CT scans. Unless there is special emphasis on these organs, no special preparation is needed but it can be recommended to discontinue solid foods some 3–4 hours prior to the examination.

In special investigations of the *stomach and pancreas*, solid foods should be discontinued the evening before the examination. The patient may continue to take oral medications, however. This makes it possible to achieve optimum distension of the stomach and duodenum following the administration of butylscopolamine or glucagon and (negative) oral contrast medium.

For special CT examinations of the small bowel (*CT enteroclysis*), solid foods are discon-

Table 3.**5** Possible prophylactic strategies for patients with thyroid disease (according to Hehrmann, 1996)

Patients at risk		
Graves disease, latent hyperthyroidism in patients with autonomous adenoma Papillary thyroid cancer, follicular thyroid cancer		
Elective CT studies:		
Sodium Perchlorate	3 dd 300 mg	Start 1 day before CT and continue for 8–14 days
Thiamazol	1 dd 30 mg	Start 1 day before CT and continue for 28 days
Emergency CT studies:		
Sodium perchlorate	1 dd 800 mg	Directly prior to CT and continue with 3 x 300 mg for 8–14 days
Thiamazol	1 dd 30 mg	Directly prior to CT and continue for 28 days
Therapy should be clinically controlled with measurements of serum free T_3 and TSH Barium 2% should be used for bowel opacification		

Table 3.**6** Bowel cleansing for CT examinations

Stomach, duodenum, pancreas
No solid food for 12 h No food or liquids for 6 h
Small intestine (CT enteroclysis)
No solid food for 24 h Low-residue diet High fluid intake (3 l/d) Mild laxative on day before examination
Colon
No solid food for 2 days, but copious liquids Laxative medication for 2 days (preferably 'dry' preparations) Mini-enema on morning of examination (optional)

tinued 24 hours before the examination. Although multiple methods will provide good results, a regimen of a low-residue diet, high fluid intake (3000 ml/day) and a combination of laxative medications (magnesium sulfate and bisacodyl) for one day is simple and works well. (Table 3.**6**).

Special CT examinations of the colon (*CT colonography*) require the same kind of bowel preparation that would precede a barium enema. The regimen suggested above (low-residue diet, high fluid intake, and combination of laxative medications) can be used for two days, but prepackaged kits (e.g., Fleet) are also available (Table 3.**6**). "Dry" preparations, typically given for barium enemas, are superior to "wet" preparations (e.g. Golytely), typically given for colonoscopy, because there is less fluid left within the colon, and air can be used as a negative contrast agent.

Positioning

Positioning includes placing the patient in a comfortable, symmetrical position and providing adequate radiation protection. Padding should be placed beneath the head, knees, or lower legs to keep the patient comfortable and reduce motion artifacts. One should consider protecting highly radiosensitive areas such as the breasts and gonads with lead shielding in those examinations in which they are outside the scanned field. A wrap-around lead apron may be used in place of a gonadal shield. Keeping a lead shield in place within the scan range will cause major artifacts and mandates a repeat examination of that region. It has been reported, however, that partially radio-opaque shielding with bismuth garments (for the breasts) allows the shield to be kept within the scan field.

To avoid artifacts, at least one arm (preferably both) should be removed from the scanning field (e.g., extended above the head). All metallic objects (zippers, wallets, ECG electrodes, metal-reinforced ventilation tubing, etc.) should also be removed from the field.

Vascular Access

Peripheral Venous Access

Intravenous access is established with a sufficiently large cannula (18–20 G), preferably placed in an antecubital vein. The vein should be substantial enough to accommodate the 3–5 ml/s injection rate that is used in most protocols. Higher flow rates mandate larger cannulas (16–17 G).

Central Venous Access

A central venous catheter (triple-lumen catheter or other catheter with a 6 G lumen) is suitable for contrast injection only at relatively low flow rates of 1.5–2.5 ml/s (see manufacturer's guidelines). Depending on the type and length of the catheter it may become ruptured or dislodged due to excessive flow rates. If doubt exists, a trial NaCl injection should be performed manually to test catheter function, and the power injector should be coupled to a pressure-limiting device.

Large central venous catheters such as an introducer sheath, a dialysis catheter, etc. allow for higher flow rates of 4 ml/s or more, again depending on the catheter type used.

Femoral Venous Access

Femoral venous access may be useful for CT angiography of the thoracic aorta but it is generally avoided where possible because of the higher risk of extravasation associated with such a technique when performed on the CT table. It should be noted that many ordinary antecubital venous cannulas are not long enough to provide secure access in obese patients. In these cases a small insertion set can be used to thread a somewhat longer catheter safely

through the femoral vein into the iliac vein (i.e., using the Seldinger technique).

If femoral access is required or if contrast medium must be injected through a pedal vein (especially in children) for abdominal scanning, it should be noted that high-contrast streak artifacts can persist in the inferior vena cava for up to 10 seconds after the end of the injection and can hamper the evaluation of adjacent structures. For this reason, lower contrast material concentrations can be recommended in these situations.

Arterial Access

Certain examinations, such as CT during arterial portography (CTAP), require the placement of an intra-arterial catheter under fluoroscopic guidance in an angiography room. On the CT table a scanogram should be taken prior to contrast administration to recheck the catheter position.

Planning the Scan

Planning the examination should be done as early as possible so that the patient can be adequately prepared and any missing information can be acquired prior to the examination. A scanning protocol that is appropriate for the scanner and for the actual requirements of the examination should be formulated and documented. In most cases, one will chose from a set of standard protocols, which may be modified according to individual requirements (e.g., in slim or obese patients, patients with impaired renal function or bad venous access).

Such standard protocols should include information about patient preparation, data acquisition and image reconstruction technique as well as 3D postprocessing and filming.

We recommend taking a written record of the individual scanning protocol on the request form, using an abbreviated code that simplifies the adaptation of standard protocols. We suggest using the notations listed in Table 3.**7**. This information should also be included in the patient comment on the CT scanner so that any subsequent problems can be investigated retrospectively to find explanations for unexpected effects in a particular examination.

To optimize image quality and to minimize radiation exposure of the patient either automated programs can be employed (most of which are just about to enter the market), or estimates of the required mAs settings based on the patient's size and weight may be used. Most of these approaches are still in their infancy, and

Table 3.**7** Suggested notation for examination parameters

Scan parameters		Example	
Spiral CT:	SC/TF/RI ↑ ↓	5/8/4 ↑	
Multislice CT:			
Acquisition:	N×SC/TF ↑ ↓	4×1/5.5 ↑	thin section acquisition
Reconstruction:	SW/RI ax/cor/sag	5/4 ax, 1.5/3 cor	5 mm axial, 1.5 mm coronal reformations

SC = section collimation (mm), TF = table feed (mm/rotation), RI = reconstruction interval (mm), ↑ ↓ = scan direction, SW = section width (mm), ax/cor/sag = section orientation

Contrast parameters		Example	
Standard:	V/F/D	100/2/100	
Contrast dilution:	V:N/F/D	60 : 60/4/30	1 : 1 dilution = 150 mg/ml
NaCl bolus:	V+N/F/D	100 + 50/4/20	50 ml saline flush
Bolus triggering:	V/F/DX	120/4/5A	bolus triggering 5 s after aortic threshold
Biphasic injection:	$V_1/F_1+V_2/F_2/D$	50/5 + 50/2/20	fast injection followed by slower injection
Biphasic scan:	$V/F/D_1+D_2$	150/4/20 + 70	arterial and portal phase scans

V = contrast volume (ml), F = flow rate (ml/s), D = scan delay (s), N = volume (ml) of dilution medium or NaCl bolus, DX = delay after reaching trigger level at position X, contrast concentration 300 mg iodine/ml

no general recommendations can be made (see Chapter 5, p. 149). Documentation of kVp, mAs, scanning mode, pitch and section collimation is required to be able to determine the patient's individual radiation exposure. If available, it is easier to use the volume CT dose index ($CTDI_{vol}$) instead. This number is an indicator of the locally applied dose and is displayed on the scanner console of most modern CT units for the specific protocols selected by the user. However, some manufacturers only display the $CTDI_{vol}$ if explicitly asked by their customer.

Gastrointestinal Contrast Media

Bowel opacification is necessary for the adequate evaluation of the gastrointestinal tract and for differentiating it from other structures of soft-tissue density. With good bowel opacification, pathologic changes in the bowel wall and lumen can be appreciated on the opacified scans.

Types of Gastrointestinal Contrast Media

Contrast media for the bowel are classified as positive or negative, depending on whether the material is hyperattenuating or hypoattenuating relative to the walls of the gastrointestinal tract (Table 3.**8**).

Water or methyl cellulose preparations are negative contrast media that facilitate evaluation of the mucosa following intravenous administration. They also do not superimpose on abdominal vessels and are therefore becoming a new standard for multislice CT of the abdomen. For use in CT examinations water or juice should not be carbonated. Methyl cellulose preparations can be administered orally (given adequate additives for taste) and have the advantage of a higher viscosity. The higher viscosity makes methyl cellulose ideally suited for CT enteroclysis or colonography. Water-based negative contrast media, however, provide insufficient detail if the bowel is not fully distended, and can hamper the detection of cystic lesions in the female pelvis. For this reason they are often used in conjunction with a spasmolytic compound (n-butylscopolamine, e.g., Buscopan) or are administered by enema or pump injection.

Oily or fat-containing contrast media are not recommended for oral administration because of their unpleasant taste, which may lead to noncompliance. However, (full fat) milk has been described as a useful contrast medium for the upper abdomen. For administration by enema (colon) or pump injection (small bowel enteroclysis) an oily contrast preparation improves the contrast between the bowel wall and the lumen, and makes it easier to distinguish between extra-enteric fluid and bowel.

Air or CO_2 as contrast media produce a very high negative contrast, which is particu-

Table 3.**8** Types of gastrointestinal contrast media

Medium	Region	Applications
Negative contrast media		
Water (non-carbonated)	Stomach, pancreas	Tumor diagnosis
Methyl cellulose preparations	Small bowel, colon	CT enteroclysis
Paraffin suspension, vegetable oils	Small bowel, colon	Rectal application, poor oral compliance
Air	Colon, stomach	Only for virtual endoscopy
Positive contrast media		
$BaSO_4$ suspension	Stomach + bowel	Universal (contraindicated if perforation may be present)
Iodinated solutions	Stomach + bowel	Universal (contraindicated in hyperthyroidism)

larly useful in virtual endoscopy of the colon (or stomach). CO_2 has the advantage over air that it is readily absorbed by the body and is eliminated by respiration. It induces less spastic response of the bowel wall and therefore is better tolerated by most patients. In addition, colon distension was reported to be superior with CO_2 as compared to air. Bowel distension can be further improved with injection of 20–40 mg of n-butylscopolamine (e.g., Buscopan) as soon the first symptoms (bowel colics) occur.

Barium sulfate ($BaSO_4$) suspensions and *iodinated solutions* are positive contrast media that have universal applications. Intestinal structures are clearly identifiable as such even when they are poorly distended. One disadvantage of positive contrast media is that they make mucosal surfaces more difficult to evaluate following IV administration of contrast material. Barium suspensions have an agreeable taste and reportedly produce somewhat better opacification of the upper gastrointestinal tract. They are contraindicated, however, in patients who may have a perforated bowel (clinical suspicion, immediate postoperative period, or after endoscopic intestinal biopsy). Iodinated contrast media should be avoided in hyperthyroidism and are contraindicated when patients are scheduled for scintigraphy or radiotherapy with iodine 131.

Technique of Gastrointestinal Contrast Administration

With few exceptions, oral contrast medium should be used routinely for CT examinations of the abdomen. With *spiral CT* the bowel is opacified with a *positive contrast medium*, in which case an iodinated solution or $BaSO_4$ suspension may be used with equal success. Care should be taken that the medium is sufficiently diluted (3–4% for agents such as Telebrix Gastro or Gastrografin, 2% for barium suspensions). Spasmolytic agents are administered only if adequate distension of the duodenum is required.

Iodinated contrast media produce better opacification of the stomach and duodenum if the last cup of oral contrast is more highly concentrated (5% = 10 ml in 200 ml water) and is ingested in the examination room. This will correct for the frequent increase in gastric secretions that occurs before the examination.

For examinations of the upper abdominal organs, only the proximal small bowel requires opacification. This is accomplished by having the patient drink 500 ml of contrast medium over a 30 minute period. Examinations covering the entire abdomen also require opacification of the distal ileum and perhaps the colon (for pelvic imaging), achieved by having the patient drink 1 to 1.5 l of contrast medium. The doses should be fractionated to distribute them evenly over the ingestion period of 60 to 90 minutes prior to the examination. Starting the scan too early leads to insufficient opacification of the distal bowel segments, while an excessive delay between the last ingested portion of contrast medium and the CT scan leads to contrast problems in the proximal small bowel. Optimum bowel opacification requires accurate timing and adequate patient instruction. Excellent colon opacification is achieved when oral contrast administration is started the evening before the examination day. With their appointment, patients receive a bottle of 20 ml of contrast agent that they have to dilute to 600 ml. This can be taken with food in two portions and gives a good large bowel delineation.

With *multislice CT*, especially when thin-section imaging is performed, delineation of the abdominal vessels becomes more important and requires use of *negative contrast agents*. Distinction between lymph nodes, masses and non-opacified bowel loops is less of a problem because of the increased spatial resolution of multislice CT.

For the stomach and pancreas we recommend methyl cellulose preparations because of their increased viscosity, while water is sufficient for the upper abdominal examinations. The contrast material (500–1000 ml) should be given over a short period of time to ensure proper distension of the stomach and duodenum. For examinations of the whole abdomen, larger amounts of negative contrast material are required (1–1.5 l), and should be given 30–60 minutes prior to the examination. For the lower abdomen, some authors suggest a combination of 500–1000 ml of positive contrast material given over a period of 30–90 minutes prior to the examination, followed by 500–1000 ml of negative contrast material given during the last 15 minutes prior to the scan. Sufficient time between ingestion of the two types of contrast material is required to avoid mixing. Even then,

some portions of the small bowel or even the stomach may retain a luminal opacification that is identical to the attenuation of the bowel wall, which makes it impossible to evaluate mucosal or intraluminal abnormalities.

Special techniques to achieve optimum opacification of the stomach, small and large bowel are summarized in Table 3.**9** and are discussed in Chapter 15, Gastrointestinal Tract.

Table 3.**9** Gastrointestinal contrast administration

Region	Technique	Anti-spasmodics	Comments
Standard protocols			
Upper abdomen	500 ml positive contrast medium	–	Taken orally in fractionated amounts over 30 min period
Abdomen	1–1.5 l positive contrast medium	–	Taken orally in fractionated amounts over a 60–90 min period
Special GI protocols			
Esophagus	200 ml positive contrast medium on examination table *or* thick barium paste on exam table	–	Done occasionally to mark the lumen
Stomach	500 ml water before exam 250 ml water on table	+	Tumor detection/staging In left lateral decubitus position, repeat for contrast series
Small bowel	Up to 2 l methylcellulose *or* up to 2 l highly dilute $BaSO_4$	–	CT enteroclysis via duodenal catheter
Rectum	500 ml positive contrast rectally	–	Done only to mark the rectum for tumor staging in the small pelvis
Colon	1–2 l positive contrast rectally or 1–2 l negative contrast	+ +	Inflammatory disease Tumor staging/inflammatory disease
Virtual endoscopy			
Stomach	3 packets of effervescent powder	+	N.p.o. for 6 h
Colon	Rectal air or CO_2 insufflation	+	Bowel preparation essential

Parenteral Contrast Media

Intravascular contrast medium is necessary for most CT examinations of blood vessels and parenchymal organs. The contrast volume and mode of contrast administration vary with the nature of the study. CT scanning with intravascular contrast may have any of six objectives:

- CT angiography (vessel evaluation)
- vascular opacification (to differentiate vessels from lymph nodes in nodal staging)
- parenchymal enhancement (lesion detection and characterization)
- interstitial enhancement (inflammatory lesions, tumors)
- Urinary enhancement (excretion, pyelocalyceal system)
- perfusion analysis (lesion characterization, tissue perfusion).

The same contrast media can also be used for the opacification of anatomic and pathologic spaces, like the spinal canal, lower urinary tract, pleura, peritoneal cavity, abscesses, or fistulas.

Types of Contrast Media

Ionic High-osmolar Contrast Media

Ionic contrast media are moderately well tolerated, depending on the injection rate used for IV administration (Table 3.**10**). Some patients experience warmth, pain, or burning at injec-

Table 3.**10** Risks of parenteral contrast media (after Katayama, 1990)

Risk group	Number of cases (ionic/nonionic)	All adverse reactions		Severe adverse reactions*	
		Ionic	Nonionic	Ionic	Nonionic
Total population	169, 284/168, 363	12.7%	3.1%	0.22%	0.04%
Known allergy	12, 913/15, 058	23.4%	6.9%	0.53%	0.10%
Known contrast allergy	5785/9667	44.0%	11.2%	0.72%	0.18%

* Severe adverse reactions: severe dyspnea, fall in blood pressure, cardiac arrest, loss of consciousness

tion rates higher than 2 ml/s. For this reason, ionic contrast media are not recommended for use in spiral or multislice CT. They are still used in intracavitary applications such as fluoroscopic studies of the bladder and bowel. In many Western countries, most radiological departments have completely switched to nonionic media for all (intravascular) indications and therefore only few ionic media are still on the market.

Nonionic Low-osmolar Contrast Media

Nonionic contrast media are generally preferred over ionic media because of their lower osmolarity and significantly lower rate of adverse events (Table 3.**10**). There is also a lower incidence of reactions related to chemo- or osmotoxicity during contrast injection, making it safe to use rapid injection (flow) rates. The main disadvantage of nonionic media is their higher cost.

Most contrast media used for intravenous application are monomeric molecules. They are in general better tolerated than dimeric molecules despite the fact that the latter are nearly iso-osmolar. Dimeric agents have a substantially higher viscosity and different hydrophilicity, and need to be heated up to body temperature prior to intravenous injection. Dimeric contrast agents are preferentially used for intrathecal and intra-articular applications (CT arthrography).

Complications of Contrast Material Injection

Contrast Extravasation

The commonest complication of intravascular injections is contrast extravasation. Most often, this involves small volumes (< 10 ml), but when large volumes extravasate serious injury to skin and subcutaneous tissues may be produced.

A number of risk factors have been identified: non-communicative patients (children, elderly), severely debilitated patients, multiple punctures in the same vein, and injections on the dorsum of the hand and foot. Treatment guidelines are outlined in Table 3.**11**.

Adverse Reactions to Contrast Media

Parenteral contrast media can incite a variety of adverse reactions (Table 3.**12**), which may occur early (usually < 20 minutes) or late. The reactions may have an anaphylactoid etiology but can also result from osmolar effects (e.g., direct irritation of the venous wall) or the number of carboxylic and hydroxylic side chains (chemotoxicity). The incidence of adverse reactions depends on whether the medium is ionic or nonionic and on

Table 3.**11** Treatment of contrast extravasation

Initial treatment
• Elevation of the affected extremity above the heart • Cold packs—15–60 min applications, three times daily (day 1–3) • Close observation for 2–4 hours • Inform referring physician
Plastic surgery consultation when
• Extravasated volume >30 ml of ionic high-osmolar CM • Extravasated volume >100 ml of nonionic low-osmolar CM • Skin blistering • Altered tissue perfusion (capillary refill) or change in sensation in hands (compartment syndrome)

Table 3.**12** Symptoms of adverse reactions to contrast media

Early reactions (up to 60 min postinjection)
Mild to moderate
• Nausea or vomiting • Urticaria • Diffuse erythema, angioedema • Bronchospasm • Vasovagal reaction
Severe (requiring treatment)
• Laryngeal edema, pulmonary edema • Hypotension • Anaphylactic shock • Respiratory arrest • Cardiac arrest
Delayed reactions (60 min to 7 days post-injection)
Skin reactions
• Skin rash, itching, swelling
Systemic reactions
• Headache, dizziness • Nausea, diarrhea • Chills, rigors • Flu-like symptoms
Delayed Arm pain
Other reactions

Table 3.**13** Selected risk factors for adverse reactions to contrast media

General risk factors
• Ionic contrast media • Overt hyperthyroidism (contraindication) • Female gender (especially delayed reactions)
Anaphylactoid reactions
• Previous serious contrast reaction • Bronchial asthma requiring treatment • Multiple allergies (atopy) requiring treatment
Chemotoxic reactions
Most important ones include: • Cardiovascular instability • Congestive heart failure grade III–IV • Diabetic nephropathy • Autonomous thyroid nodules in elderly • Liver and kidney disease

the specific product that is used. It is also influenced by the concentration and volume of the contrast medium, the rate of contrast injection, and a number of patient-related factors (Table 3.**13**). Published incidence data vary dramatically depending on how adverse reactions are defined. A possible grading is as follows:

- Minor reactions: nausea, vomiting, heat sensation, flushing, mild urticaria, sneezing
- Intermediate reactions: mild hypotension, generalized urticaria, mild bronchospasm, diffuse erythema, angioedema, vasovagal reaction
- Severe reactions: hypotension (systolic pressure < 70 mm Hg), pulmonary edema, epiglottic edema, severe bronchospasm, cardiac arrhythmia, cardiac arrest.

As a general rule, nonionic contrast media are well tolerated but are still associated with a 2–4% incidence of early adverse reactions and a 4–30% incidence of late reactions (depending on definition). According to the study by Katayama in 1990, most early reactions are mild to moderate (3.1%), and only 0.4% are severe (Table 3.**10**). The incidence of very severe reactions (causing critical illness or death) was 0.1%. Late reactions are not uncommon but occur more frequently in patients who received interleukin-2 therapies (10–30%). They often cause nonspecific symptoms like rash, mild fever, dizziness, chills, or rigors. In most cases no or only supportive treatment is indicated.

Cutaneous Reactions

Patients with cutaneous reactions are usually cooperative. Urticaria are anaphylactoid reactions resulting in raised focal areas of the skin and are most common in the face, neck and chest. They are associated with pruritus (itching) and can be mild or generalized. Patients may also develop diffuse erythema or subcutaneous (angio)edema that may develop into hypotension or airway edema and therefore should be closely monitored.

Respiratory Reactions

Respiratory reactions usually result in agitation. Airway or laryngeal edema is associated with a feeling of tightness in the throat, a change of voice, or even inspiratory stridor. It can be preceded by swelling of lips or tongue. Bronchospasm can be seen in asthmatics and cause dyspnea with wheezing and difficulty exhaling. Pulmonary edema may be seen in patients with

underlying congestive heart failure. The symptoms often develop slowly and dyspnea is the most important symptom. Anxiety is a diagnosis of exclusion, but it can cause hyperventilation with chest tightness.

Cardiovascular Reactions

These are usually the more dramatic reactions in which patients are looking for help but may become unresponsive. Hypotensive patients often complain of light-headedness or weakness. Mild reactions often respond well to fluids and leg elevation. Vasovagal reactions are associated with bradycardia (pulse < 60 bpm) and are more frequent in younger males, while tachycardia is suspect for an anaphylactoid reaction. It may be difficult to differentiate these two in patients that use β-blocking agents. If patients do not improve after initial measures or if they become unresponsive, direct assistance should be sought.

Treatment of Adverse Reactions

Oxygen should be administered at high dosage (10–12 l/min) via a face mask, preferably with an oxygen reservoir. This enables administration of 100% concentrations. Nasal cannulae are suboptimal for delivery of such high doses. All patients should receive a high dose regardless of the existence of chronic obstructive pulmonary disease.

H_1 and H_2 antihistamines are used primarily to reduce symptoms of skin reactions such as urticaria and diffuse erythema. They can also be used as a second-line drug for respiratory reactions after epinephrine has been given.

Corticosteroids do not play an important role in the treatment of the acute reaction. They are effective in prevention of delayed recurrences for as long as 48 hours, especially in respiratory reactions. When administered, a high loading-dose of 500–1000 mg hydrocortisone is advised which can be followed by constant infusion of 500 mg in 250 ml saline at a rate of 60 ml/h. Overdosing in the acute phase is generally not problematic. 500–1000 mg hydrocortisone is therapeutically equivalent to 125–250 mg Prednisolone, 100–200 mg methylprednisolone or 20–40 mg dexamethasone.

Epinephrine (adrenalin) is the most important medication. The 1 : 1000 dilution (1 mg/ml) is used for subcutaneous or intramuscular injection for milder symptoms and is often available in 0.3 ml preloaded syringes (e.g., Epipen®). The 1 : 10 000 dilution (0.1 mg/ml) is used for intravenous injection in moderate to severe symptoms and may also be available in preloaded syringes. In a recent UK report from the Project team of Resuscitation Council, IV administration by nonexperienced personnel is strongly discouraged and requires monitoring. Instead, IM injection of 0.5 ml 1 : 1000 adrenalin is recommended. Care should be taken in patients using β-blocking agents, as the selective α-adrenergic stimulation with vasoconstriction may lead to a hypertensive crisis (use isoproterenol instead).

A detailed outline of the most important reactions and suggested treatment is given in Table 3.**14**.

Table 3.**14** Treatment suggestions for adverse reactions to contrast media (protocols have to be checked with local regulations and available medication)

Cutaneous reactions
Nausea or vomiting: • Antiemetic drug when severe or protracted
Mild or asymptomatic urticaria: • No treatment needed
Generalized or symptomatic urticaria: • 50 mg diphenhydramine po/im/iv[a] • 50 mg ranitidine in 20 ml saline slowly iv[b]
Angioedema or diffuse erythema: • 50 mg diphenhydramine iv[a] • 50 mg ranitidine in 20 ml saline slowly iv[b]
Angioedema with signs of laryngeal edema: • Add 0.5 ml epinephrine 1 : 1000 im—may be repeated after 5 min
Diffuse erythema with hypovolemia: • Add 0.5 ml epinephrine 1 : 1000 im—may be repeated after 5 min • Saline 0.9% or Ringer's lactate rapidly iv
Respiratory reactions
Mild laryngeal edema: • Oxygen 10 l/min by face mask • 0.5 ml epinephrine 1 : 1000 im—may be repeated after 5 min
Severe laryngeal edema—add: • 50 mg ranitidine in 20 ml saline slowly iv[b] • Call emergency code—consider tracheal intubation
Mild bronchospasm: • Oxygen 10 l/min by face mask • Albuterol, terbutaline or metaproterenol dose-inhaler—2–3 deep inhalations

Continue ▶

Table 3.**14** (Continue)

Severe bronchospasm—add:
- 0.5 ml epinephrine 1 : 1000 im—may be repeated after 5 min
- 500–1000 mg hydrocortisone iv or equivalent (optional—see text)
- Call emergency code if patient does not respond —consider tracheal intubation

Cardiovascular reactions

Hypotension with bradycardia (vagal reaction):
- Elevate legs and release any abdominal compression
- Oxygen 10 l/min by face mask
- Saline 0.9% or Ringer's lactate rapidly iv
- 0.6–1.0 mg atropine slowly iv—may be repeated in 0.5 mg doses every 5 min up to 3 mg

Mild, isolated hypotension with tachycardia:
- Elevate legs and release any abdominal compression
- Oxygen 10 l/min by face mask
- Saline 0.9% or Ringer's lactate rapidly iv

Generalized anaphylactic reaction (shock)—add:
- Call emergency code
- 0.5 ml epinephrine **1 : 1000 im**
- Treat associated pulmonary or cutaneous reactions as indicated above
- Transfer to ICU

Pulmonary edema:
- Elevate head or have patient sit up
- Oxygen 10 l/min by face mask
- 40–80 mg furosemide slowly iv
- 500–1000 mg hydrocortisone iv or equivalent
- Call emergency code if patient does not respond

Angina:
- 0.4 mg nitroglycerin sublingual
- Oxygen 10 l/min by face mask
- Call emergency code for cardiologist and ECG

Cardiac arrest:
- Start cardiopulmonary resuscitation
- Call emergency code immediately

Neurological reactions

Anxiety reaction:
- Monitor vital signs and reassure patient
- Paper bag for breathing (when hyperventilating)
- If severe—2.5 mg midazolam or 5 mg diazepam slowly iv

Seizures:
- Turn on side to avoid aspiration
- Oxygen 10 l/min by face mask
- 2.5 mg midazolam or 5 mg diazepam slowly iv

[a] Alternative: 2 mg clemastine
[b] Alternative: 300 mg cimetidine in 20 ml saline
All **adverse reactions should be adequately documented** in the radiology report—type of CM used, patient symptoms, therapy, outcome and follow-up.

Contrast Injection Parameters

The most important parameters for intravascular contrast injection are:

1 Contrast volume **V** (ml)
2 Flow rate **F** (ml/s)
3 Scan delay **D** (s)
4 Saline flush **N** (ml)
5 Position **X** (of the reference region for bolus triggering)
6 Concentration **C** (mg iodine/ml)
7 Osmolarity (osmol/l)
8 Viscosity (kP)

Parameters 1 through 3 are the main ones for contrast injections, while parameters 6 through 8 are specific for the product used and generally are not modified by the examiner. The injected contrast material can be more fully utilized for contrast enhancement if the contrast material is pushed forward and the injection vein is flushed by a bolus of isotonic NaCl (normal saline, parameter 4). If the initiation of scanning is determined by the appearance of contrast medium in a reference region X (parameter 5), the scan delay D (parameter 3) denotes the interval from that point until a designated level of enhancement is achieved in that region.

The contrast parameters should be documented as a comment on the images, as they may have important implications for image interpretation. We suggest using the notations from Table 3.**7**.

Intravenous Contrast Administration

In the great majority of cases, parenteral contrast medium is administered by an intravenous route. Such an access route is quite long and leads to a defined sequence of vascular and organ enhancement with various mixing processes along the way to the target organ.

Basic Principles

Contrast material has to flow through the injection veins into the vena cava, enter the right atrium, pass the pulmonary circulation and finally arrive in the aorta. Mixing with non-opacified blood occurs along the way to the right atrium. In the right ventricle, mixing of opacified and non-opacified blood should be completed.

Once the contrast material has entered the aorta, it enhances various capillary beds during an arterial phase, enters draining veins that either join the vena cava or enter the portal venous system. Contrast material in the portal system enhances the liver parenchyma and drains into the liver veins before it reaches the right atrium again. As the contrast material flows back to the right heart from various organs, recirculation effects occur. Typical arrival times for various organ systems are shown in Table 3.**15**.

Aortic enhancement ideally reaches a plateau phase shortly after the contrast material arrives in the aorta. The slope of this initial enhancement is an indicator of the cardiac output of the patient but may be slowed if there are any obstructions along the venous inflow. As more contrast medium is injected, the aortic "plateau" increases further from cumulative effects that culminate as the final amount of contrast material enters the aorta. Thus, the aortic enhancement "plateau" is not a real horizontal plateau but increases as the scan progresses (Fig. 3.**1**). Peak aortic enhancement is seen at the end of this phase. This peak enhancement should not be regarded mistakenly as the ideal time for imaging the arteries but it is well suited for imaging arterially perfused organs.

Since the spontaneous flow in the injected veins is often slower than the injection rate, the inflow of contrast material slows as the injection is completed. This leads to a premature end of the aortic plateau and does not take full advantage of the injected contrast material. A saline flush, injected at identical flow rates immediately after contrast administration, pushes the contrast material forwards and thus prolongs the aortic plateau phase. In theory, the time from contrast arrival to peak enhancement in the aorta should last about as long as the injection time (= V/F), but it often ends earlier in patients with a high cardiac output and lasts longer in patients with a low cardiac output.

Most organs have an exclusively arterial blood supply. Only the liver and the lungs have a

Table 3.**15** Contrast arrival times after injection into the right cubital vein

Right atrium	6–12 s
Main pulmonary artery	9–15 s
Left atrium	13–20 s
Aorta	15–22 s
Carotids	16–24 s
Renal arteries	18–27 s
Femoral arteries	22–33 s
Jugular vein	22–30 s
Renal veins	22–30 s
Suprarenal IVC	24–32 s
Infrarenal IVC	120–250 s
Splenic vein	30–45 s
Mesenteric veins	35–50 s
Liver veins	50–80 s
Femoral veins	120–250 s

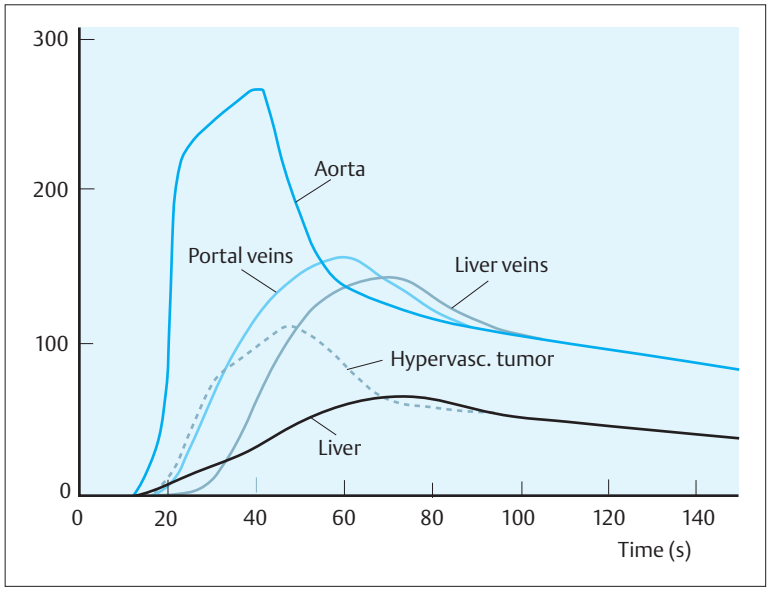

Fig. 3.**1** Contrast enhancement for the liver: example of a time-density curve for 150 ml contrast material injected at 4 ml/s.